AD-A076 566 RECOGNITION SYSTEMS INC VAN NUYS CALIF F/G 5/8
FEASIBILITY OF USING OPTICAL POWER SPECTRUM ANALYSIS TECHNIQUES--ETC(U)
JUN 79 H L KASDAN DAAK70-78-C-0019
UNCLASSIFIED KS-77-370 ETL-0186 NL

1 OF 3
AD A076566

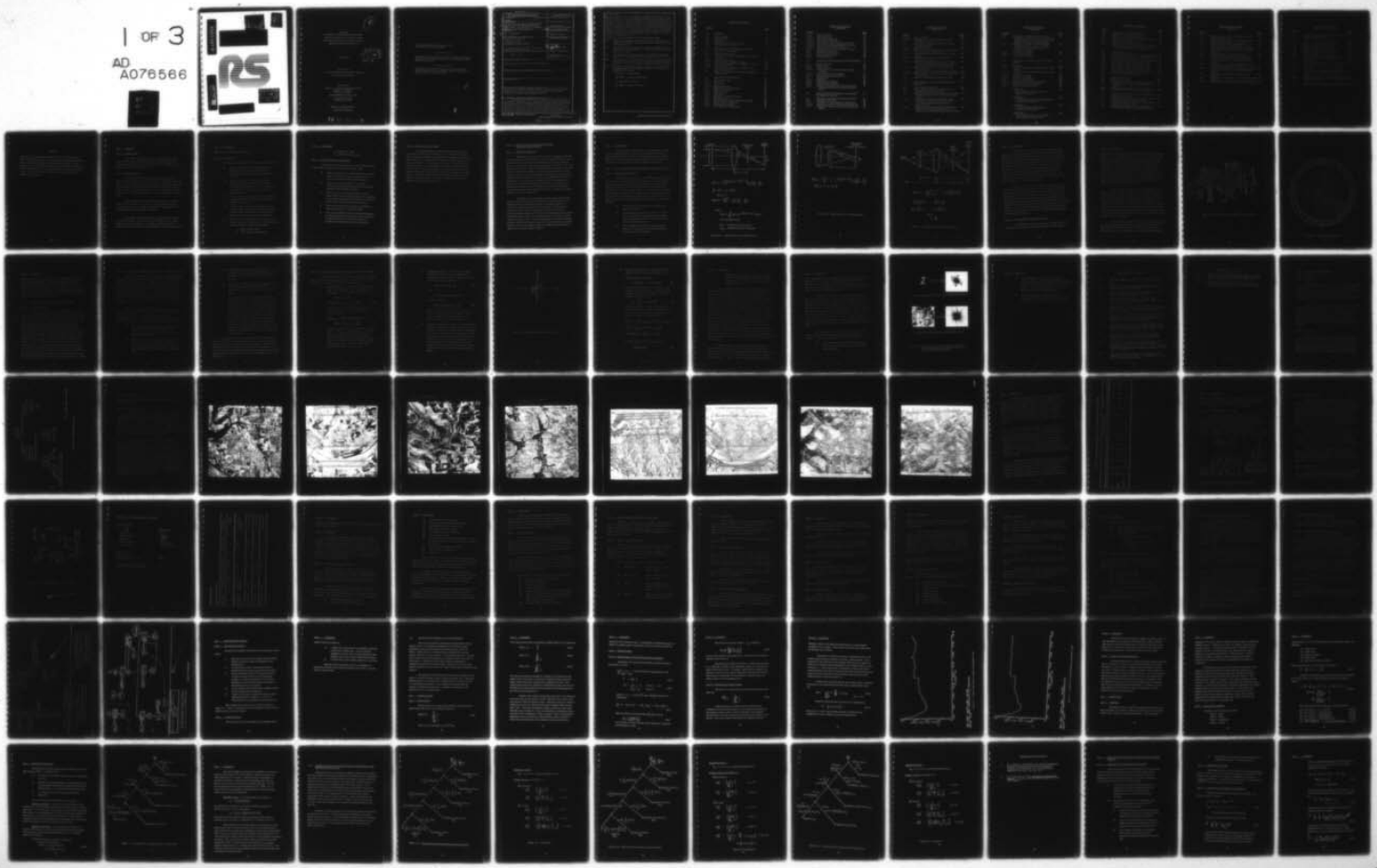

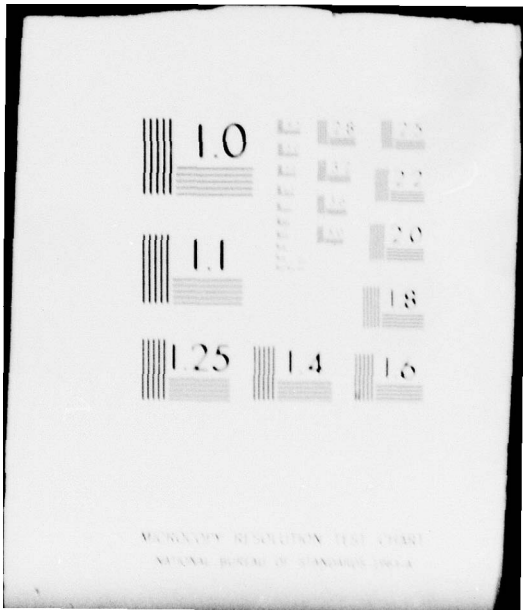
1.0
1.1
1.25
1.4
1.8
2.2
2.0
1.8

LEVEL II

4

Recognition Systems, Inc. | 5383 Cabrito Road | Van Nuys, California 91406 | (213) 785-2179

4

ETL-0186

Feasibility of Using Optical Power Spectrum Analysis Techniques for Automatic Feature Classification from High Resolution Thermal, Radar and Panchromatic Imagery

1 June 1979

Prepared for:

U.S. Army Engineer Topographic Laboratory
Fort Belvoir, VA 22060

Prepared by:

Harvey L. Kasdan, Principal Investigator
Thomas J. Middleton
Michael A. Snyder

RECOGNITION SYSTEMS, INC.

15531 Cabrito Road
Van Nuys, CA 91406

Approved for Public Release
Distribution Unlimited

Destroy this report when no longer needed.
Do not return it to the originator.

The findings in this report are not to be construed as an official Department of the Army position unless so designated by other authorized documents.

The citation in this report of trade names of commercially available products does not constitute official endorsement or approval of the use of such products.

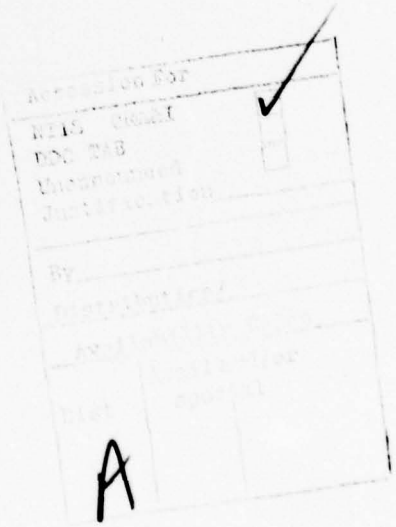

UNCLASSIFIED

SECURITY CLASSIFICATION OF THIS PAGE (When Data Entered)

(19) REPORT DOCUMENTATION PAGE	READ INSTRUCTIONS BEFORE COMPLETING FORM
1. REPORT NUMBER (18) ETL-0186	2. GOVT ACCESSION NO.
3. RECIPIENT'S CATALOG NUMBER	
4. TITLE (and Subtitle) (6) FEASIBILITY OF USING OPTICAL POWER SPECTRUM ANALYSIS TECHNIQUES FOR AUTOMATIC FEATURE CLASSIFICATION FROM HIGH RESOLUTION THERMAL, RADAR, AND PANCHROMATIC IMAGERY	5. TYPE OF REPORT & PERIOD COVERED Contract Report
	6. PERFORMING ORG. REPORT NUMBER (14) KS-77-370 / MS-79-404
7. AUTHOR(s) (10) Harvey L. Kasdan	8. CONTRACT OR GRANT NUMBER(s) (15) DAAK70-78-C-0019
9. PERFORMING ORGANIZATION NAME AND ADDRESS Recognition Systems, Inc. 15531 Cabrito Road Van Nuys, California 91406	10. PROGRAM ELEMENT, PROJECT, TASK AREA & WORK UNIT NUMBERS
11. CONTROLLING OFFICE NAME AND ADDRESS U.S. Army Engineer Topographic Laboratories Fort Belvoir, Virginia 22060	(11) 12. REPORT DATE 1 June 1979
	13. NUMBER OF PAGES 182
14. MONITORING AGENCY NAME & ADDRESS (if different from Controlling Office) (12) 194	15. SECURITY CLASS. (of this report) Unclassified
	15a. DECLASSIFICATION/DOWNGRADING SCHEDULE

16. DISTRIBUTION STATEMENT (of this Report)

Approved for public release; distribution unlimited.

17. DISTRIBUTION STATEMENT (of the abstract entered in Block 20, if different from Report)

18. SUPPLEMENTARY NOTES

19. KEY WORDS (Continue on reverse side if necessary and identify by block number)

Optical Power Spectrum Analysis, Terrain Classification, Panchromatic Imagery Processing, Radar Imagery Processing, Thermal Imagery Processing, Coherent Optics, Optical Processing

20. ABSTRACT (Continue on reverse side if necessary and identify by block number)

The objective of this study was to determine experimentally the feasibility of using optical power spectrum analysis techniques for automatic topographic feature classification from high resolution radar, panchromatic and thermal imagery. A data base of radar, panchromatic and thermal imagery was assembled. Radar and panchromatic imagery were available over the same geographical area with the same scale and perspective. An optical power spectrum data base of 6,216 individual aperture samples from

DD FORM 1 JAN 73 1473 EDITION OF 1 NOV 65 IS OBSOLETE

UNCLASSIFIED

SECURITY CLASSIFICATION OF THIS PAGE (When Data Entered)

390 603

20. (continued)

the three types of imagery was collected. Included in this data base were samples over the same area with different aperture sizes. Feature analysis and decision software required in addition to standard FACEL routines was developed. Using this software, features and a decision rule were developed for radar imagery that achieved 90% correct classification of four classes of terrain. A quantitative statistical analysis was performed to determine the effects of aperture and sensor type on the performance of the optical power spectrum based features. In addition, a qualitative analysis was performed in order to present examples that illustrate signature differences between radar and panchromatic imagery.

The following general conclusions were drawn from this study:

(1) There are statistically significant performance differences for optical power spectrum based algorithms for radar, panchromatic and thermal sensors.

(2) No statistically significant trend is evident associating better or worse performance as aperture size increases that is independent of the imagery type.

(3) For a given type of imagery, there is a statistically significant variation in decision performance that depends on aperture size.

(4) For the samples used in this study, the single best sensor is radar. It is presumed that this is because of the greater texture variations present in radar imagery compared to panchromatic or thermal.

(5) No single sensor performs best for all classes. The results ~~of this study would~~ lead to the following choices for the detection of particular terrain types:

a. Urban - panchromatic

b. Water - radar or panchromatic

c. Agriculture - radar

d. Forest - thermal or radar

TABLE OF CONTENTS

Section		Page
1.0	SUMMARY	1
1.1	Study Objective	1
1.2	Work Performed	1
1.3	Conclusions	2
1.4	Additional Studies Recommended	3
1.5	Organization of the Report	4
2.0	OPTICAL POWER SPECTRUM ANALYSIS - TECHNICAL BACKGROUND	5
2.1	Historical Development	
2.2	Generic Configurations for Optical Power Spectrum Analysis	6
2.2.1	Optical Configuration	6
2.2.2	Power Spectrum Sampling Techniques	10
2.3	Applications of Optical Power Spectrum Analysis	14
2.3.1	General Applications	14
2.3.2	Image Analysis Applications of Optical Power Spectrum Analysis	15
2.4	Optical Power Spectrum Properties Important for for this Study	17
3.0	EXPERIMENT DESCRIPTION	27
3.1	Experiment Design	27
3.1.1	Philosophy	27
3.1.2	Design Tree	27
3.1.3	Design Discussion	29
3.2	RHDAS Data Collection System	40
3.2.1	Optical Components	41
3.2.2	Film Transport	41
3.2.3	Electronics	45
3.2.4	Controller and Control Software	45
3.3	Analysis Software	47
3.3.1	Data Acquisition Software (HDAS29, BASICT)	48
3.3.2	Plotting Software (PRPLOT)	48
3.3.3	Listing Software (LIST)	49
3.3.4	File Editing and Classification	49

TABLE OF CONTENTS
(continued)

Section		Page
3.3.5	File Partitioning	50
3.3.6	Clue Processing	50
3.3.6.1	Clue Executive (KLUE)	51
3.3.6.2	Normalization (KLUE01)	52
3.3.6.3	Generation of Vector Statistics (KLUE02)	53
3.3.6.4	Threshold Classification (KLUE03, KLUE04)	54
3.3.6.5	Top of Form Generation (KLUE05)	55
3.3.7	Overlay Grid Generation (CIRGN, DECPLT)	55
3.3.8	Operations Flowcharts	55
3.4	Data Collection Procedure	58
3.4.1	Pan and Radar Imagery	58
3.4.2	Thermal Imagery	58
4.0	FEATURE AND DECISION RULE DEVELOPMENT	60
4.1	Feature Analysis	60
4.1.1	Ring Features	60
4.1.2	Wedge Features	62
4.1.2.1	Panchromatic and Thermal Imagery Wedge Features	62
4.1.2.2	Radar Imagery Wedge Features	63
4.1.3	Feature Evaluation Methodology	67
4.2	Decision Rule	67
4.2.1	Motivation	67
4.2.2	Decision Rule Definition	68
4.2.3	Decision Rule Properties	70
4.2.4	Specific Realizations of the Decision Rule for Panchromatic, Radar and Thermal Imagery Cases	73
5.0	QUANTITATIVE STATISTICAL EVALUATION OF DECISION RESULTS	81
5.1	Statistical Formulation of the Study Questions	81
5.2	Statistical Framework	82
5.2.1	Chi Square Test for Multinomial Equivalence	82
5.2.1.2	Applications of the Chi Square Multinomial Test	84
5.2.2	Analysis of Variance for the Linear Hypothesis Model	84

TABLE OF CONTENTS
(continued)

Section		Page
5.2.2.1	Test Description	84
5.2.2.2	Applications of the Linear Hypothesis Model Analysis of Variance	87
5.3	Discussion of Results - Statistical Answers to the Study Questions	88
5.3.1	Confusion Matrices	88
5.3.2	Comparison of Panchromatic, Radar and Thermal Imagery Decision Performance	97
5.3.3	Detailed Comparison of Panchromatic and Radar Imagery	100
5.3.3.1	Application of the Linear Hypothesis Model Analysis of Variance	100
5.3.3.2	Statistically Significant Differences Between Pan and Radar Independent of Aperture Size and of Aperture Size Independent of Pan or Radar	103
5.3.4	Effect of Aperture Size for Panchromatic and Radar Imagery	104
5.3.4.1	Application of the χ^2 Test for Multinomial Equality	104
5.3.4.2	Statistically Significant Differences Depending on Aperture Size	105
5.4	Summary of Statistically Significant Results	108
6.0	COMPARISON OF RESULTS FOR INDIVIDUAL SAMPLES	114
6.1	Urban Sample Comparison	115
6.2	Representative Samples Comparing Water 50 Panchromatic and Radar Results	116
6.3	Comparison of Results for Forest Using Diffraction Pattern Samples from Radar and Panchromatic Imagery	120
6.4	Comparison of Non-Plowed Agriculture (70) Performance Utilizing OPS Samples Derived from Radar and Panchromatic Imagery (2mm aperture)	128
6.5	Comparison of Plowed Agriculture (20) Decision Performance Utilizing OPS Samples from Radar and Panchromatic Imagery (2mm aperture)	128

TABLE OF CONTENTS
(continued)

Section		Page
6.6	Comparison of Results for Water (60) and Agriculture Utilizing Optical Power Spectrum Measurements from Radar and Panchromatic Imagery with a 2mm Sampling Aperture	132
6.7	Qualitative Examination of the Results for Water (60) When 2, 4 and 6mm Aperture Samples are Taken from Radar and Panchromatic Imagery	139
6.7.1	2mm Aperture Results	142
6.7.2	4mm Aperture Results	142
6.7.3	6mm Aperture Results	
7.0	CONCLUSIONS AND SUGGESTED FURTHER STUDY	146
7.1	Conclusions	146
7.1.1	Overall Performance for Different Sensor Types Differ	146
7.1.2	Certain Sensors are Better for Specific Terrain Types	146
7.1.3	Aperture Size Effect	149
7.1.4	Conclusion Generality	149
7.2	Areas for Further Study	150
7.2.1	Expanded and Generalized Experiment	150
7.2.2	Terrain Boundary Determination	150
7.2.3	Decision Rule Improvement	151
	APPENDIX 1 Linear Hypothesis Model Analysis of Variance Test Results	153
	APPENDIX 2 χ^2 Test Results for Panchromatic Aperture Performance Comparison	160
	APPENDIX 3 χ^2 Test Results for Radar Aperture Performance Comparison	166
	APPENDIX 4 Class Statistics Plots - 2mm Aperture Panchromatic and Radar Cases	170

LIST OF ILLUSTRATIONS

Figure		Page
2-1a	Object before lens in collimated beam	7
2-1b	Object after lens in converging beam	8
2-1c	Object before lens in diverging beam	9
2-2	Lendaris and Stanley Diffraction Pattern Sampler	12
2-3	WRD 6400 Photodetector	13
2-4	Conjugate Points in the Fourier Plane	19
2-5	Objects and their diffraction patterns illustrating the relationship between lines, circles, gratings and corresponding diffraction patterns	23
3-1	Experiment Design Tree	
3-2a	Panchromatic Imagery Frame 1 with Sampling Grid	30
3-2b	Panchromatic Imagery Frame 2 with Sampling Grid	31
3-2c	Panchromatic Imagery Frame 3 with Sampling Grid	32
3-2d	Panchromatic Imagery Frame 4 with Sampling Grid	33
3-2e	Radar Imagery Frame 1 with Sampling Grid	34
3-2f	Radar Imagery Frame 2 with Sampling Grid	35
3-2g	Radar Imagery Frame 3 with Sampling Grid	36
3-2h	Radar Imagery Frame 4 with Sampling Grid	37
3-3	Block Diagram of RHDAS OPS Sampling System	40
3-4	ROSA Optical Configuration Used for Study	42
3-5	ETL Non-Visual Support Software	56
4-1	Typical Urban Sample	65
4-2	Typical Forest Sample	66
4-3	Hierarchical Tree Representation of Decision Rule	71
4-4a	Decision Rule and Features for Panchromatic Imagery	74
4-4b	Decision Rule and Features for Radar Imagery	76
4-4c	Decision Rule and Features for Thermal Imagery	78
6-1	Comparison of Urban Areas in Panchromatic and Radar Imagery - 2mm	117
6-2	Comparison of Features for Urban Samples Derived from Panchromatic and Radar Imagery	118
6-3	Comparison of Water (50) Areas in Panchromatic and Radar Imagery - 2mm	121
6-4	Comparison of Features for Water (50) Samples Derived from Panchromatic and Radar Imagery	122

LIST OF ILLUSTRATIONS
(continued)

Figure		Page
6-5	Comparison of Forest Areas in Panchromatic and Radar Imagery - 2mm	125
6-6	Comparison of Features for Forest Samples Derived from Panchromatic and Radar Imagery	126
6-7	Comparison of Non-Plowed Agriculture (70) Areas in Panchromatic and Radar Imagery - 2mm	129
6-8	Comparison of Features for Non-Plowed Agriculture Samples Derived from Panchromatic and Radar Imagery	130
6-9	Comparison of Plowed Agriculture (20) Areas in Panchromatic and Radar Imagery - 2mm	133
6-10	Comparison of Features for Plowed Agriculture Samples Derived from Panchromatic and Radar Imagery	134
6-11	Comparison of Water (60) and Agriculture Areas in Panchromatic and Radar Imagery - 2mm	136
6-12	Comparison of Features for Water (60) and Agriculture Samples Derived from Panchromatic and Radar Imagery	137
6-13	Comparison of Water (60) Areas in 4mm Radar Imagery	140
6-14	Comparison of Water (60) Areas in 4mm Panchromatic Imagery	141
6-15	Radar Imagery Wedge Clue Comparison for Water (60)	143

LIST OF ILLUSTRATIONS

Table		Page
3-1	Training Set and Validation Samples Breakdown for Each Aperture Size	39
3-2	ROSA Beam and Lens Parameters	43
5-1	Confusion Matrix 1mm Pan Hardclipped	89
5-2	Confusion Matrix 2mm Pan Gaussian	90
5-3	Confusion Matrix 4mm Pan Gaussian	91
5-4	Confusion Matrix 6mm Pan Gaussian	92
5-5	Confusion Matrix 2mm Radar Gaussian	93
5-6	Confusion Matrix 4mm Radar Gaussian	94
5-7	Confusion Matrix 6mm Radar Gaussian	95
5-8	Confusion Matrix 10mm Thermal Gaussian	96
5-9	Pan/Radar/Thermal Decision Performance Comparison	99
5-10	Linear Hypothesis Model Analysis of Variance for All Class Performance	101
5-11	Linear Hypothesis Model Analysis of Variance Summary	102
5-12	X^2 Test Comparing Panchromatic 1mm Hard-clipped Aperture Results to 2mm Gaussian Results	106
5-13	Aperture Comparison - X^2 Test Results Summary	107
5-14	Aperture Performance Comparison Summary for Panchromatic Imagery	109
7-1	Sensor Percent Correct Performance Comparison	148

Preface

This study was performed by Recognition Systems for the Geographic Sciences Laboratory of the U. S. Army Engineer Topographic Laboratories to investigate the feasibility of using optical power spectrum analysis techniques for automatic topographic feature classification under Contract No. DAAK70-78-C-0019. The contract duration was 31 January 1978 to 1 June 1979. D. Craig Baker was the USAETL Contracting Officer's Technical Representative.

1.0 SUMMARY

1.1 Study Objective

The objective of this study was to determine experimentally the feasibility of using optical power spectrum analysis techniques for automatic topographic feature classification from high resolution radar, panchromatic and thermal imagery.

1.2 Work Performed

In conjunction with ETL personnel, a data base of radar, panchromatic and thermal imagery was assembled. Radar and panchromatic imagery were available over the same geographical area with the same scale and perspective. An optical power spectrum data base of 6,216 individual aperture samples from the three types of imagery was collected. Included in this data base were samples over the same area with different aperture sizes.

Feature analysis and decision software required in addition to standard FACEL routines was developed. Using this software, features and a decision rule were developed for radar imagery that achieved 90% correct classification of four classes of terrain.

A quantitative statistical analysis was performed to determine the effects of aperture and sensor type on the performance of the optical power spectrum based features. In addition, a qualitative analysis was performed in order to present examples that illustrate signature differences

1.2 --Continued.

between radar and panchromatic imagery.

1.3 Conclusions

The following general conclusions were drawn from this study:

1) There are statistically significant performance differences for optical power spectrum based algorithms for radar, panchromatic and thermal sensors.

2) There is no universal statistically significant aperture size effect. In other words, no trend is evident associating better or worse performance as aperture size increases that is independent of the imagery type.

3) For a given type of imagery, there is a statistically significant variation in decision performance that depends on aperture size.

4) For the samples used in this study, the single best sensor is radar. It is presumed that this is because of the greater texture variations present in radar imagery compared to panchromatic or thermal.

5) No single sensor performs best for all classes. The results of this study would lead to the following choices for the detection of particular terrain types:

   a. urban - panchromatic
   b. water - radar or panchromatic

1.3 --Continued.

c. agriculture - radar

d. forest - thermal or radar

1.4 Additional Studies Recommended

The following are recommended areas where additional effort would extend or improve the results obtained in this study:

1) Utilize similar features and decision rules on a larger data set representing more geographical areas to extend the statistical validity of these results.

2) Improve the decision algorithm and study the relationship of the present algorithm to the previously developed FACEL MISTIC algorithm.

3) Obtain a data base containing thermal, radar and panchromatic imagery of identical scale and perspective over a single geographical area to obtain a more precise performance comparison for the three sensors.

4) Formalize the approaches to boundary definition that appear promising as a result of this study.

5) Use boundary definition or other appropriate techniques to implement contextual processing in order to improve decision making in areas where local texture is insufficient to differentiate between terrain types.

1.5 Organization of the Report

It is intended that this report be self contained to the extent reasonable. Therefore, the report begins with a discussion of optical power spectrum sampling history, techniques and equipment in Section 2. This is followed by a discussion of the experiment design, equipment and software in Section 3. A description of the features and decision rule is found in Section 4. A detailed discussion of the statistical procedures used to analyze the effects of aperture and imagery type is presented in Section 5 along with the quantitative results that were obtained. Section 6 contains a qualitative discussion of specific sample OPS signatures that illustrate differences due to sensor type. Conclusions and areas for further study are discussed in Section 7.

2.0 OPTICAL POWER SPECTRUM ANALYSIS - TECHNICAL BACKGROUND

2.1 Historical Development

Diffraction phenomena have been observed since the early days of the development of optical science. Huygens observed[1] that if a screen was placed to intercept a portion of a light beam, then at some distance beyond the screen, light was visible as expected on the side of the beam not obscured by the screen. But, in addition, light was also visible on the side of the beam blocked by the screen. This observation by Huygens and his use of the secondary wavefront construction to predict the wavefront at an arbitrary distance beyond the screen are early formulations of the theory of diffraction. As the theory of electromagnetic wave propagation, in particular, the propagation of optical disturbances was developed. The superposition principle embodied in Huygens' principle was developed more formally as the Fresnel-Kirchhoff integral as a result of the suitable application of Green's theorem.[2]

Regardless of the historical and mathematical development leading to the result, it became apparent that the relationship between a diffraction pattern and the object causing the diffraction pattern was a two-dimensional Fourier transform relationship. Until low power helium neon lasers became available toward the end of the 1960's, forming diffraction patterns that could be easily photographed or measured was difficult because non-laser monochromatic sources could not easily supply the requisite power. Once the capability to generate the diffraction patterns associated with scenes imaged on transparencies became readily available, many workers began to experiment with diffraction pattern or optical power spectrum analysis systems.

2.1 --Continued.

In the remainder of this section, we shall briefly review the general optical configuration used to develop a diffraction pattern, the type of equipment that is available to sample diffraction pattern data at high speed, some references to general applications of the technique and a summary of the important work that is applicable to the study.

2.2 Generic Configurations for Optical Power Spectrum Analysis

2.2.1 Optical Configuration[3]

The Abbe Theory of Image Formation[1] implies that whenever a point source is imaged to a point source the image plane will contain the diffraction pattern of a transmission object placed anywhere in the path between the object and image point sources. Specifically, three situations are possible as shown in Figure 2-1. The transmission object may be placed after the lens or before the lens in a diverging beam or, if the point source is at infinity, in a collimated beam. In general, it is better to have the transmission object in the converging beam for several reasons:

1) The lens pupil does not limit the rays diffracted toward the detector.

2) The aberration requirements on the lens are much less severe since the incident illumination will be either a collimated beam or a diverging beam with a known spherical wavefront.

3) The possibility of ghost images at the detector is minimized because there is not a direct path from the lens surface to the detector.

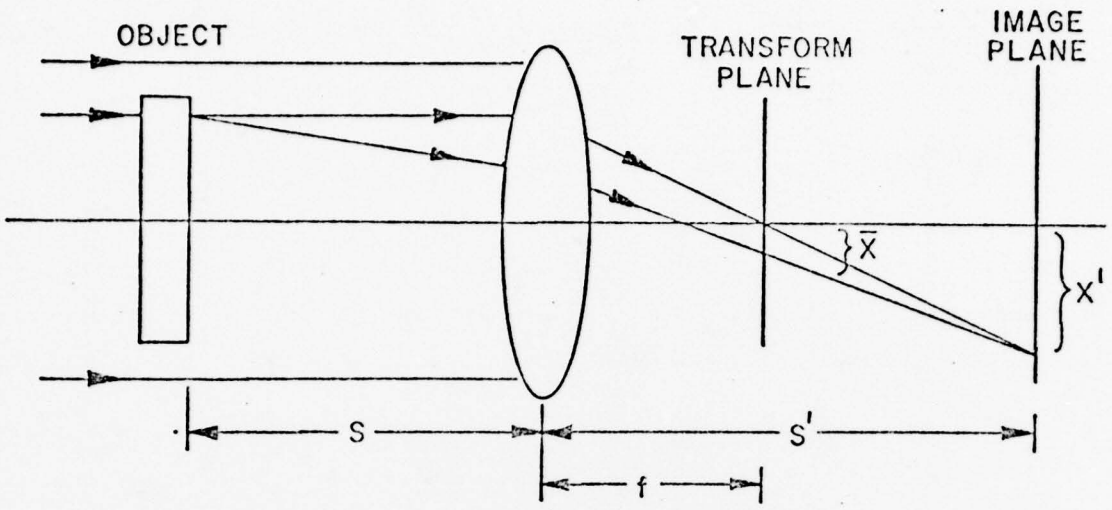

$$\tilde{E}(\bar{x},\bar{y},f) = \frac{je^{-jk(S+f)}}{\lambda f} e^{(jk/(S'-f))(\bar{x}^2+\bar{y}^2)} E_0 \hat{\tau}_0\left(\frac{-\bar{x}}{\lambda f}, \frac{-\bar{y}}{\lambda f}\right)$$

$$\left[f_x = \bar{x}/\lambda f \ , \ f_y = \bar{y}/\lambda f\right]$$

When S = f

$$\tilde{E}(\bar{x},\bar{y},f) = \frac{je^{-jk2f}}{\lambda f} E_0 \hat{\tau}_0\left(\frac{-\bar{x}}{\lambda f}, \frac{-\bar{y}}{\lambda f}\right)$$

where,

$$\hat{\tau}(u,v) = \iint_{-\infty}^{\infty} \tau(x',y')\, e^{-2\pi j(ux'+vy')}\, dx'\, dy'$$

f = focal length of lens

$\bar{x},\bar{y}$ = position in transform plane

f_x, f_y = spatial frequencies coordinates

Figure 2-1A. Object before lens in collimated beam.

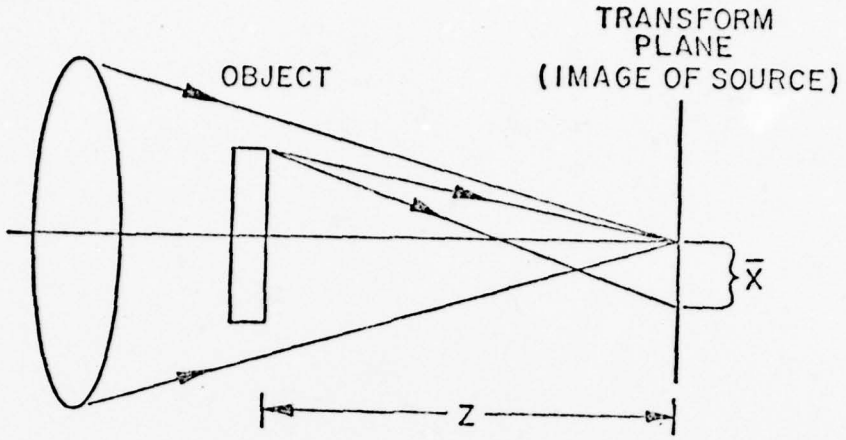

$$\tilde{E}(\bar{x}, \bar{y}, z) = \frac{je^{-jkz}}{\lambda z} \quad \frac{f}{z} \quad e \left[j \frac{k}{2z} (\bar{x}^2 + \bar{y}^2) \right] E_0 \hat{\tau}_0 \left(\frac{\bar{x}}{\lambda z}, \frac{\bar{y}}{\lambda z} \right)$$

$$\left[f_x = \bar{x}/\lambda z \, , \quad f_y = \bar{y}/\lambda z \right]$$

Figure 2-1B. Object after lens in converging beam.

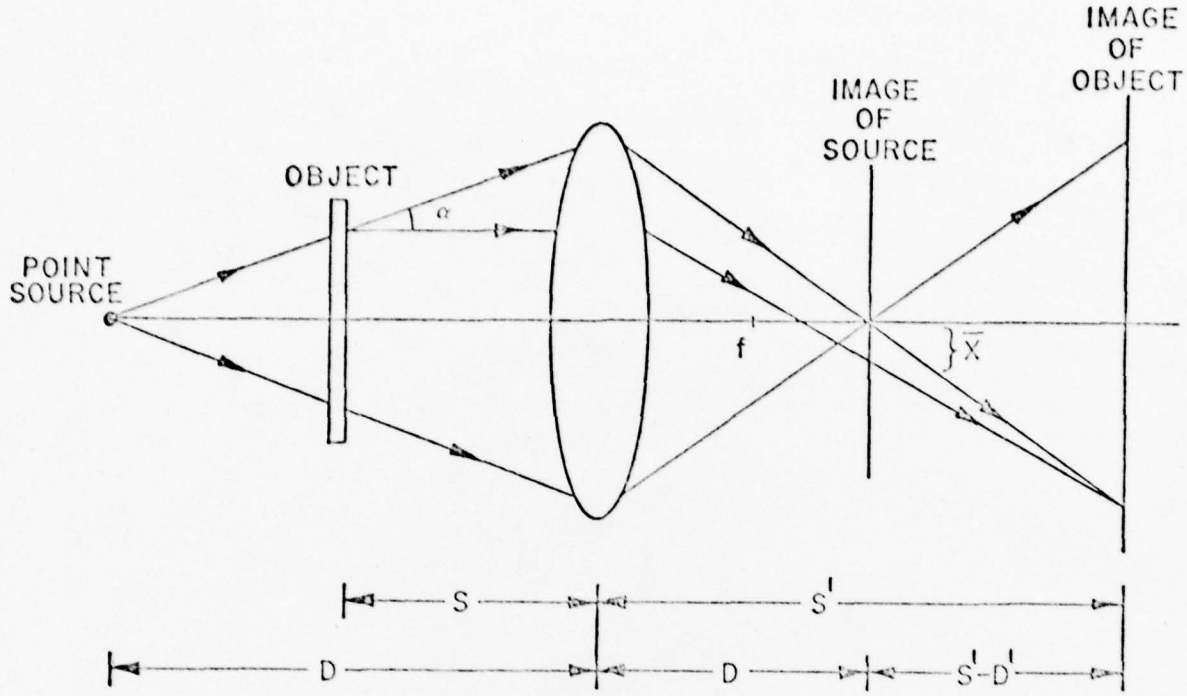

$$\tilde{E}(\bar{x}, \bar{y}, D') = \frac{-jm}{\lambda(S' - D')} e^{-jk(S + D')} \quad E_0 \exp\left[\frac{jk(\bar{x}^2 + \bar{y}^2)}{2(S' - D')}\right]$$

$$\hat{\tau}_0 \left[\frac{m\bar{x}}{\lambda(S'-D')} \quad , \quad \frac{m\bar{y}}{\lambda(S' - D')}\right]$$

$$\left[f_x = \frac{m\bar{x}}{\lambda(S'-D')} \quad , \quad f_y = \frac{m\bar{y}}{\lambda(S'-D')}\right]$$

where,

$$m = \frac{-S'}{S}$$

Figure 2-1C. Object before lens in diverging beam.

2.2.1 --Continued.

The only situation in which it may be desirable to have the transmission object before the lens is when the incident illumination is collimated. In this case, with the transmission object in the collimated beam, the position of the object relative to the lens or the detector does not affect the magnification of the diffraction pattern. Furthermore, if the object is placed in the back focal plane of the lens the quadratic phase factor in the expression for the diffraction pattern disappears. Thus, an exact Fourier transform relationship holds between the transmission object and the amplitude pattern in the diffraction plane. Of course, in general, it is the intensity pattern that is sampled so that the phase factor is of no practical importance.

Finally, we make one additional observation concerning the general diffraction pattern optical configuration. Note that although the development has been for transmissive and refractive optical elements, the analysis holds for reflective elements as well. Thus, in general, any optical element in the path between the point source object and its image will contribute to the disturbance in the diffraction plane. Therefore, all elements in the optical path of a diffraction pattern analysis system are critical. Limiting pupils within the system may minimize high spatial frequency scatter from surfaces far from the detector but each situation must be carefully analyzed.

2.2.2 Power Spectrum Sampling Techniques

To this point we have not addressed the problem of how one is to measure the diffraction plane intensity pattern. Early workers

photographed the intensity pattern in the diffraction plane and attempted to analyze these photographs. In many cases this approach is not viable because of the wide dynamic range of the intensity pattern as a function of position in the diffraction plane. The limited dynamic range of film does not allow a single exposure to adequately represent the entire range of intensity in the diffraction plane. Thus one is confronted with a situation in which an exposure designed to allow low intensity values to be visible causes high intensity regions to saturate the film. If the exposure is set so that high intensity regions do not saturate the film, low intensity regions do not expose the film. Clearly, some wide dynamic range readout mechanism is required.

One of the earliest systems developed specifically to sample and record diffraction patterns as well as perform pattern recognition studies on sampled diffraction patterns was developed by Lendaris and Stanley.[4] The optical portion of their system is pictured in Figure 2-2. By utilizing a wide selection of mechanical apertures and physically moving the input transparency, they were able to realize the wide variety of diffraction pattern sampling geometries and configurations. Although extremely general, and suited for laboratory experimentation, this system was limited by its inherent mechanical nature insofar as diffraction pattern acquisition speed was concerned.

To overcome the limitations of this type of mechanical approach, the solid state photodetector pictured in Figure 2-3 was developed by Recognition Systems specifically to allow high speed acquisition of diffraction pattern data. This detector has subsequently been interfaced

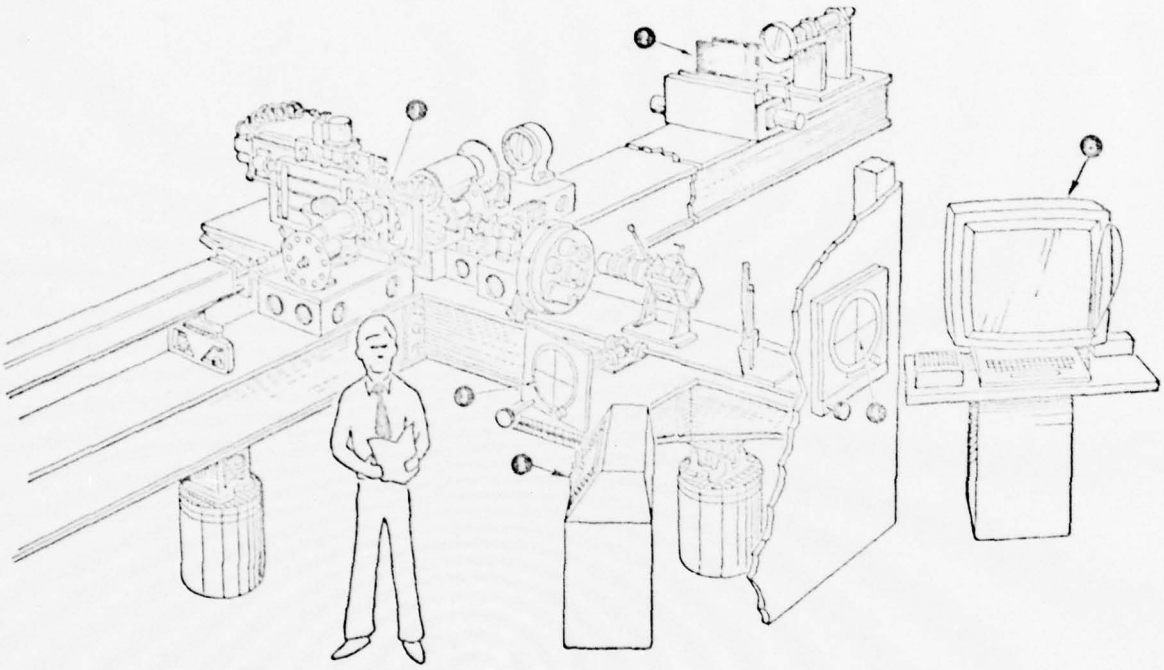

Figure 2-2. Lendaris and Stanley Diffraction Pattern Sampler

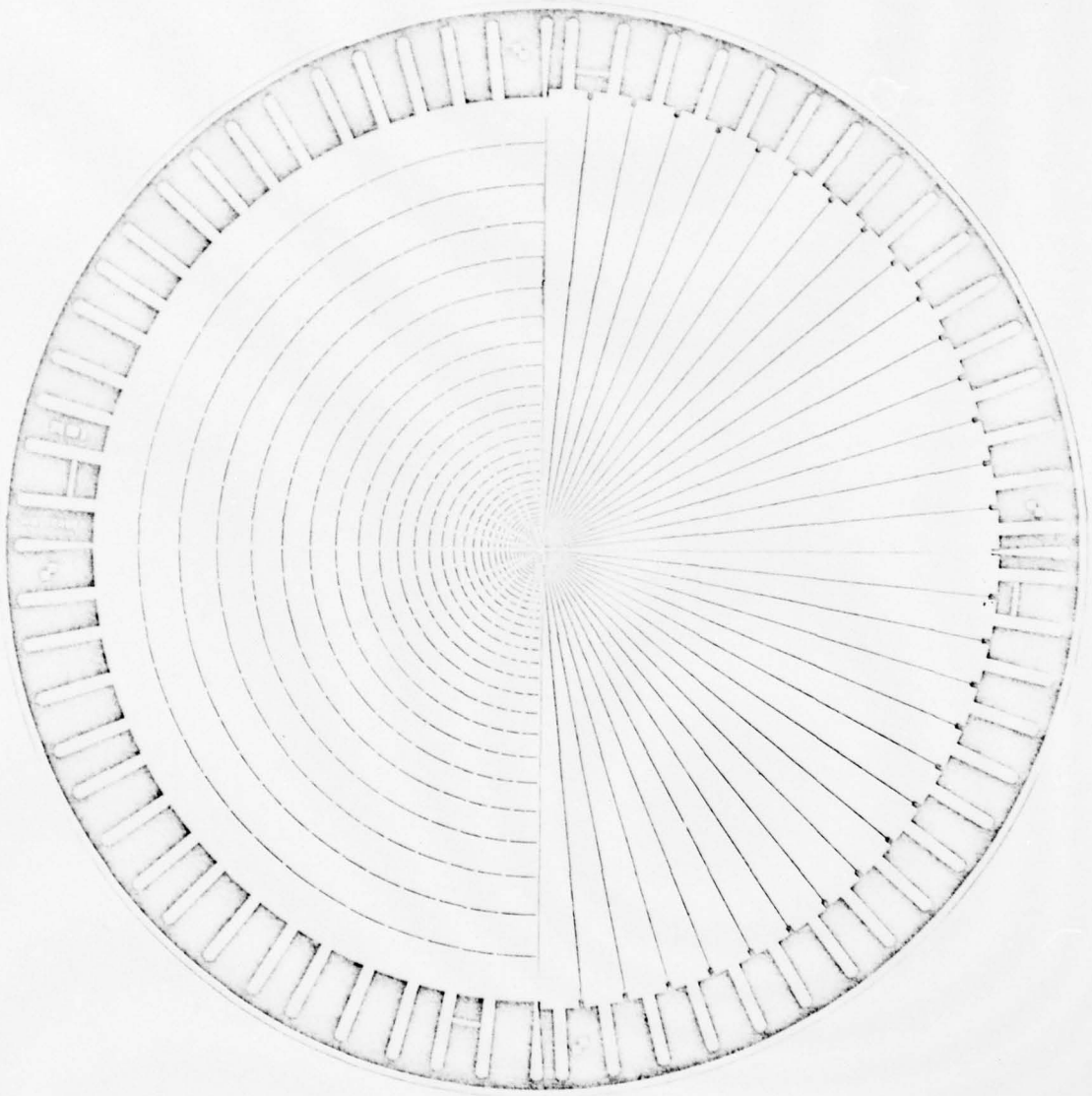

Figure 2-3. WRD 6400 Photodetector

2.2.2 --Continued.

to a wide variety of high speed analog signal conditioning and analog to digital conversion circuitry. This has enabled the development of a number of optical power spectrum analysis systems for automatic inspection of industrial production and automatic imagery analysis. The earliest of these systems, ROSA (Recording Optical Spectrum Analyzer), has been in use at ETL since 1972. A system similar to the ETL ROSA was used to acquire the data for this study.

2.3 Applications of Optical Power Spectrum Analysis

2.3.1 General Applications

Since the work of Lendaris and Stanley[4] in the late 60's, optical power spectrum analysis and related scattering analysis have been applied to a wide variety of pattern recognition, automatic inspection and imagery analysis problems. Applications to transparency analysis have included pneumoconiosis (black lung disease) detection from x-ray radiographs[5], determination of the type of dystrophy disease from muscle biopsy photomicrographs[6], analysis of pap smear material from photomicrographs of slides and real time spatial light modulator images of smear material.[7] Direct analysis of the scattered illumination from biological cells has been used to determine cell type distributions and cell characteristics.[8] Scatter from large numbers of particles has been used to determine cell size distributions both in terms of dimension and weight.[9] Reflected scatter from paper and machine surfaces has been used to determine paper quality and machine surface finish.[10] Aside from these non-imagery based applications, substantial number of image analysis applications (both classified and unclassified) have been developed.

2.3.2 Image Analysis Applications of Optical Power Spectrum Analysis

The original work of Lendaris and Stanley is directly applicable to the problem being considered in this study. In the Goleta Valley study described in their paper, Lendaris and Stanley utilized diffraction pattern information to distinguish between man-made and non-man-made areas in the Goleta Valley in Southern California. The features which they found most useful to effect the discrimination were ring features that measured the non-airy disc intensity roll-off and wedge features that measured the non-uniformity of the energy distribution on the wedges. Utilizing these features they were able to correctly identify 94% of the sample in a set of 275 samples.

Subsequent work by Lukes[11] demonstrated the capability of optical power spectrum analysis for cloud screening applications and the form of diffraction pattern signatures for various terrain types. In general, the work of Lendaris and Stanley and Lukes suggests the following general attributes associated with terrain diffraction pattern signatures:

1) Man-made objects typically have many straight line structures resulting in diffraction pattern energy that is distributed in preferred rectangular orientations within the diffraction plane.

2) Often man-made objects such as city streets or plowed fields appear as gratings that cause the diffracted energy at a particular angular orientation to break up into a dot pattern similar to that caused by a diffraction grating.

3) Natural objects tend to have a uniform angular distribution of energy. (One exception to this general perception cited by Lukes[11] is the case of ocean waves.)

4) The spatial frequency content of natural objects tends to be concentrated at lower frequencies than the spatial frequency content associated with man-made objects.

5) Generally lines and edges associated with buildings, roads and other man-made structures tend to be sharp relative to the transmission changes normally found in nature so that as a result higher spatial frequencies are more prevalent in man-made objects compared to natural objects. There are of course some exceptions. For example, mountain regions with an illumination angle such that crags and crevices are in sharp relief compared to the other mountain areas will typically have high spatial frequency content associated with them. However there is generally no preferred orientation so that the angular distribution of energy even in this case is quite uniform.

To summarize, various terrain types are characterized both by the spatial frequency distribution of energy and the spatial orientation of diffracted energy. Preferred orientation distributions and distributions with relatively high spatial frequency content are characteristic of man-made objects. More generally, highly textured scenes will have high spatial frequency content compared to scenes that one would identify as having very little texture.

2.4 Optical Power Spectrum Properties Important for this Study

The major properties of optical power spectrum are essentially those of two-dimensional Fourier transforms described by Lendaris and Stanley[4] and Kasdan.[12] Specifically the properties are:

1) Spatial Invariance - If $t(x,y)$ represents the spatial transmission at the object plane and $\mathbb{F}\{t(x,y)\} = T(f_x, f_y)$ the Fourier transform of this function, then

$$\mathbb{F}\{t(x-x_o,\ y-y_o)\} =$$

$$\mathbb{F}\{t(x,y)\} \exp(-2\pi i (f_x x_o + f_y y_o)). \qquad (1)$$

where f_x, f_y are the spatial frequency coordinates. From Eq. (1) we see that the magnitude of the transform given by

$$\left|\mathbb{F}\{t(x-x_o,\ y-y_o)\}\right| = \left|\mathbb{F}\{t(x,y)\}\right| \cdot \left|\exp(-2\pi i (f_x x_o + f_y y_o))\right| \qquad (2)$$

is unchanged regardless of the position of the object determined by x_o, y_o. (This of course assumes that that as a result of the translation all of $t(x,y)$ is still within the entrance pupil of the transform lens.) Thus we have the very important result that regardless of the position of the object in the entrance pupil, the diffraction pattern remains constant.

2) Conjugate Symmetry - Assuming that the spatial transmission at the object plane, $t(x,y)$ is a real function of x, y (which will be true if $t(x,y)$ represents a transparency for example) then

$$T(f_x, f_y) = T^*(-f_x, -f_y) \tag{3}$$

where

T^* is the complex conjugate of T.

From Eq. (3) we have

$$\left| T(f_x, f_y) \right| = \left| T(-f_x, -f_y) \right| \tag{4}$$

In other words, the light intensity at a point P is the same as the intensity at the conjugate P* found at the same radius as P but 180 degrees away in the Fourier plane as illustrated in Figure 2-4.

3) Preservation of Rotation - We have seen that translation of the object affects only the phase of the Fourier transformation. Rotation of the object about the optical axis, the center of spatial coordinates, causes the transform or diffraction pattern to be rotated about its center of spatial frequency coordinates (also the optical axis in this case) by the same angular displacement as the object. Thus rotation of the object is preserved in the transformation by an equal rotation of the diffraction pattern.

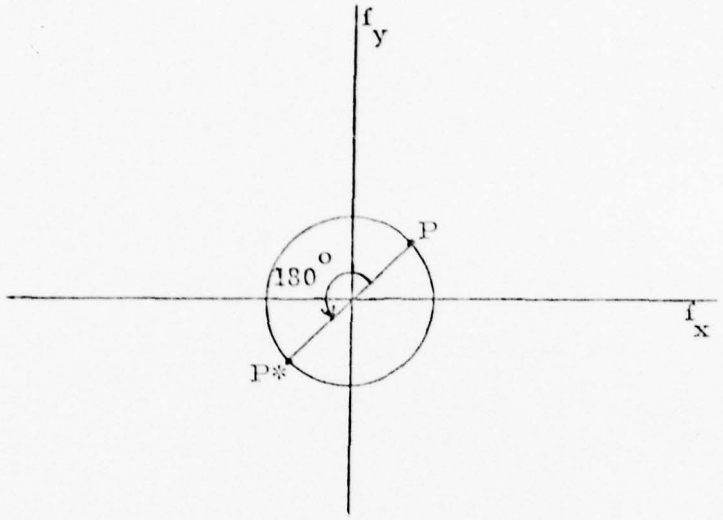

Figure 2-4. Conjugate Points in the Fourier Plane

4) Linearity or Additivity - The well known linearity property of the Fourier transformation given by

$$\mathbb{F}\left\{a_1\, t_1(x,y) + a_2\, t_2(x,y)\right\} =$$

$$a_1\left\{t_1(x,y)\right\} + a_2\ \mathbb{F}\left\{t_2\ (x,y)\right\} \tag{5}$$

has interesting consequences when determining the intensity in the Fourier plane. Using Equations (1) and (5) we have that the magnitude of n objects in the entrance pupil is given by

$$M_n = \left| \sum_{j=1}^{n} \mathbb{F}\left\{t_j(x,y)\right\} \right| \tag{6}$$

Assuming that all these objects have identical transmission functions t (x, y), and random spatial location in the object plane, the expected value of the intensity in the Fourier plane is given by

$$E\, M_n^2 = E \sum_{j=1}^{n} T(f_x, f_y) \exp\left(-2\pi i\,(f_x x_j + f_y y_j)\right)$$

$$\cdot \sum_{k=1}^{n} T^*(f_x, f_y) \exp\left(2\pi i\,(f_x x_k + f_y y_k)\right)$$

$$= n\left|T(f_x,f_y)\right|^2 + \sum\sum_{j \neq k} \left|T(f_x, f_y)\right| \cdot$$

$$E \exp\left(2\pi i\,(f_x\,|x_k - x_j| + f_y\,|y_k - y_j|\right)$$

$$= n\left|T(f_x, f_y)\right|^2 \tag{7}$$

2.4 --continued.

Thus, for the case of incoherent addition of identical diffractors, the diffraction pattern intensity of the composite is n times the intensity of the individual diffraction pattern.

In addition to these properties it is important to recognize that the diffraction pattern of an area on an aerial photograph limited by a finite aperture is a function of the aperture size. Precisely, the diffraction pattern of the aperture image area is the convolution of the unapertured image diffraction pattern with the aperture diffraction pattern. Thus, we see that the effect of a very small aperture (which has a diffraction pattern that is large in extent) is in fact to blur the sampling of the input diffraction pattern. On the other hand, a very large aperture (whose diffraction pattern approaches that of an impulse) will result in a faithful reproduction of the input diffraction pattern. Thus we are faced with a situation that is mathematically equivalent to the Heisenberg Uncertainty Principle. Namely, we cannot simultaneously isolate an arbitrarily small region in the input plane and measure the diffraction pattern due to this input with as perfect fidelity as we wish. This is due to the Fourier transform relationship that exists between the input plane and the diffraction plane. Precisely the same relationship exists between a particle's position and momentum if the particle satisfies the Schroedinger Wave Equation.

Within an aperture, however, the linearity and conjugate symmetry properties are still valid. Thus, an aperture that includes multiple terrain types will have a diffraction pattern signature that in many cases closely approximates a linear combination of the intensity patterns of the individual terrain types. Since the resulting diffraction pattern is

a linear combination, it is not possible to determine where within the aperture boundaries exist nor in fact the constituents of the linear combination. The conjugate symmetry property implies that a wedge ring detector geometry is sufficient to analyze both the radial distribution of energy and angular distribution of energy.

One final comment concerning the position of objects within the aperture. For objects that are small compared to the aperture size, property 1 is a good approximation to the actual situation. Thus, the position of the object within the aperture does not significantly affect the diffraction pattern. On the other hand for objects that are large compared to the aperture, the position of the object within the aperture clearly will affect diffraction pattern. As an example consider an opaque line within an aperture of approximately the same dimension. Depending upon the location of the line within the aperture we have the diffraction pattern of either a single slit or a double slit. These diffraction patterns are quite different.

To summarize the discussion in this section, consider the spatial objects and corresponding diffraction patterns pictured in Figure 2-5. These patterns illustrate the following principles:

1) The diffraction pattern corresponding to a line is also a line oriented at 90^{o} with respect to the line in the input plane.

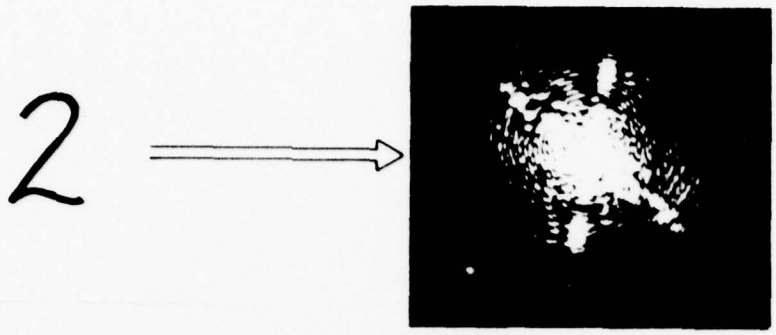

a) Handwritten Numeral and Corresponding Diffraction Pattern

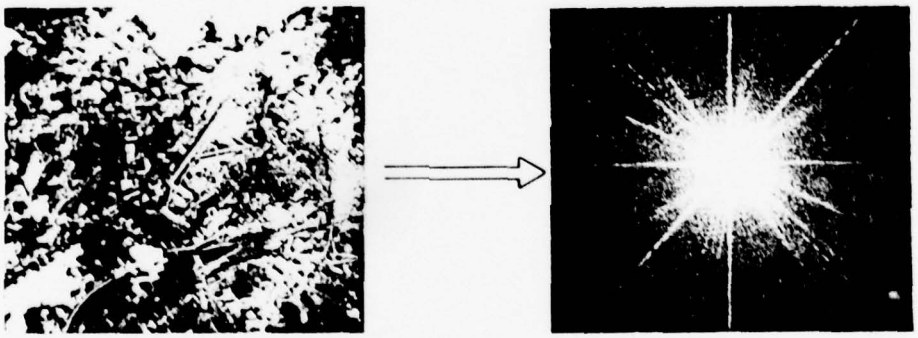

b) "Random" Scene and Corresponding Diffraction Pattern

Figure 2-5. Objects and their diffraction patterns illustrating the relationship between lines, circles, gratings and corresponding diffraction patterns.

2.4 --continued.

2) The diffraction pattern of a circular grating is a circular grating, grating spacing inversely proportional to the grating spacing in the input plane. More generally, circularly symmetric input patterns transform into circularly symmetric diffraction patterns.

3) The diffraction pattern of a linear grating is a sequence of "diffraction spots" arrayed along the line orthogonal to the direction of the lines in the grating.

REFERENCES FOR SECTION 2

1. M.V. Klein, Optics, John Wiley and Sons, Inc., New York 1970.

2. J.W. Goodman, Introduction to Fourier Optics, McGraw-Hill Book Company, New York 1968.

3. H.L. Kasdan, "Industrial Applications of Diffraction Pattern Sampling", Optical Engineering (to appear).

4. G.G. Lendaris and G.L. Stanley, "Diffraction Pattern Sampling for Automated Pattern Recognition", Proceedings of the IEEE, Vol. 58, pp. 198-216, 1970.

5. P. Krueger, W.B. Thompson and A.F. Turner, "Computer Diagnosis of Pneumoconiosis", IEEE Transactions on Systems, Man and Cybernetics, Vol. SMC-4, No. 1 January 1974.

6. S.C. Suffin, P.A. Cancilla and H.L. Kasdan, "Feasibility of Computer Evaluation of the Histopathologic Findings in Human Skeletal Muscle Disease", American Journal of Pathology, Vol. 85, No. 3, December 1976, pp. 609-618.

7. B. Pernick, R.E. Kopp, J. Lisa, J. Mendelsohn, H. Stone, and R. Wohlers, "Screening of Cervical Cytological Samples Using Coherent Optical Processing - Part I", Applied Optics, Vol. 17, No. 1, 1 January 1978, pp. 21-34.

8. G.C. Salzman, et al, "A Flow-System Multiangle Light-Scattering Instrument for Cell Characterization", Clinical Chemistry, Vol. 21, No. 9, 1975, pp. 1297-1304.

9. J. Swithenbank, et al, "A Laser Diagnostic Technique for the Measurement of Droplet and Particle Size Distribution", published in "Experimental Diagnostics in Gas Phase Combustion Systems", Progress in Astronautics and Aeronautics, Vol. 53, ed B.T. Zinn, 1977.

10. B.J. Pernick, "Surface Roughness Measurements with an Optical Fourier Spectrum Analyzer", Applied Optics, Vol. 18, No. 6, 15 March 1979, pp. 796-801.

11. G. E. Lukes, "Rapid Screening of Aerial Photography by OPS Analysis", Proceedings of SPIE Data Extraction and Classification from Film, Vol. 117, pp. 89-97, August 1977.

12. H. L. Kasdan, "Nonparametric Feature Analysis Methods for Sampled Diffraction Patterns", Proceedings of the SPIE, Vol. 4, Oct. 1972, pp. 187-206.

3.0 EXPERIMENT DESCRIPTION

3.1 Experiment Design

3.1.1 Philosophy

The objective of the experiment design is to allow a comparison of the effects of imagery type and aperture size on ability to determine topographic features. In particular, visual representations of synthetic aperture radar reconstructions, panchromatic imagery and passive thermal scan imagery were compared. Topographic classes represented in the available imagery were urban, water, agriculture and forest.

The most desirable situation is to minimize the effects of other variables such as scale differences, perspective differences, different geographical areas and optical power spectrum equipment variation. Huntsville, Alabama area imagery was available from both radar and panchromatic sensors with virtually identical scale and perspective. Unfortunately, among the sources investigated, thermal and panchromatic imagery with the same good match of scale and perspective was not available.

3.1.2 Design Tree

Based on the considerations above, the experiment design described in Figure 3-1 was selected. Imagery for the experiment came from two major geographical areas. Area 1 is the Huntsville, Alabama area. Area 2 is a region in Europe. Synthetic aperture radar and panchromatic imagery over the same Huntsville area with virtually the same scale was available. Thus, a direct comparison of the ability to

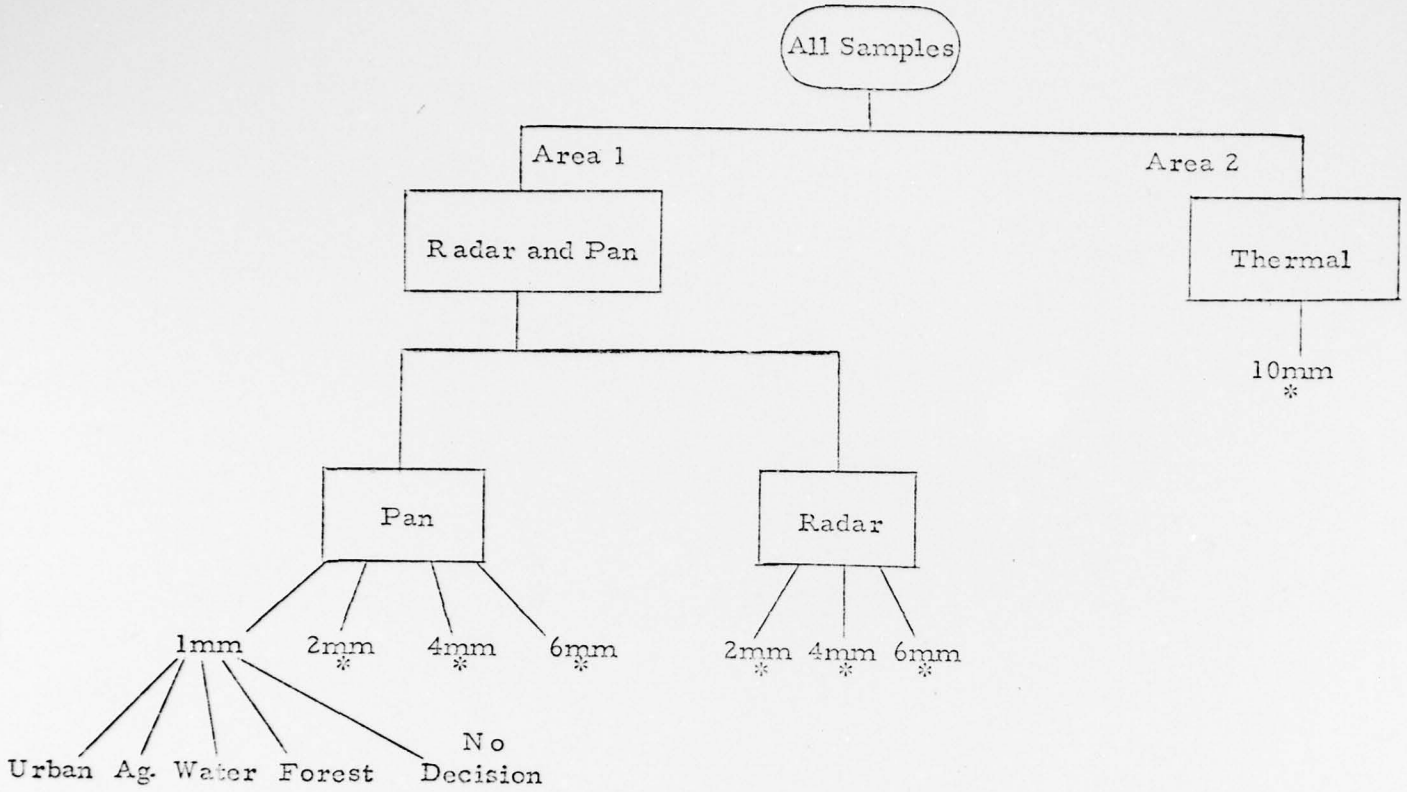

*Same decision actions as 1mm Pan

Figure 3-1. Experiment Design Tree

3.1.2 --Continued.

classify terrain type from panchromatic and synthetic aperture radar images was possible.

3.1.3 Design Discussion

Initial experiments were conducted with a 1mm hardclipped flat field illumination aperture. Initial interpretation of these results indicated that the small aperture contributed significantly to smearing the optical power spectrum data. In fact the most pronounced aspect of the optical power spectrum plots for this particular aperture size was the clearly visible contribution of the aperture. To overcome the aperture effect, subsequent experiments were conducted with 2, 4 and 6mm Gaussian shaped beams with no limiting apertures.

These three aperture sizes were then applied to both the sampling grid for the panchromatic and synthetic aperture radar. These sampling grids were virtually identical with some modification of the radar grid to take into account slight differences in perspective and scale to eliminate a strong specular return from the surface of the river water in the radar that would obviously be incorrectly classified. Shown in Figure 3-2 are the four image areas selected from both the panchromatic and synthetic aperture radar reconstruction imagery. In each case a sampling grid of 1 mm centers was selected. Five scan lines in each image area were used so that a total of 820 samples each were collected for panchromatic and radar for a given aperture size. The sample spacing was maintained independent of aperture size.

Figure 3-2a. Panchromatic Imagery Frame 1 with Sampling Grid (1mm spacing and apertures)

Figure 3-2b. Panchromatic Imagery Frame 2 with Sampling Grid (11mm spacing and apertures)

Figure 3-2c. Panchromatic Imagery Frame 3 with Sampling Grid (1mm spacing and apertures)

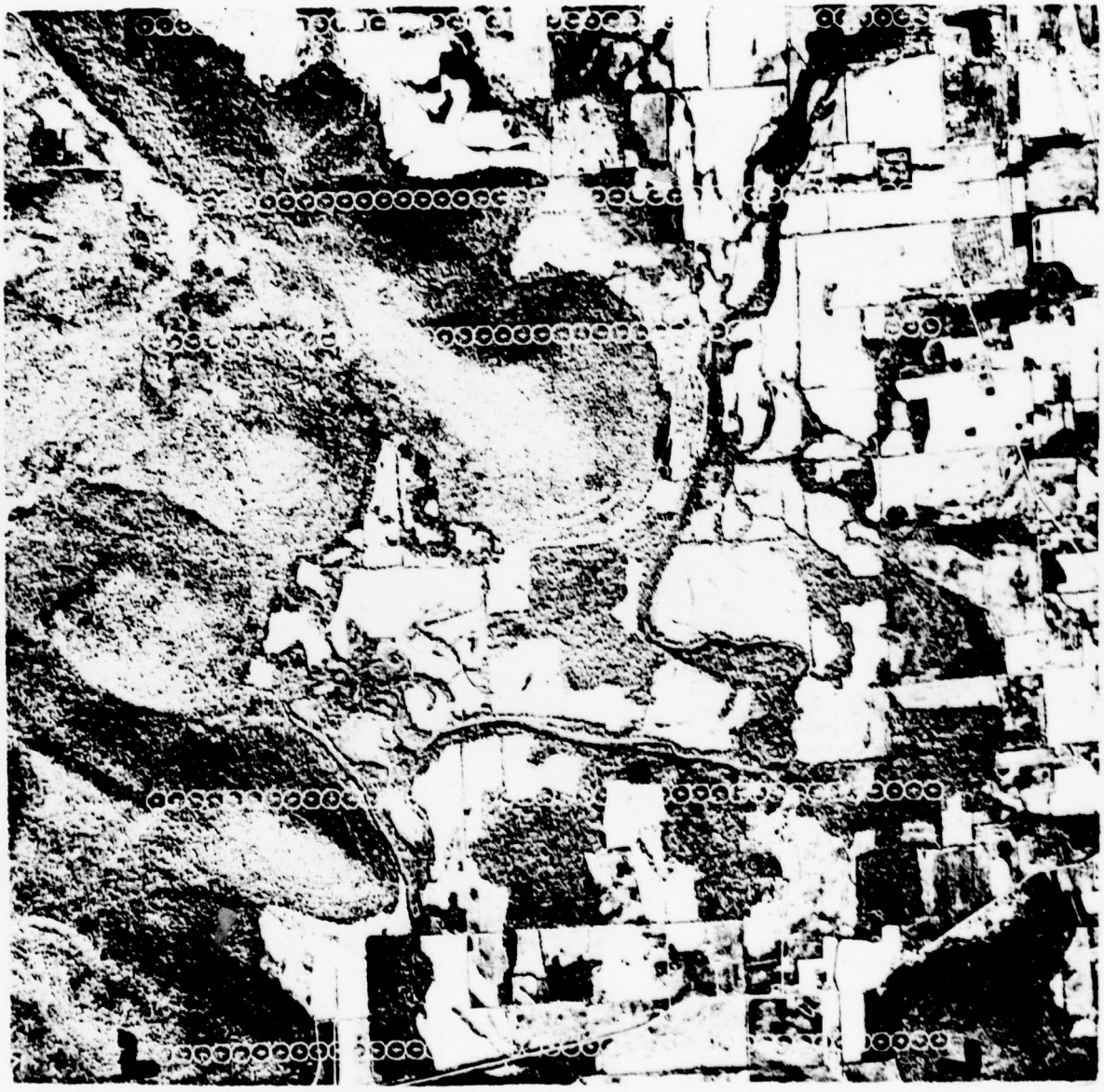

Figure 3-2d. Panchromatic Imagery Frame 4 with Sampling Grid (1mm spacing and apertures)

Figure 3-2e. Radar Imagery Frame 1 with Sampling Grid
(1mm spacing and apertures)

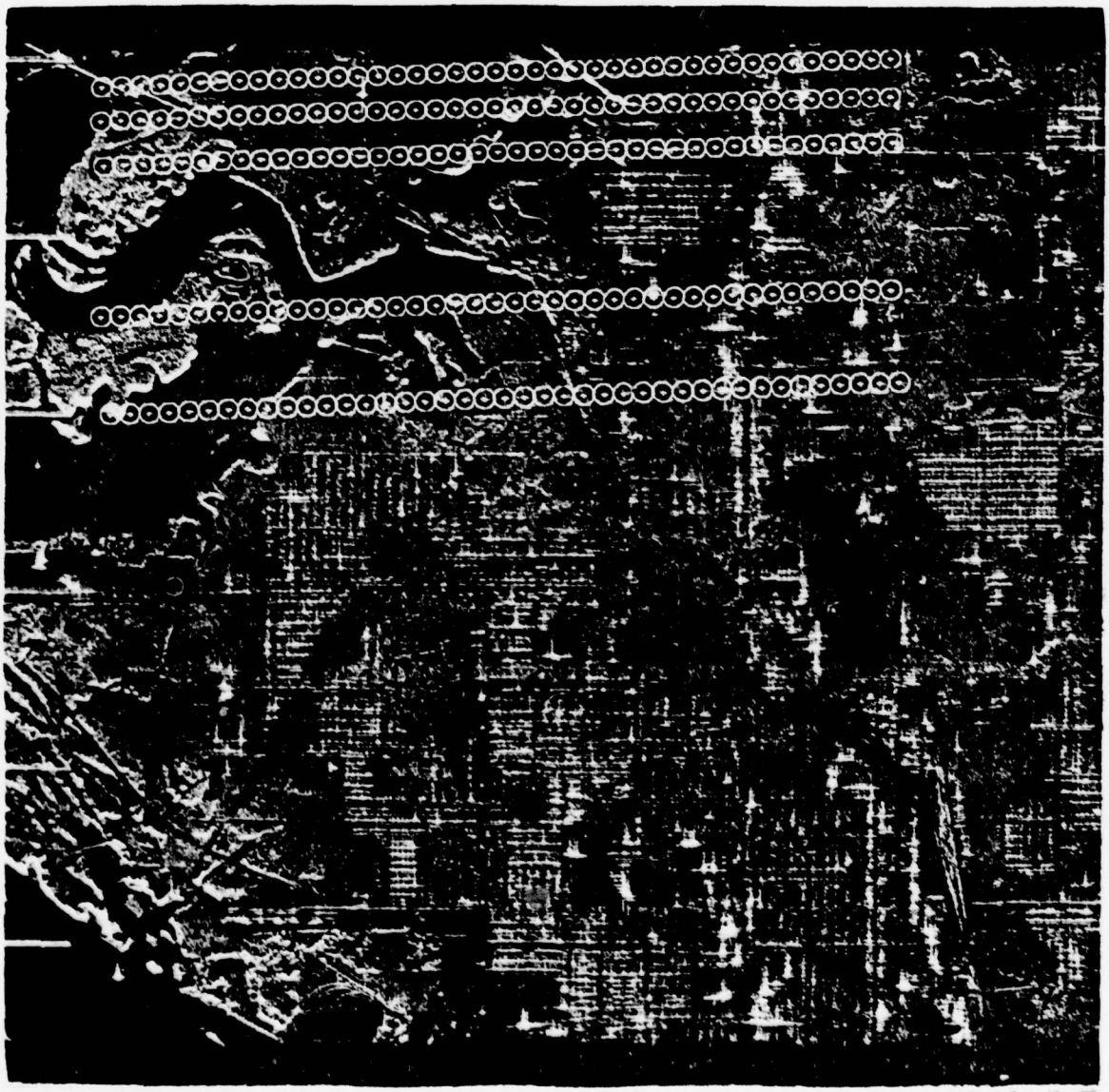

Figure 3-25. Radar Imagery Frame 2 with Sampling Grid
(1mm spacing and apertures)

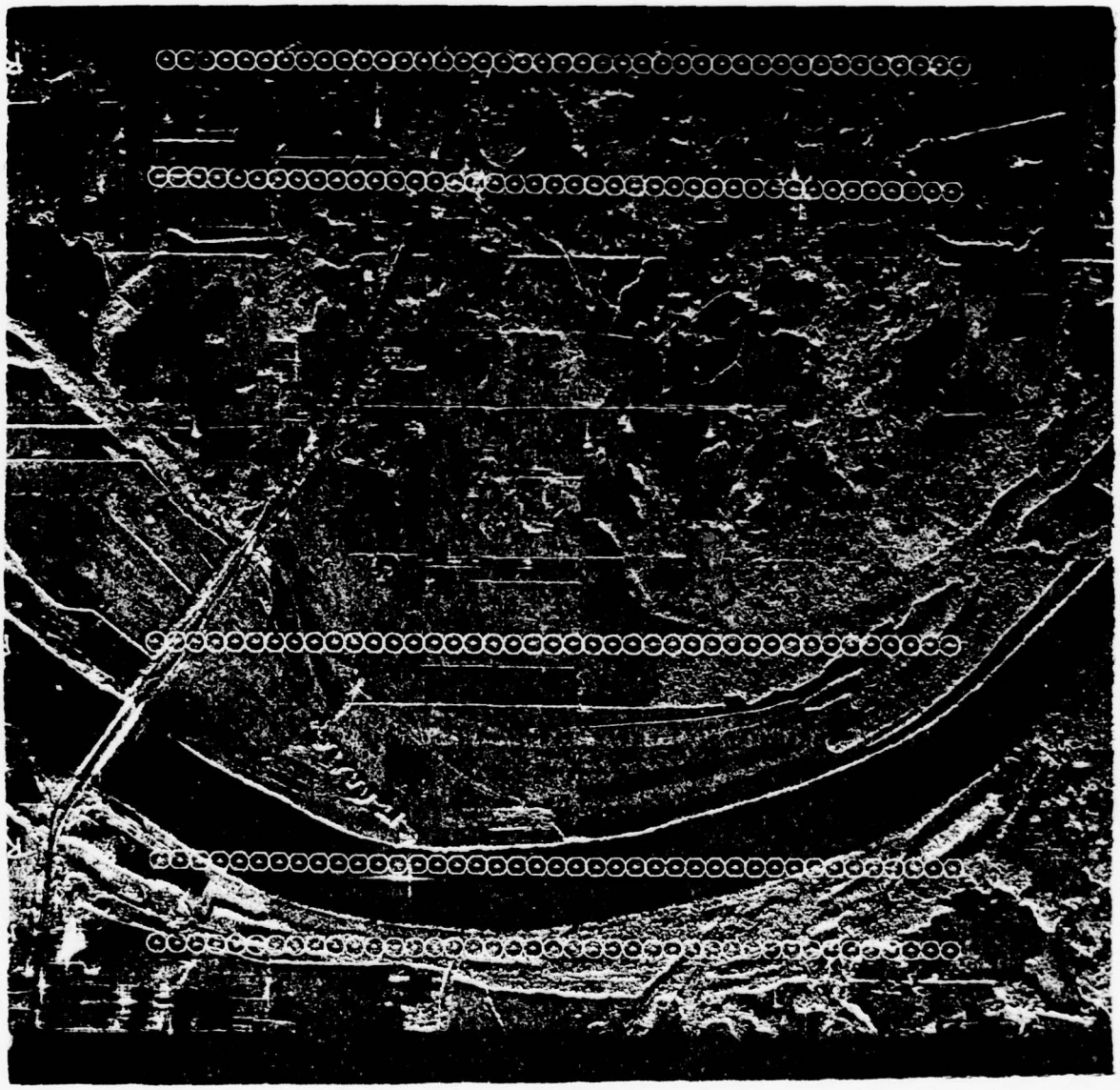

Figure 3-4g. Radar Imagery Frame 5 with Sampling Grid (1mm spacing and apertures)

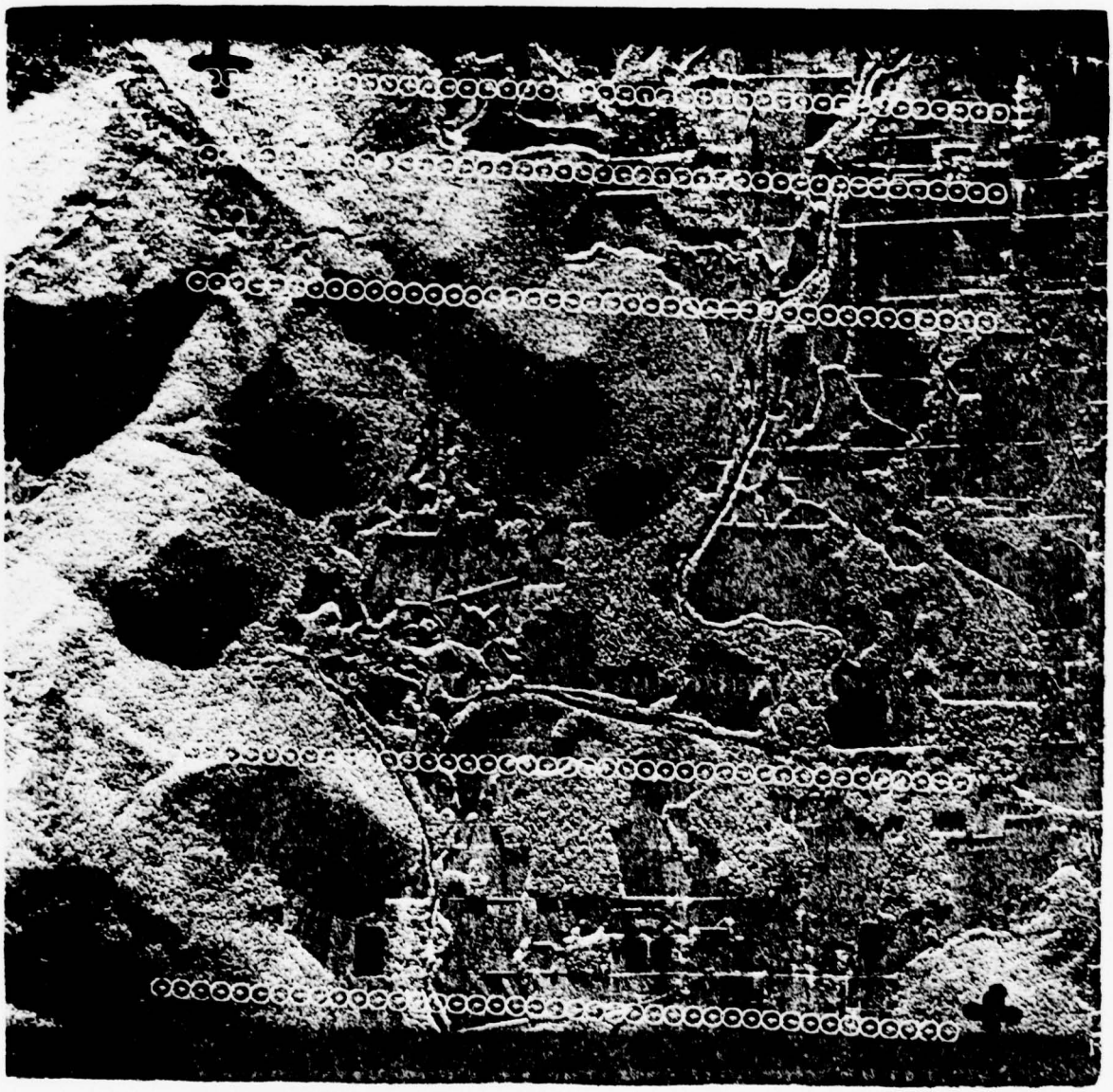

Figure 3-2h. Radar Imagery Frame 4 with Sampling Grid
(1mm spacing and apertures)

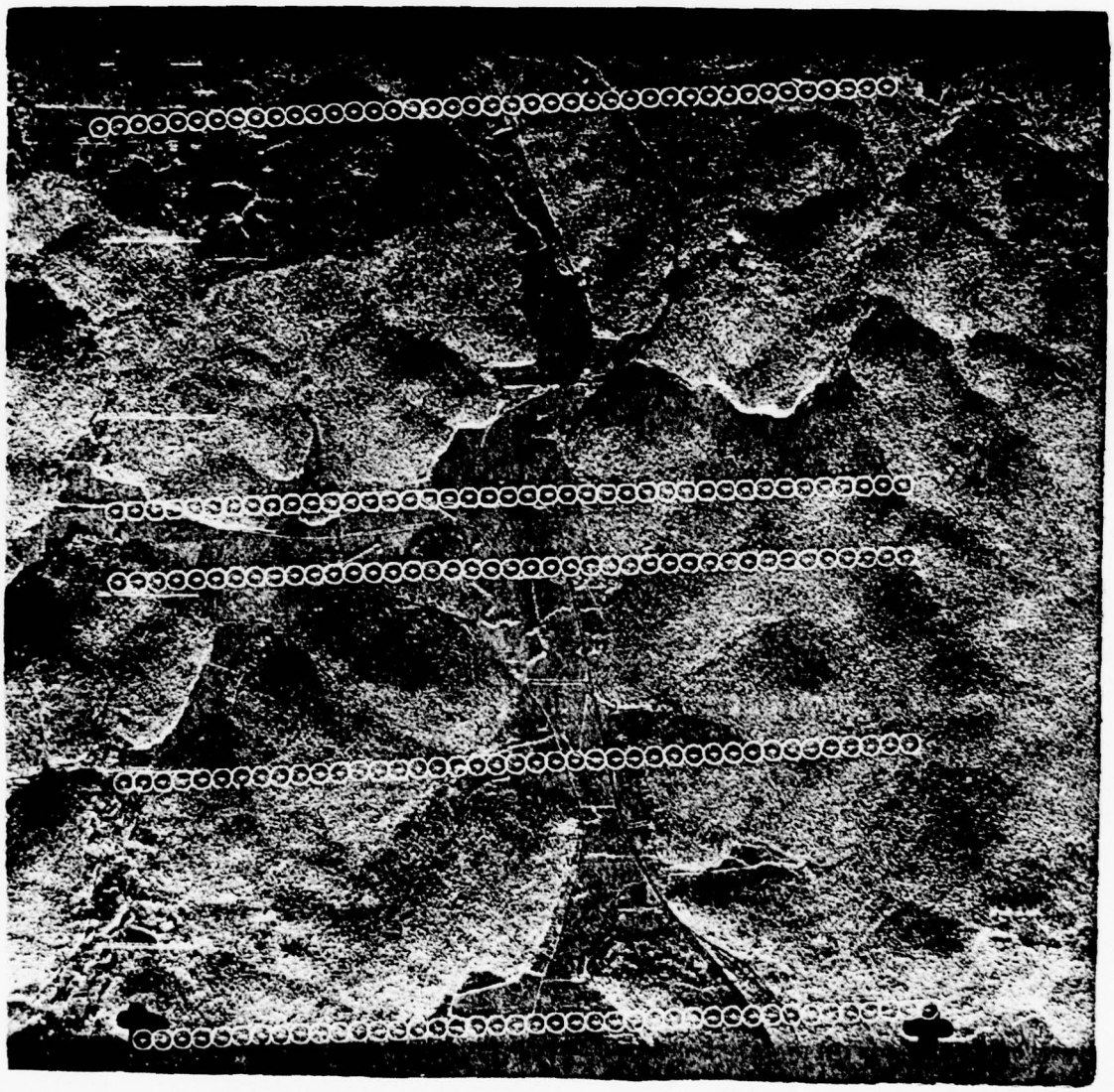

3.1.3 --Continued.

Only apertures containing a single terrain type were used in the training set. In general, several classes were sampled on each scan line, thereby minimizing the effect of equipment drift and variation. Additionally, since each class was represented on one or more frames, the effect of time variation was minimized. The samples not used for training in each scan line were available to be part of the validation set. Table 3-1 summarizes the number of training set and validation set samples as well as the number of training set samples available for each class.

Thermal imagery was available over a region in Europe. The perspective and scale of the corresponding panchromatic imagery was significantly different than the perspective and scale of the thermal scan imagery. In addition, the flight paths used to record the two different types of imagery had very little overlap so that comparisons of large numbers of apertures over identical areas would be difficult. Thus it was decided that a detailed comparison of thermal imagery to panchromatic imagery would not be attempted. Rather a gross comparison of the results for thermal would be compared to the gross results for radar and panchromatic.

Due to limitation in the optical configuration, it was impossible to project on the imagery a good quality aperture larger than about 15 mm. For the thermal imagery, approximately a 10 mm sample aperture corresponds to the same ground area as a 2 mm aperture for either the radar or panchromatic imagery. Therefore, a 10 mm aperture was selected. Results for this aperture were compared to the 2 mm results

Table 3-1. Training Set and Validation Sample Breakdown for Each Aperture Size

Imagery Type	Urban	Other	Water (50)	Water (60)	Plowed Agriculture (20)	Non-Plowed Agriculture (70)	Forest	Total for Training	Validation	Total Sampled
Pan	31	-	11	26	83	48	214	413	407	820
Radar	26	-	9	19	72	53	211	390	430	820
Thermal	64	62	54	-	49	44	41	314	162	476

3.1.3 --Continued.

for radar and panchromatic. It was possible to find representative areas on the thermal imagery for the four classes (urban, water, agriculture and forest) present on the radar and panchromatic imagery.

3.2 RHDAS Data Collection System

The ROSA High Speed Data Acquisition System (RHDAS) provides an efficient mechanism for generating, sampling, and recording of the Optical Power Spectrum of roll film imagery. The major components of this system are outlined in the following Block Diagram (Figure 3-3).

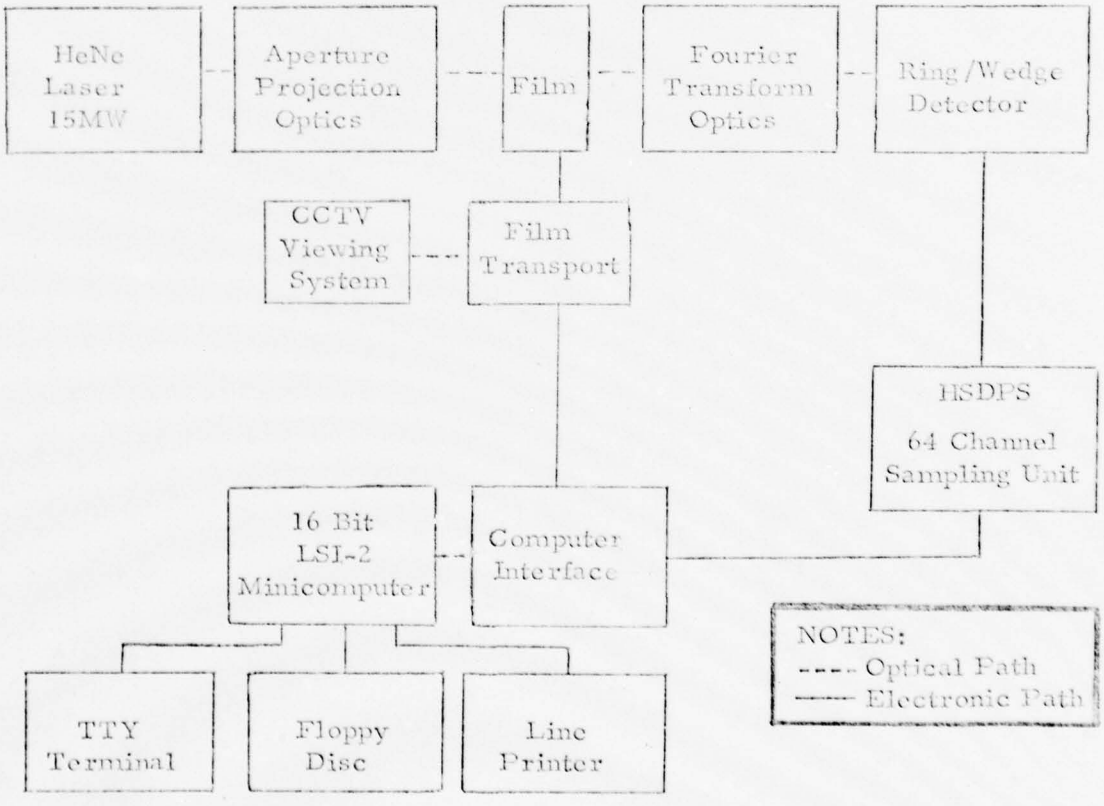

Figure 3-3. Block Diagram of RHDAS OPS Sampling System

3.2.1 Optical Components

This system contains optical components to generate the optical Fourier transform of imagery placed in the film plane (Figure 3-4). A He-Ne laser in conjunction with the Aperture Projection Optics package provides coherent, circularly apertured or Gaussian illumination of the film. The Fourier Transform Optics collects this light as it is diffracted from the film and resolves it into the Optical Power Spectrum. The patented RSI Wedge/Ring Photodetector samples this spectrum in a polar coordinate geometry and produces analog electrical signals proportional to the light energy incident on the detector elements. All of the optical components are securely mounted to a rigid optical platform.

Sampling apertures of 1 to 15 mm are readily accommodated. The Transform Optics can handle transform lenses from 3 inch to 120 inch focal length; these provide for sampling of the film with cutoff frequencies of from 329 cycles/mm to 8 cycles/mm respectively. The lens combinations and optical parameters used are summarized in Table 3-2.

A closed circuit TV is incorporated into the viewing system. This provides a simultaneous magnified view of the apertured laser illumination on the film and white light illumination of the surrounding film area. With this scheme the experimenter can obtain absolute verification of the sample point on the film.

3.2.2 Film Transport

The Film Transport provides precision incremental translation of the film across the stationary laser illumination. It can accommodate roll film up to 9 1/2 inches wide. Motion resolution along the film is

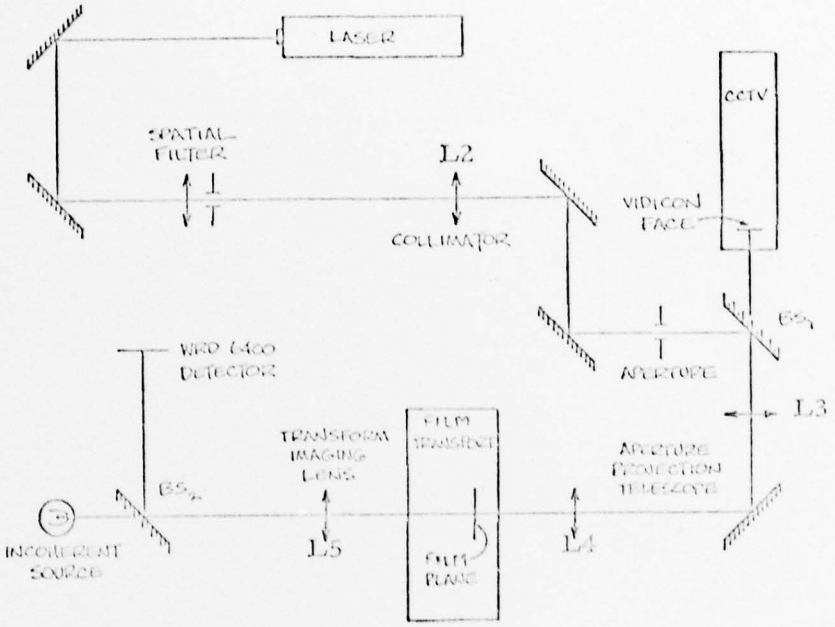

Figure 3-4. ROSA Optical Configuration used for Study

Table 3-2. ROSA Beam and Lens Parameters

Lens Parameters

Lens	Focal Length
10X Objective	16mm
First Collimator	variable
Relay Lens	300mm
Second Collimator	117.8mm (7")
Transform Lens	628.65mm (24.75")

Other Parameters

Film aperture size to aperture stop size ratio	$\frac{1}{1.687}$
Ratio of $(1/e)^2$ points to aperture diameter for 15% intensity fall off	3.51

Table 3-2 (continued)

Configuration Parameters

Desired Film Aperture Size	Physical Aperture Beam Size	First Collimator Desired Focal Length	First Collimator Actual Focal Length	Actual Film Aperture Size
F_D	$D_D = (1.687)F_D$	$C_D = \frac{16}{1.1} D_D$	C_A	$F_A = \frac{C_A}{24.54}$
1mm hardclip (15% intensity fall-off)	1.687mm hard-clip (5.92mm Gaussian)	86.1mm	93.98mm	1mm hardclip (13% intensity fall-off)
2mm Gaussian	3.374mm	49.1mm	58.23mm	2.37mm Gaussian
4mm Gaussian	6.748mm	98.1mm	93.98mm	3.84mm Gaussian
6mm Gaussian	10.12mm	147.2mm	140mm	5.7mm Gaussian

3.2.2 --Continued.

0.1 mm; across the film it is 0.01 mm. The Film Transport is controlled by the system computer.

3.2.3 Electronics

The sixty-four (64) (32 ring, 32 wedge) analog electrical signals from the Ring/Wedge Photodetector are individually amplified, multiplexed, and A/D converted by the RSI HSDPS Sampling Unit. Auto-ranging is provided to preserve precision in the widely varying dynamic range data. The digital output to the computer for each channel consists of an eight bit mantissa and a three bit exponent. The HSDPS is equipped with sample and hold circuitry for each channel. Sampling can readily be accomplished at 30 μs. per channel.

3.2.4 Controller and Control Software

The Computer Automation minicomputer is the system controller. It contains a Floppy Disc drive to load the system software as well we record data acquired during sampling. A TTY terminal provides the experimenter with an interactive interface to the system. The line printer allows on-line printout and plots of the ring/wedge data.

The operational system software provides the user with a powerful, easy-to-use language to control the sampling experiment. The commands are introduced by keywords and are followed by optional parameters. The following list outlines the major command capabilities:

1) Redefine default sampling parameters
2) Provide prompts for all optional input

3.2.4 --Continued.

3) Define a file name and comment
4) Define present film coordinates to system
5) Move film to a specified film location
6) High speed wind/rewind of film
7) Sample film at present coordinates
8) Take samples in a loop
9) Sample over a grid. Terminal coordinates and step size table defined. Raster scan with/without retrace is provided.
10) Place end of file on output Floppy Disc
11) List contents of a Floppy Disc
12) Terminate.

Many sampling parameters are default initialized in a table; they may be changed at any time. Some of the more important parameters allow definition of the sampling grid and stepsize, whether the data is to be saved on a Floppy Disc or plotted, the sample index, etc.

A unique feature of the operational software is that it is written in the BASIC language and executes in an interpretive mode under control of the BASIC compiler. Thus, new commands and capabilities may be added to the system by the experimenter on-line and used immediately.

The system can readily perform automatic grid sampling and recording at about five (5) samples per minute, exclusive of initial manual film positioning. This rate includes automatic averaging of up to 127 consecutive samples to reduce the effect of random system noise.

3.2.4 --Continued.

Considering the above-listed capabilities, the RHDAS does indeed supply the OPS experimenter with a unique, efficient mechanism for acquiring data. This implementation is the product of several man-years of research effort at Recognition Systems, Inc. and represents the current state-of-the-art in OPS sampling techniques.

3.3 Analysis Software

The software described here was designed to support the analysis tasks in this study. These routines were designed to augment the existing RSI developed FACEL modules. The prime design motivation of this new software was to aid the experimenter in feature selection. The data consisted of ring/wedge values. The classes to be separated were characterized by various topological features.

In contrast to the controller software written in BASIC, all of this analysis software was written in FORTRAN IV. It runs on a Computer Automation LSI-2 computer. Many of the lower level library routines are drawn from RSI library 'TJMLIB'. All user supplied parameter inputs are free format (except in routine 'SORTD').

The software described herein performs the following tasks:

1) acquire data in the RSI RHDAS facility
2) plot the data or clue files
3) list the data or clue files
4) edit and classify the data
5) partition the data into training and recognition files
6) clue processing (normalize the data, generate clue files, generate threshold test limits, and classify vectors based on a threshold test)
7) generate overlay grid for classification

3.3.1 Data Acquisition Software (HDAS29, BASICT)

'HDAS29' is a BASIC language source file used for controlling the data acquisition process in the RHDAS facility at RSI. It runs under control of the BASIC Executive 'BASICT' which has several machine language routines to access the HSDPS, Motor Controller interface, and the computer front panel.

3.3.2 Plotting Software (PRPLOT)

'PRPLOT' was developed to produce three dimension contour perspective data plots on the Versatec plotter. The perspective display did not provide the desired visibility. However, this routine is an excellent mechanism for overlay plotting and this has been the chief feature and data display vehicle in the study.

'PRPLOT' is controlled by four types of control cards:

1)	title card (#1)	Places selected symbolic text on the plot.
2)	title card (#2)	Places Facfile header and name on the plot.
3)	axis card	Selects graph type, scale parameters, labeling, etc., and draws axes.
4)	graph card	Selects files, vectors, labeling, and line patterns to be drawn.

3.3.2 --Continued.

All data plotting is done using the Calcomp compatible calls to standard Versatec software. A new graph is started for each appearance of the 'TITLE' (optional), and 'AXIS' parameter set. Each subsequent 'GRAPH' card directs the plotting of its vectors on axes specified by the immediately preceeding 'AXIS' card.

Data to be plotted can be in either the RHDAS (source) or FACFILE format.

3.3.3 Listing Software (LIST)

Program 'LIST' lists out a selected range of contiguous vectors from a file. The vectors may be specified by physical index, designator, and class label. The range of components to list is also selectable. The format of the line (narrow for terminal, wide for line printer) is selected automatically depending on the output device type.

All parameters are specified on the /EX Command which invokes LIST. The first null option terminates the parameter scan. Defaults are assumed for null options.

Input files may be either RHDAS or FACFILE, the proper read mode being automatically determined by 'LIST'.

3.3.4 File Editing and Classification

Program 'CLMG' provides the capability to generate an output file composed of selected vectors from selected files. It is a merging program where the vectors to be merged can be individually selected from the input files in any order. Not all input vectors need be copied to the output file. Thus it 'edits' the file.

3.3.4 --Continued.

'CLMG' can generate a descriptor in the output file even if the input had no descriptor; in general, it can change the output descriptor to any arbitrary length, including zero.

Input vectors may be selected by physical index, designator, or input class label.

Output class label (if any) can be set to a specified value or remain the same as input. Thus vector classification can be performed on designators, with a possible prerequisite class label.

Input files may be either RHDAS or FACFILES, the proper read mode being automatically determined by 'CLMG'.

3.3.5 File Partitioning

Program 'SORTD' selects groups of vectors from an input file by class and creates a new output file. A typical use is to select every n^{th} vector for a training data set and every k^{th} vector for a recognition data set.

The input file may be RHDAS or a FACFILE, the proper read mode being automatically determined by 'SORTD'.

3.3.6 Clue Processing

Generation of new features and training and recognition is accomplished with a set of routines analogous to the classic CLUEIT/CLUE software of FACEL. The executive routine in this package, 'KLUE',

3.3.6 --Continued.

provides I/O services similar to 'CLUEIT' with several enhancements. The actual clue processor routines are named 'KLUE**', where ** = (01, 02, etc.).

Whereas the classic 'CLUEIT' executive could access at most one clue subroutine, one input file, and only call the clue routine when each vector was read, the new improved 'KLUE' can access multiple clue routines and files, and can also call the clue routine upon completion of processing a particular vector data set. The 'KLUE**' subroutines can make a vector by vector decision concerning generation of an output data vector and make the decision about when to place an EOF on the output file.

This facility has been used to implement normalization, automatic threshold selection, recognition, and accumulation of performance statistics.

3.3.6.1 Clue Executive (KLUE)

The clue executive reads free format parameter cards to determine the mode of operation. Each card can specify:

1) input file name and device
2) input start and end vector (designator or physical index specification
3) input class label
4) output file name
5) output file comment
6) index to clue routine
7) parameters for clue routine.

3.3.6.1 --Continued.

All parameters are optional, with a default assumption for null. For example, if no input file name is specified, 'KLUE' assumes there is no input file; similarly for the output file. The comments of the listing provide complete details.

In order to be legally specified as a clue index parameter, the corresponding 'KLUE**' subroutine must exist in the load module. If it doesn't, an error message is reported.

'KLUE' can read either RHDAS files or FACFILES, the proper read mode being automatically determined by 'KLUE'. Output files are FACFILE format.

Each parameter card read by 'KLUE' is listed on the printer for subsequent reference as are the names and locations of the effective files.

Prior to each call to a 'KLUE**' subroutine, the input vector designator, descriptor, and data components are copied to the corresponding output vector arrays. This feature obviates the clue subroutine from having to copy unchanging vector data to the output array.

3.3.6.2 Normalization (KLUE01)

Clue subroutine 'KLUE01' performs various user selected normalizations on vector input data. It is called by 'KLUE' and specified by the clue index parameter = 1.

3.3.6.2 --Continued.

'KLUE01' allows specification of:

1) independent scale value for ring, wedge normalization
2) independent starting and ending components for ring, wedge normalization
3) various normalization methods such as
    a. none
    b. simple range of elements with possible rank ordering
    c. ranked differences, etc.

3.3.6.3 Generation of Vector Statistics (KLUE02)

Clue subroutine 'KLUE02' generates a set of six vectors representing several statistics of a range of vectors. All statistics are acquired on a component by component basis over all vectors processed. The statistics produced include:

1) minimum envelope vector
2) maximum envelope vector
3) average vector
4) standard deviation vector
5) average vector - k * standard deviation vector
6) average vector + k * standard deviation vector

A typical usage of this routine is to determine the envelope of a set of vectors of a particular class. These vectors might then be used in a threshold decision rule classifier.

3.3.6.4 Threshold Classification (KLUE03, KLUE04)

Clue routines 'KLUE03' and 'KLUE04' implement a threshold decision rule classifier. A typical application is to compare a set of components of a set of vectors against a limit vector. The decision rule is that any single component of the suspect vector passing the limit test (polarity is user specified) is called a success; otherwise it is a failure. Prerequisite class labels may be specified thus allowing implementation of a layered decision rule. The decision class label may be specified for success or failure, or may be left undisturbed (e.g., if test fails, don't change label).

In a typical experiment several 'KLUE03' parameter cards would be input to define the limit vectors and test parameters. This would be followed by a 'KLUE04' parameter card to specify the recognition data set and printout formats desired. Each individual decision may be printed, or simply can be summarized in transition matrices (true class versus decision class, or previous class decision versus current decision class).

In actual operation, the 'KLUE03' routine stores the decision parameters and threshold limits in a table in core memory. For each 'KLUE04' parameter card, a pass is made through the input file and decisions rendered on a vector by vector basis by sequencing through each of the 'KLUE03' parameter tests defined in core. The final class label after all tests is the decision class label. This label is recorded in the transition matrices and on a scratch disk file. A subsequent 'KLUE03'/'KLUE04' sequence may be input to continue the layered decision-making process - such subsequent sequences may specify that the 'input class label' comes from the scratch file. Such a procedure is necessary, for example, to continue a layered process using differently normalized data. This process requires only one caution: the vectors presented to 'KLUE04' on each pass must have the same sequence of designators, otherwise processing is terminated.

3.3.6.5 Top of Form Generation (KLUE05)

Clue routine 'KLUE05' is a simple routine to issue a top of form on the line printer and output a line of comment text. This facility is useful to separate printouts from various clue routines.

3.3.7 Overlay Grid Generation (CIRGN, DECPLT)

Programs 'CIRGN' and 'DECPLT' were designed to produce a plot of circular apertures on a regularly spaced grid. This plot may then be xeroxed onto viewgraph film sheets. The intention of this sequence is to produce an overlay sheet which can be placed over aerial photographs of appropriate magnification. This combination may then be used by an experimenter to determine the exact area on a piece of film which was diffraction pattern sampled using a sampling aperture of known size.

Program 'CIRGN' generates a file of center coordinates of the circles to be plotted. It is programmed by a control card defining the X, Y stepsize. 'CIRGN' includes different 'fudge' factors for X, Y magnification corresponding to the measured difference in magnification of the xerox process (it may not be stationary with time).

Program 'DECPLT' plots circles on the Versatec plotter at the coordinates specified on the file generated by 'DECPLT'.

3.3.8 Operations Flowcharts

The flowcharts contained on the following two pages (Figure 3-5) are intended to illustrate typical usage situations of the software modules described above.

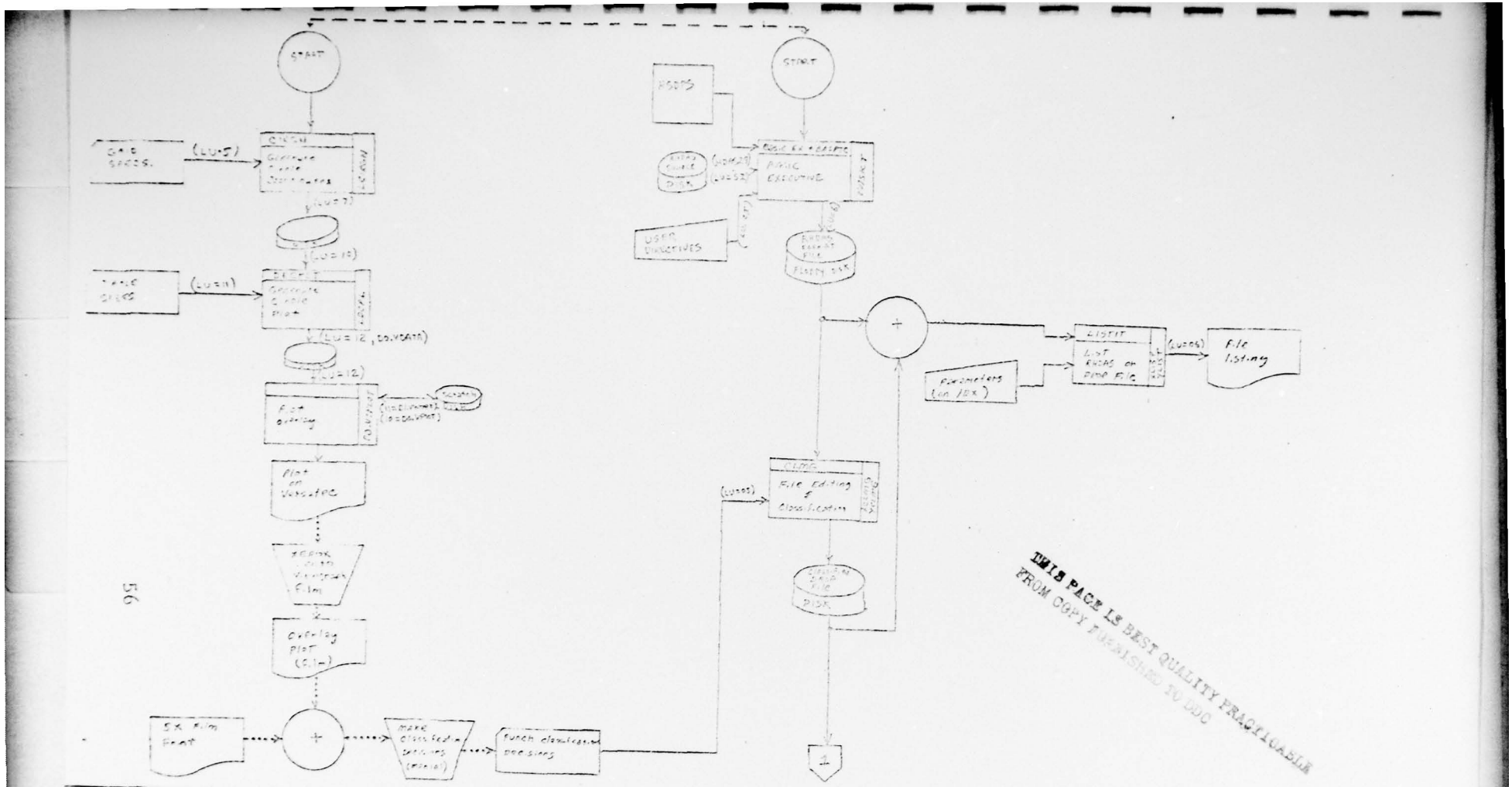

EIL NON VISUAL SUPPORT SOFTWARE (PART 1 of 2)
12/18/78 TJM

Figure 3-5

Notes:

1) 'DASP' format files may be either on disk (as shown) or on tape. To access tape files, the mag tape #3 (MTD3) must be loaded (8:9) auto load from disk ('TJM3') and execute the power program (see table below). Note that no MTD3 executable version of VIPLOT has been created, hence mag tape files may not be directly plotted without reloading DOS.

Source Name	Executable DOS	Executable MTD3
CHNG	XCHNG	YCHNG
LISTIT	XLIST	YLIST
SORTD	XSORTD	YSORTD
TRNFRM	XPLOT	YPLOT
VLUC	XLUC	YLUC

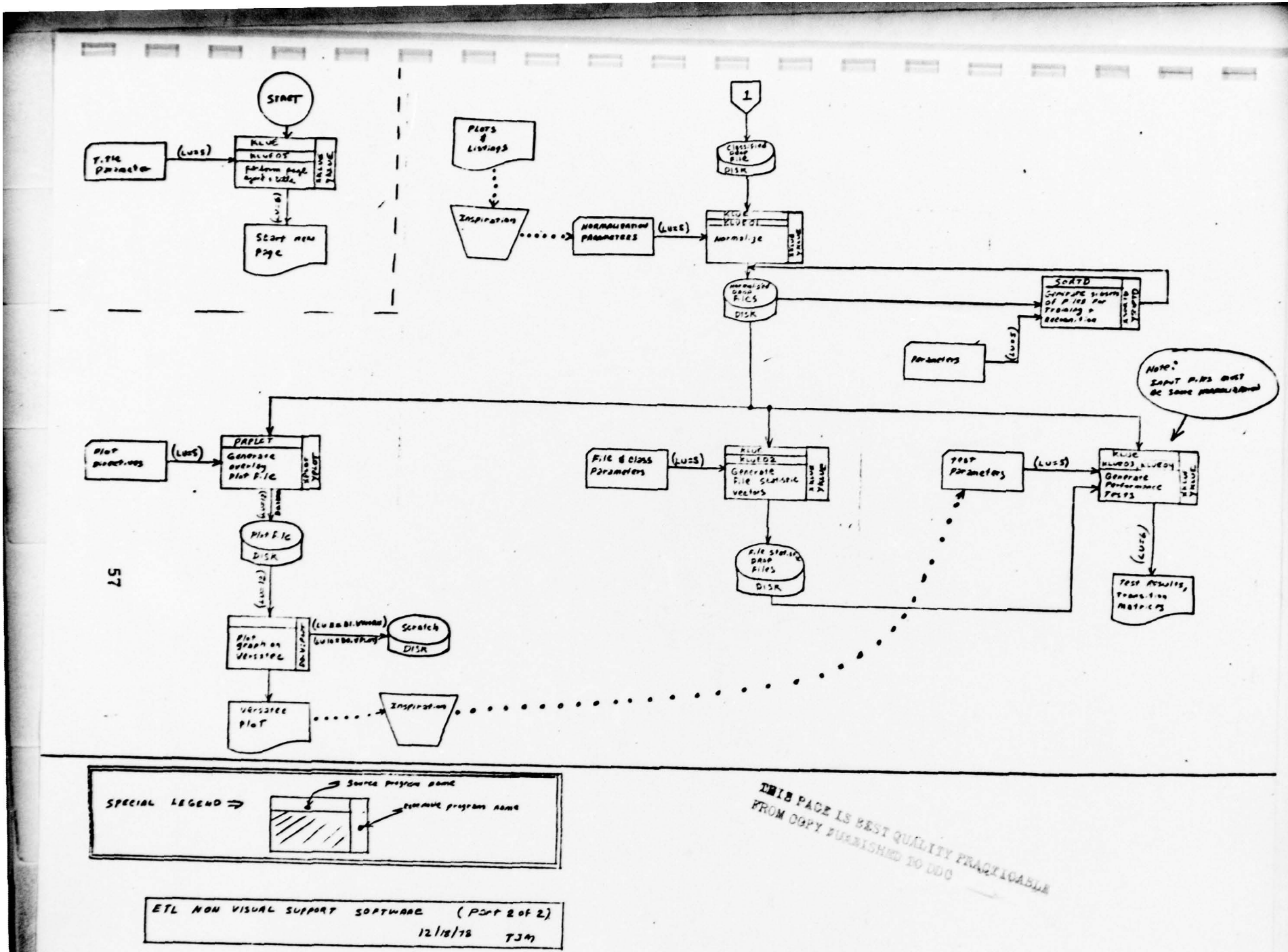

Figure 3-5 (continued)

3.4 Data Collection Procedure

3.4.1 Pan and Radar Imagery

The basic data collection procedure for Pan and Radar Imagery was to:

1) Align the frame area to be sampled using the fiducial marks on the film to define the boundaries of the sampling grid.
2) Use the motorized film transport chip holder to position the imagery to the scan line to be sampled.
3) Record individual aperture OPS samples along the scan line on floppy disk storage for subsequent analysis. (A unique designator code was used to identify the frame scan line number and location of the aperture along the scan line.)
4) Use an overlay grid to delineate the sampling location for each sample in the training set.
5) Assign a class label in accordance with the software procedure outlined in Sections 3.3.4 and 3.3.7. This procedure was repeated for each aperture size.

The sampling grid overlayed on the imagery is shown in Figure 3-2. Table 3-1 summarizes the data collected by class for radar, panchromatic and thermal imagery.

3.4.2 Thermal Imagery

The thermal imagery data collection was generally similar

3.4.2 --Continued.

with the following exceptions:

1) A single line sampling grid was developed rather than a scan area sampling grid. This was because individual scan lines were at widely separated points along the long frame format of the thermal imagery.

2) As noted above, only a single aperture size was used.

Once the data for the sample areas was collected, the processing procedure for the thermal imagery was the same as for the radar and panchromatic.

4.0 FEATURE AND DECISION RULE DEVELOPMENT

The overall development philosophy for both features and the decision rule was to continue development to the point that overall probability of correct classification approached the order of 80% or better. Additionally, it was desired that no individual class percent correct should be less than about 60%. It was decided that once a decision rule meeting these general objectives was achieved for the 2 mm pan and 2 mm radar, no additional effort would be expended attempting to significantly improve the decision results. Rather, the same algorithm would be applied to the 4 mm and 6 mm samples of the radar and panchromatic imagery.

The rationale for this approach is that the prime objective of the study is to compare effects of imagery type and aperture size. Expending effort to optimize an algorithm for a specific data set in order to achieve 5 or 10% better performance is less valuable than understanding the reasons for differing performance as a function of aperture size and imagery type for a suboptimal rule.

4.1 Feature Analysis

4.1.1 Ring Features

The generic family of ring features initially considered for the panchromatic film with a 2 mm aperture is given by

$$F(j,k;\ell,m) = \frac{\sum_{i=j}^{k} r_i}{\sum_{n=\ell}^{m} r_n} \qquad (4\text{-}1)$$

where r_i is the intensity from the i^{th} ring

4.1.1 --Continued.

From this generic family, the following specific features were considered:

$$F(j,j;\,1,1) = \frac{r_j}{r_1} \qquad (4\text{-}2a)$$

$$F(j,j;\,1,3) = \frac{r_j}{\sum_{n=1}^{3} r_n} \qquad (4\text{-}2b)$$

$$F(j,j;\,4,32) = \frac{r_j}{\sum_{n=4}^{32} r_n} \qquad (4\text{-}2c)$$

The basic presumption motivating the selection of ring features is that texture in the scene causes an increase in spatial frequency content at higher spatial frequencies relative to the undiffracted energy. Thus features that compare the diffracted to undiffracted energy or the form of the diffracted energy should be the most useful for discriminating among the various topographic classes.

Analysis of the optical configuration shows that a 2 mm Gaussian beam image spot on the detector will have virtually all the energy within the first three WRD 6400 detector rings. With this in mind, the region of undiffracted energy was taken to be the region contained within the first three rings. The region of diffracted energy was taken to be the region including rings 4 through 32. Thus, normalization to undiffracted energy was taken to be normalization to rings 1 through 3 while normalization to diffracted energy was taken to be normalization to rings 4 through 32. Both of these normalizations were evaluated using the decision rule

4.1.1 --Continued.

described in the following section. Normalization to diffracted energy was found to be slightly better and therefore used as the primary feature set.

4.1.2 Wedge Features

4.1.2.1 Panchromatic and Thermal Imagery Wedge Features

The feature sets used for panchromatic and thermal imagery are defined as follows:

Let w_i, i=1, ..., 32 be the intensity of illumination on the i^{th} wedge. Then

$$\bar{w} = \max_i w_i \tag{4-3}$$

$$\Delta w_i = \begin{cases} w_{i+1} - w_i & \text{for } i=1, \ldots, 31 \\ w_1 - w_{32} & \text{for } i=32 \end{cases} \tag{4-4}$$

Let $(s)_i$ i=1, ..., n be the i^{th} order statistic defined by the relationship

$$\min_i s_i = (s)_1 < (s)_2 < \ldots < (s)_i < (s)_{i+1} < \ldots < (s)_n = \max_i s_i. \tag{4-5}$$

Then, the first set of wedge features $\left\{F_{w1}\right\}$ is given by

$$\left\{F_{w1}\right\} = \left\{\left(\left|\frac{\Delta w}{\bar{w}}\right|\right)_i\right\} \tag{4-6}$$

or in words, the ranked absolute wedge differences normalized by the maximum wedge.

output file. Thus it 'edits' the file.

4.1.2.1 --Continued.

The second set of wedge features F_{w2} is given by

$$\left\{F_{w2}\right\} = \left\{\left(\left|\frac{\Delta w}{(|\Delta w|)_{32}}\right|\right)_i\right\} \tag{4-7}$$

or, the ranked absolute wedge differences normalized by the maximum absolute wedge difference.

Note that these families of features are rotationally invariant, i.e., rotational orientation of the diffraction pattern does not affect the value of the feature family. In addition, notice that these features are basically a measure of the angular uniformity of the diffraction pattern. This measure of uniformity is not developed in absolute terms, but rather relative to the normalizing factor.

4.1.2.2 Radar Imagery Wedge Features

The best set of wedge features used for radar imagery is the following:

$$W^{(i)}_{13,20} = \frac{w_i}{\sum_{j=13}^{20} w_j} \tag{4-8}$$

Notice that this set of features will be sensitive to the orientation of the diffraction pattern. It was designed specifically for the synthetic aperture radar in order to detect the "cross pattern" characteristic of specular returns from cornercube-like objects on the ground. These cross patterns will always be oriented in the same

4.1.2.2 --Continued.

direction relative to the flight path and therefore at a fixed angular orientation in the imagery. Thus, there is in fact no loss in generality in using this type of feature.

This feature measures an increase in diffracted energy in the central wedge elements compared to the other wedge elements. It was developed by observing that a large fraction of the aperture samples for urban areas displayed energy distributions on the wedges similar to those of Figure 4-1. On the other hand, the majority of samples from other classes typically had a dip in the center wedge elements and tended to have increased energy at the outer wedge elements compared to the center wedge elements as shown in Figure 4-2.

Finally, the observation that led to the wedge features described by Equation (4-8) motivated the following wedge autocorrelation feature set.

$$A(k) = \frac{1}{\sum_{\ell=1}^{3} r_\ell} \sum_{i=1}^{32} w_{\bar{i}}\, w_{\overline{i+k}} \qquad k=1,\ldots,32 \tag{4-9}$$

where the subscript with an overbar, $\bar{\alpha}$, is interpreted as

$$\bar{\alpha} = \left[(\alpha - 1) \bmod 32\right] + 1 \tag{4-10}$$

Thus we have a wedge autocorrelation function normalized by the "undiffracted energy" incident on rings one through three.

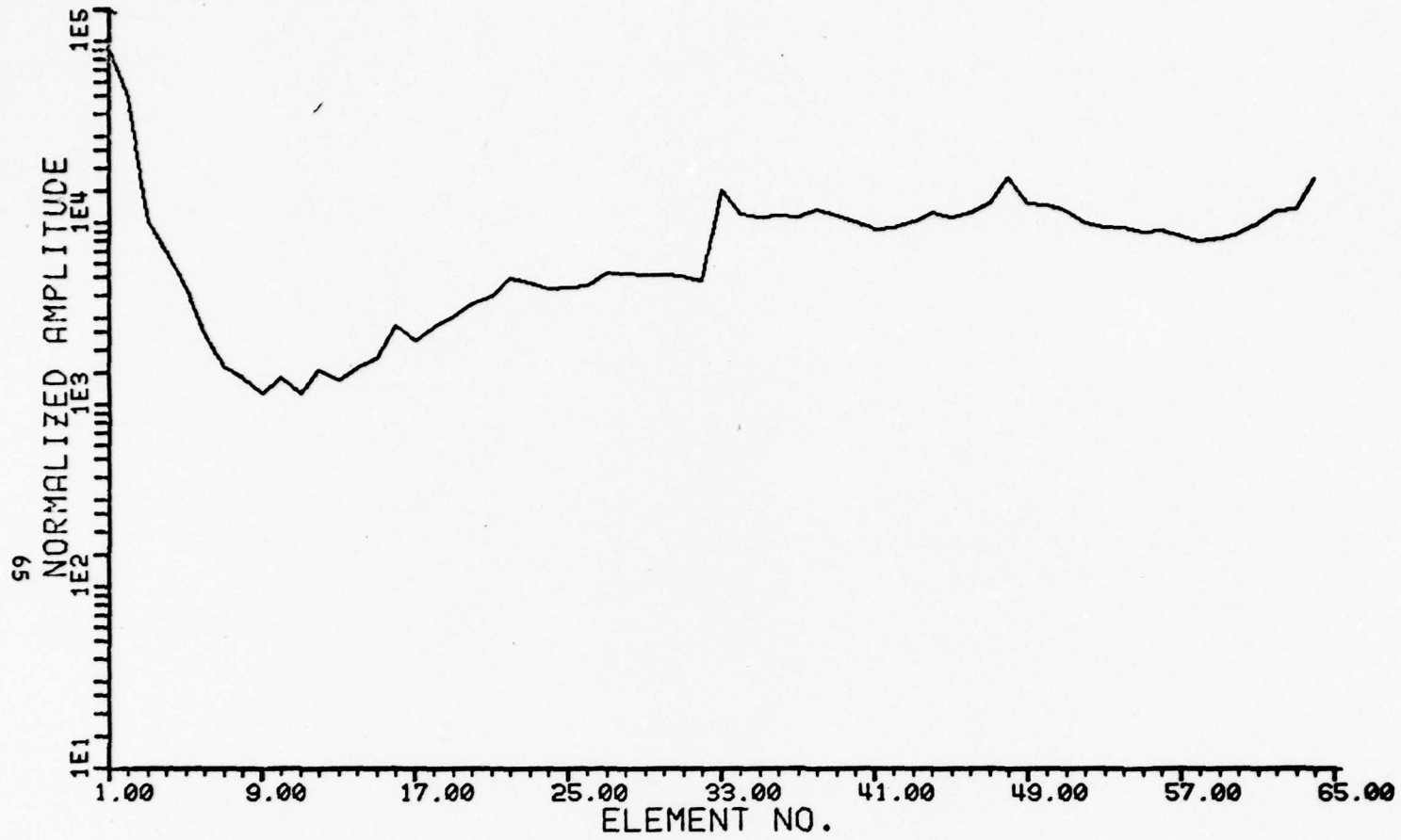

10236 <URBAN> DECISION = URBAN 2MM RADAR
FILE D1.HLK5 .NVD008- /NVD008/DECISIONS USING NVN008-NVN108
05/01/79 09:20

Figure 4-1. Typical Urban Sample (Wedges are Elements 33-64)

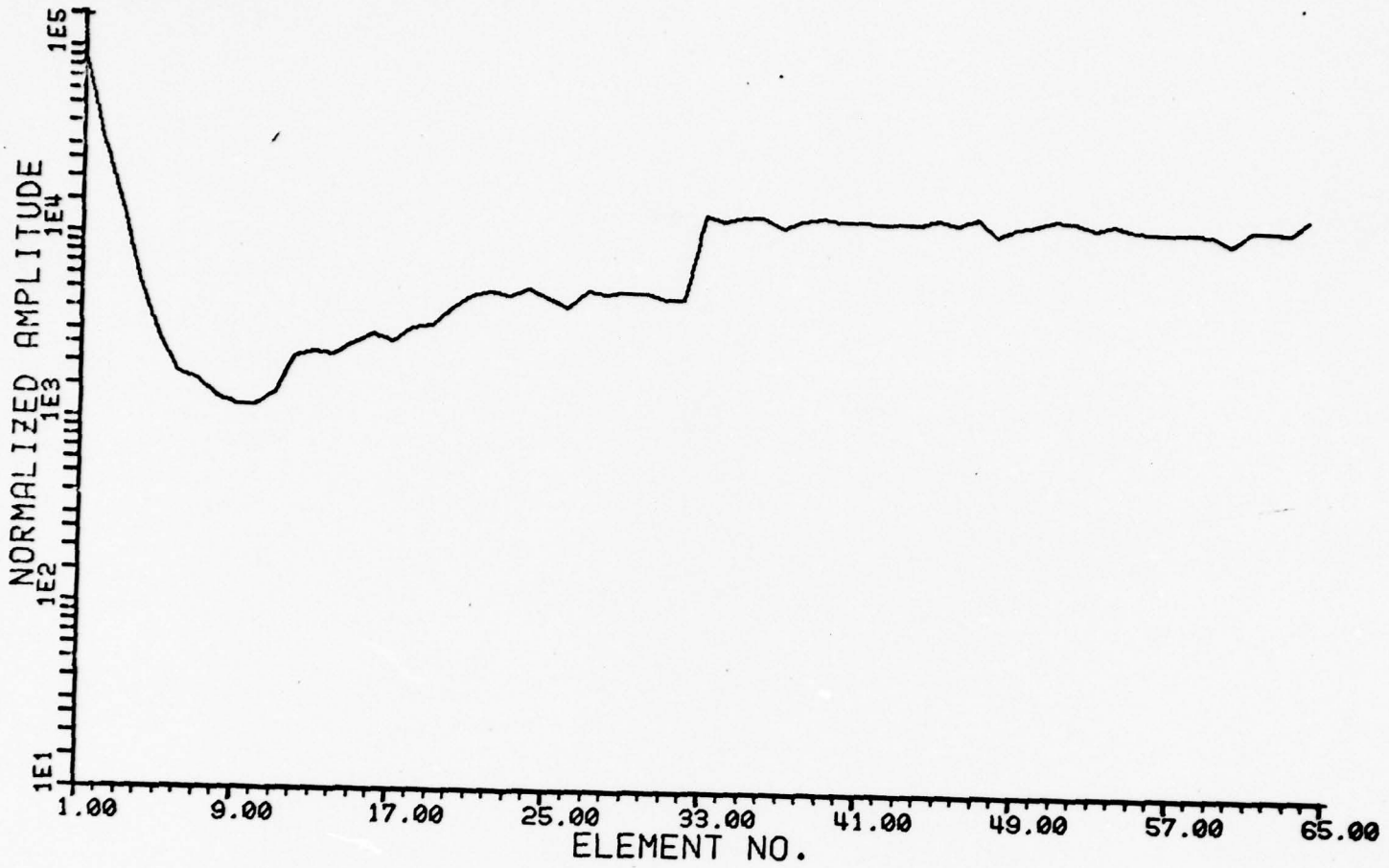

40226 (FOREST) DECISION = FOREST 2MM RADAR
FILE D1.HLK5 .NVD008- /NVD008/DECISIONS USING NVN008-NVN108
05/01/79 09:33

Figure 4-2. Typical Forest Sample (Wedges are Elements 33-64)

4.1.2 --Continued.

This feature set was not quite as effective as $\{w(i)_{13,20}\}$, but was significantly more effective in identifying those sample apertures with specular returns that typify urban areas than the normalized rings F(j,j;4,32). Note that the autocorrelation form is in fact rotationally invariant and furthermore is symmetric about a lag of 15 wedges.

4.1.3 Feature Evaluation Methodology

The basic method used to evaluate the feature families described above was to utilize the features in the general decision rule structure described in the next section. Maximum mutual information analysis was used on a limited basis to evaluate the ability of certain subsets of the feature families to separate particular classes. It was on the basis of just this type of analysis that the decision was made not to differentiate between what appeared to be plowed and non-plowed agricultural land. No significant separation of the two classes appeared to be achievable with any of the feature sets under consideration. In addition it seemed quite difficult to visually justify the initial classification of various apertures into plowed and non-plowed.

4.2 Decision Rule

4.2.1 Motivation

The MISTIC Decision Rule,[1] is perfectly general in the sense that in principle it can handle an arbitrary number of classes and feature vectors with an arbitrary number of components. From a practical

'KLUE04' on each pass must have the same sequence of designators, otherwise processing is terminated.

4.2.1 --Continued.

standpoint, 2^n samples would be required in order to utilize n components. With four classes available, and as few as 31 samples in some classes, an upper limit of four component feature vectors is imposed. In cases where the classes are well separated, four components may well be sufficient to separate the four classes. In this case here, it became obvious after initial investigation of the first data set that effective separation of the classes was not to be accomplished using only four components.

By studying the envelope of the normalized ring values it soon became clear that the urban class had the following property: each individual urban sample had a normalized ring value that exceeded the maximum normalized ring value for each of the other classes. This property defines a region in 32-space. Thus, given a sufficient number of samples, the MISTIC Decision Rule would accurately define this region. However, a small number of samples would not be sufficient for the MISTIC Decision Rule to perform this characterization. On the other hand, a decision rule which successively compared each component from an unknown sample to the maximum, minimum, mean or other selected quantile from the distribution of another class could in fact define this type of decision region in a very simple way.

4.2.2 Decision Rule Definition

Let class i i=1 to 4 be given as follows:

Class 1 = Urban

Class 2 = Water

Class 3 = Agriculture

Class 4 = Forest

4.2.2 --Continued.

Let the regions A_i i=1 to 5 be the regions where the decision action is the following:

A_1 - decide urban
A_2 - decide water
A_3 - decide agriculture
A_4 - decide forest
A_5 - abstain from making a decision

Let the generic feature vector for class i be given by

$$X^i = \left\{x_1^i,\ x_2^i,\ \ldots,\ x_n^i\right\} \tag{4-11}$$

In terms of the foregoing, define the region B_i whose boundaries are an upper bound on the region containing all the class i vectors as follows:

$$B_i = \left\{X : \underline{x}_j^i \le x_j \le \bar{x}_j^i,\ j=1, \ldots, n\right\},\ i=1, 2, 3, \ldots, 4 \tag{4-12}$$

where $\underline{x}_j^i = \min_{\substack{\text{all vectors}\\ \text{in class i}}} x_j^i$

$\bar{x}_j^i = \max_{\substack{\text{all vectors}\\ \text{in class i}}} x_j^i$

Now, the decision action regions A_i, i=1 to 5 are given by

$$A_1 = \left\{X : X \notin B_i,\ i=2, 3, 4\right\} \cap B_1 \tag{4-13a}$$

$$A_2 = \left\{X : X \notin B_i,\ i=3, 4\right\} \cap \bar{A}_1 \cap B_2 \tag{4-13b}$$

$$A_3 = \left\{X : X \notin B_4\right\} \cap \overline{(A_1 \cup A_2)} \cap B_3 \tag{4-13c}$$

$$A_4 = \left\{X : X \notin B_3\right\} \cap \overline{(A_1 \cup A_2 \cup A_3)} \cap B_4 \tag{4-13d}$$

$$A_5 = \overline{(A_1 \cup A_2 \cup A_3 \cup A_4)} = B_3 \cap B_4 \cup (\bar{B}_1 \cap \bar{B}_2 \cap \bar{B}_3 \cap B_4) \tag{4-13e}$$

4.2.3 Decision Rule Properties

The decision rule defined in the previous section has some very interesting properties. Among these are:

1) The rule is hierarchical in nature and can be represented as a tree.

2) Bounds on certain probabilities of misclassification can be determined independent of the underlying distribution. Therefore there is a nonparametric aspect to this rule.

3) An abstention action exists but not for all classes uniformly.

Let us now examine these properties in more detail.

Hierarchical Nature - Figure 4-3 is a representation of the decision rule. The hierarchical nature of the rule can easily be seen from this figure. In the first stage, the urban class is separated from the three other classes. At subsequent levels in the tree, water, then agriculture, then forest are separated from the remaining group. Those samples remaining after the forest classification are by definition the samples that fall in the abstention region for which no decision is made.

Nonparametric Nature - The nonparametric nature of the decision rule concerns an error bound for each class that is independent of the underlying distribution for the particular class. To see this, consider the following:

$$\begin{aligned} \Pr\{\text{Error} \mid \text{Class } i\} &= \Pr\{X \notin A_i \mid \text{Class } i\} \\ &< \Pr\{X \notin B_i \mid \text{Class } i\} \\ &= \Pr\{X : x_j < \underline{x}_j^i \text{ for some } j \\ &\qquad \text{or } x_j > \bar{x}_j^i \text{ for some } j\} \end{aligned} \tag{4-14}$$

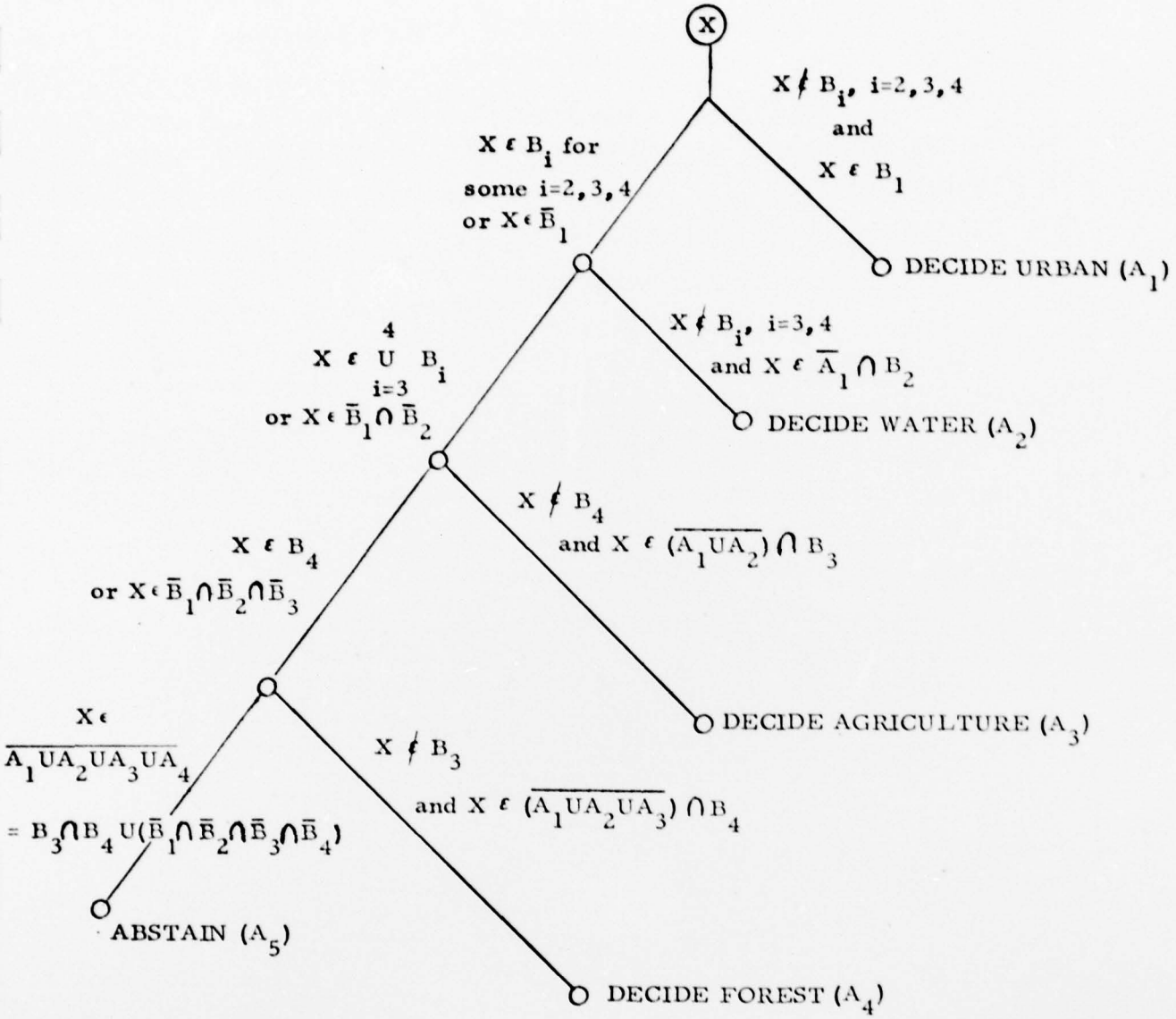

Figure 4-3. Hierarchical Tree Representation of Decision Rule

4.2.3 --Continued.

The last probability is precisely the probability of at least one component exceeding the n^{th} order statistic or being less than the 1st order statistic given n-samples. Determining these probabilities is precisely the problem of determining the probability of the first and last coverage associated with the order statistics $\left\{\left(x_j^i\right)_k\right\}$. This can be done independent of the actual distribution of the x_j^i (see Ref. 2). Thus a bound on the probability of misclassification can be determined without knowing the actual distribution.

Abstention Region - The reject region A_5 is defined as

$$A_5 = \overline{(A_1 \cup A_2 \cup A_3 \cup A_4)}$$

By application of DeMorgan's Law and the distributive property of Boolean operators, it can be shown that

$$A_5 = B_3 \cap B_4 \cup \left[\bar{B}_1 \cap \bar{B}_2 \cap \bar{B}_3 \cap \bar{B}_4\right]$$

Note that this reject region is defined only in terms of the region for accepting class 3 and class 4 simultaneously or rejecting all classes.

This obviously does not limit samples from other classes from being in this region. However the form of the rule is such that at least in the training set no sample from agriculture or forest can be misclassified. This is easy to see from the tree representation of the rule in Figure 4-3. Any sample that is outside of both B_3 and B_4 is not, by definition, agriculture or forest. Thus, for members of either of these two classes only three possibilities exist. A forest sample is only within B_4; an agriculture sample is only within B_3; or a sample from either one is in $B_3 \cap B_4$. Thus either the sample is correctly classified or falls in the common region and is assigned an abstention action.

4.2.4 Specific Realizations of the Decision Rule for Panchromatic, Radar and Thermal Imagery Cases

During the course of the analysis, additional subclasses were defined in order to better understand the performance of the decision rule. Specifically, new water classes were defined for the two river regions in the panchromatic and radar imagery when observation of the initial class statistics showed an apparent grouping into two distinct groups of the water samples. In the panchromatic imagery, Water (50) texture appears nonuniform compared to Water (60). The reflectance from Water (50) varies depending on the distance from the shoreline. The reflectance from Water (60) appears constant independent of the distance from the shoreline. In the radar imagery, the distinction between the two water classes is slight. Water (50) is not quite as dark as Water (60), but there is no variation depending on distance from the shore.

Similarly, the initial objective was to classify agriculture into plowed and non-plowed classes. Therefore these class distinctions were carried through the entire analysis. Using the notation developed above, the following figures define the exact decision rules used for the panchromatic, radar and thermal imagery cases. Also indicated in each figure is the form of the feature family used.

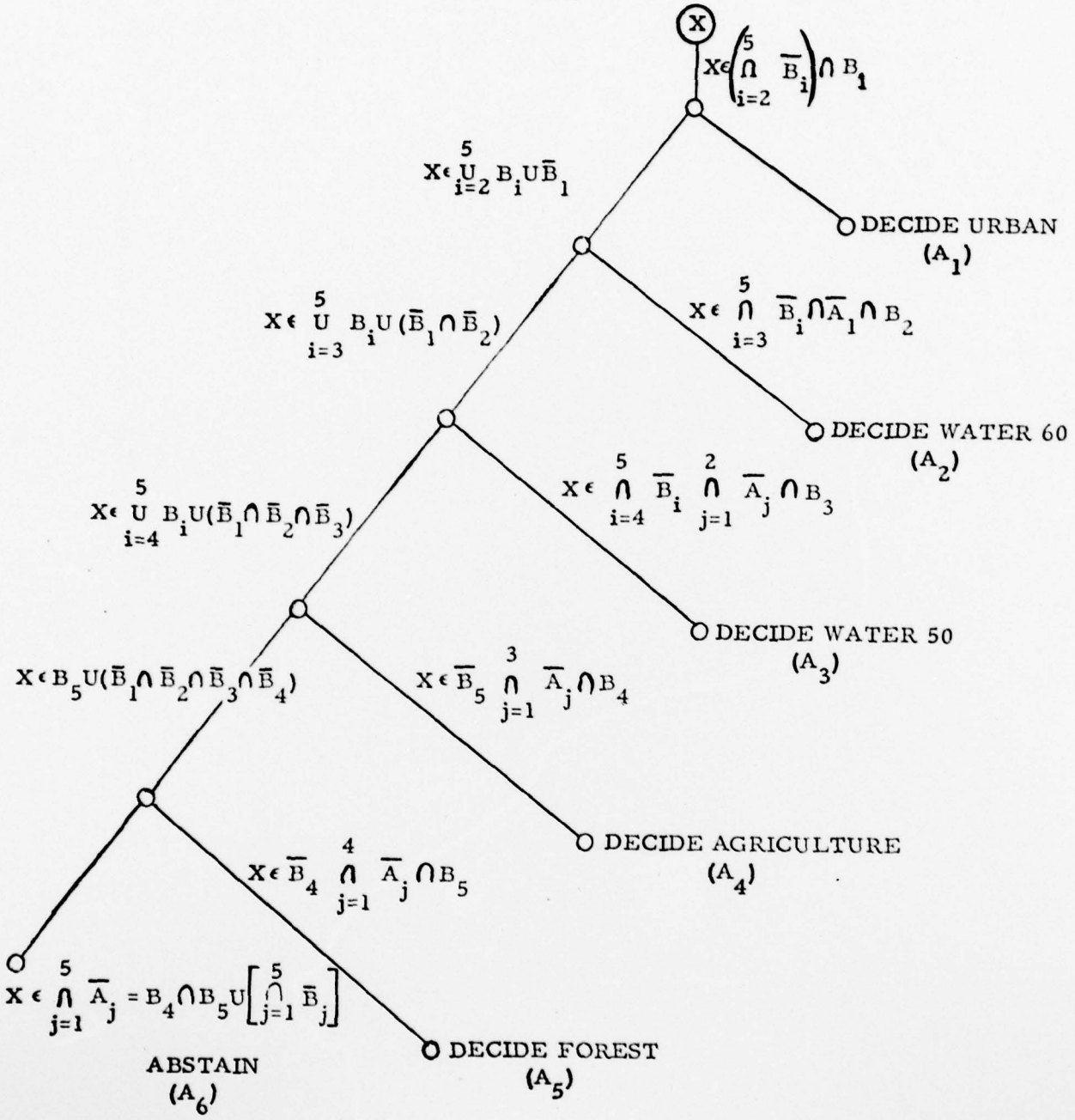

Figure 4-4a. Decision Rule and Features for Panchromatic Imagery

Acceptance Regions

B_i, i = 1, 2, 3, 4, 5 given by Equation (4-12).

Feature Vectors (see Section 4.1)

X^i, i = 1, 2, 3

$$\left\{x_j^i\right\} = \left\{\frac{r_j}{\sum_{n=4}^{32} r_n}\right\} \qquad j = 1, 32$$

$$\left\{x_j^i\right\} = \left\{\left(\left|\frac{\Delta w}{\bar{w}}\right|\right)_{j-32}\right\} \qquad j = 33, 64$$

X^i, i = 4, 5

$$\left\{x_j^i\right\} = \left\{\frac{r_j}{\sum_{n=4}^{32} r_n}\right\} \qquad j = 1, 32$$

$$\left\{x_j^i\right\} = \left\{\left(\left|\frac{\Delta w}{\bar{w}}\right|\right)_{j-32}\right\} \qquad j = 33, 64$$

$$\left\{x_j^i\right\} = \left\{\left(\left|\frac{\Delta w}{(|\Delta w|)_{32}}\right|\right)_{j-64}\right\} \qquad j = 65, 96$$

Figure 4-4a. (continued)

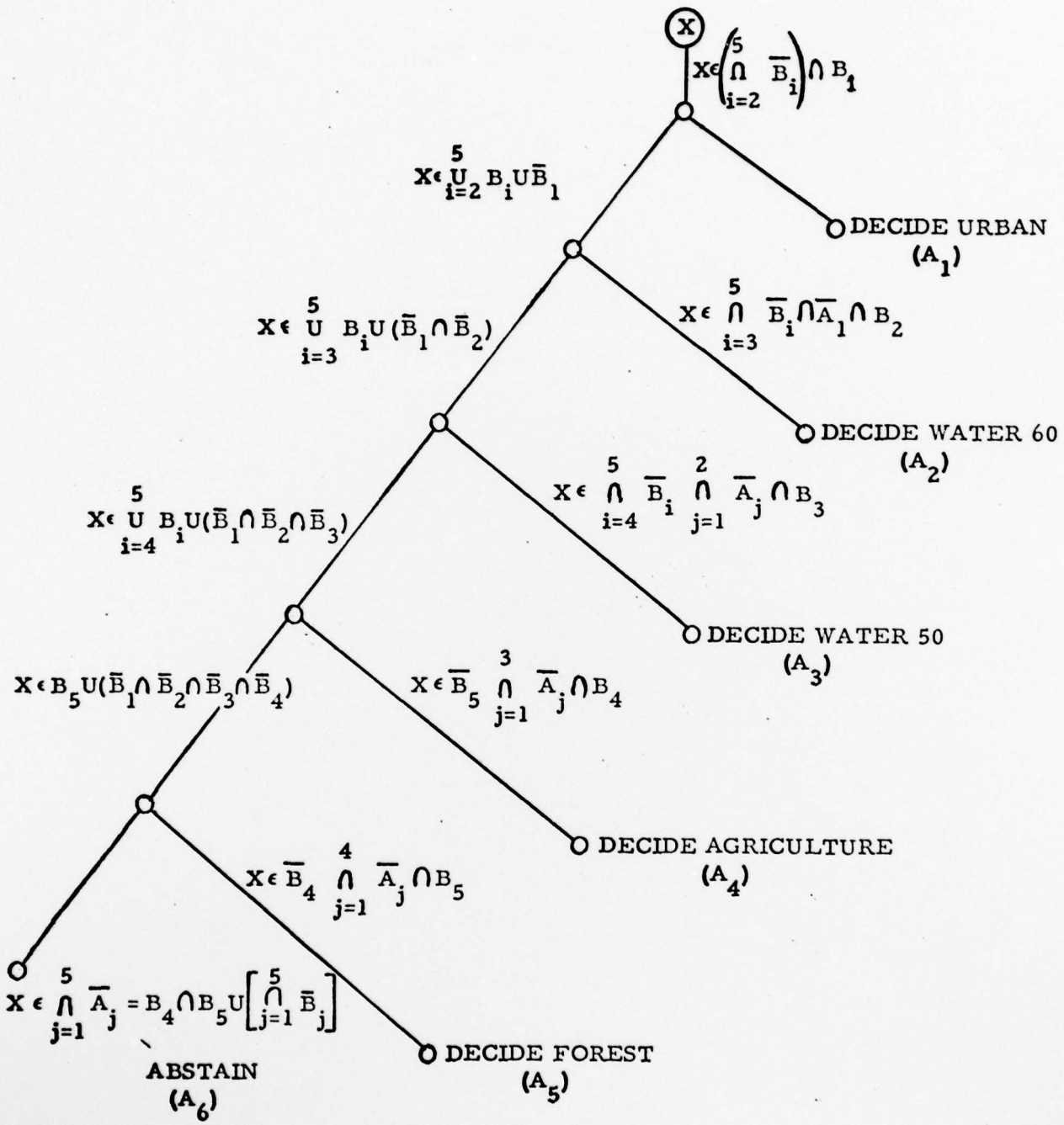

Figure 4-4b. Decision Rule and Features for Radar Imagery

Acceptance Regions

B_i, i = 1, 2, 3, 4, 5 given by Equation (4-12).

Feature Vectors (see Section 4.1)

X^i, i = 1, 2, 3

$$\left\{x_j^i\right\} = \left\{\frac{r_j}{\sum_{n=4}^{32} r_n}\right\} \qquad j = 1, 32$$

$$\left\{x_j^i\right\} = \left\{\frac{w_{j-32}}{\sum_{n=13}^{20} w_n}\right\} \qquad j = 33, 64$$

X^i, i = 4, 5

$$\left\{x_j^i\right\} = \left\{\frac{r_j}{\sum_{n=4}^{32} r_n}\right\} \qquad j = 1, 32$$

$$\left\{x_j^i\right\} = \left\{\frac{w_{j-32}}{\sum_{n=13}^{20} w_n}\right\} \qquad j = 33, 64$$

$$\left\{x_j^i\right\} = \left\{\frac{r_{j-64}}{\sum_{n=1}^{3} r_n}\right\} \qquad j = 65, 96$$

$$\left\{x_j^i\right\} = \left\{\frac{1}{\sum_{n=1}^{3} r_n} \sum_{k=1}^{32} w_{\bar{k}}\, w_{k+j-96}\right\} \qquad j = 97, 128$$

$$\bar{\alpha} = \left[(\alpha - 1) \bmod 32\right] + 1$$

Figure 4-4b. (continued)

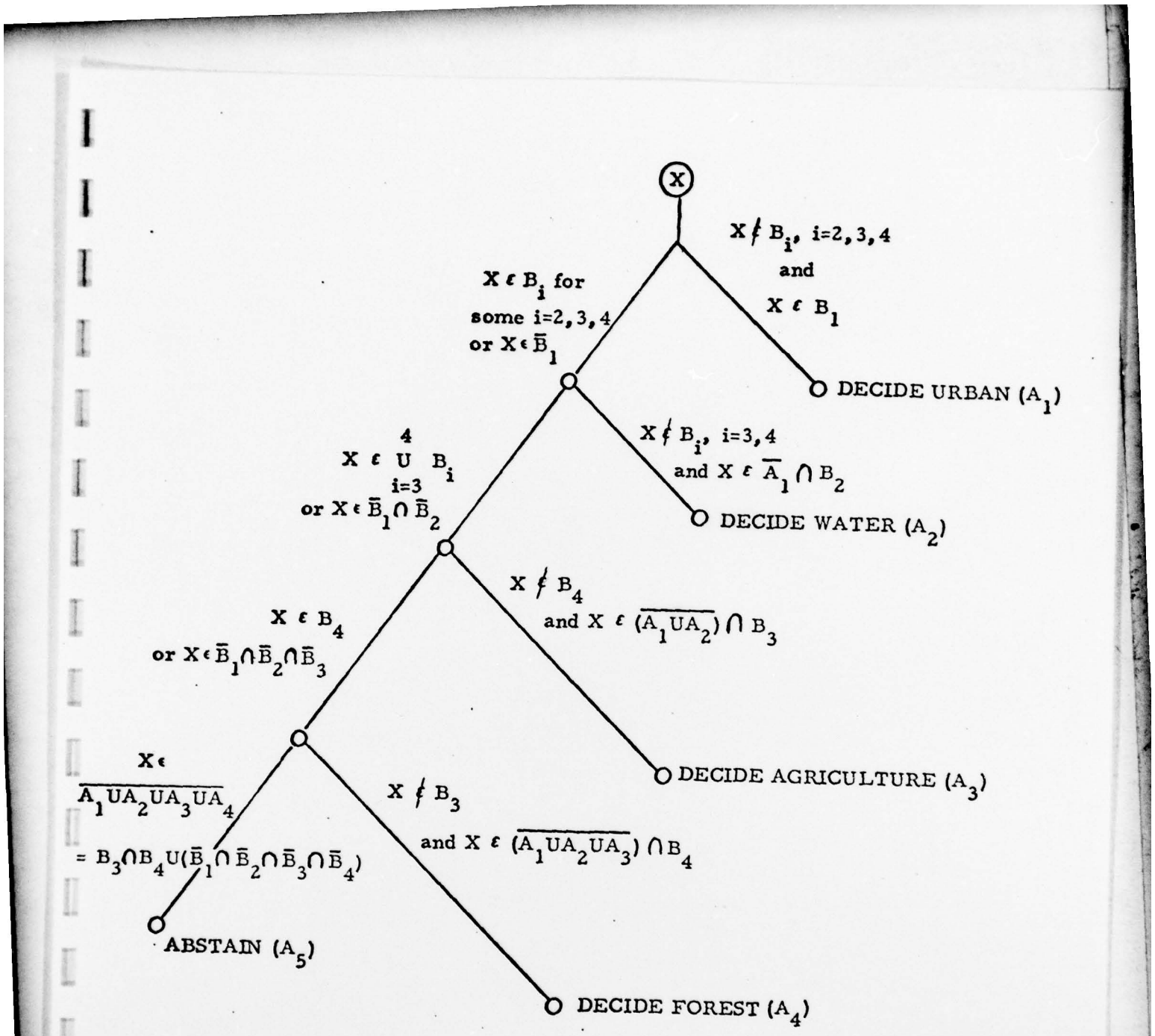

Figure 4-4c. Decision Rule and Features for Thermal Imagery

Acceptance Regions

B_i, i = 1, 2, 3, 4, 5 given by Equation (4-12).

Feature Vectors (see Section 4.1)

X^i, i = 1, 2, 3

$$\left\{x_j^i\right\} = \left\{\frac{r_j}{\sum_{n=4}^{32} r_n}\right\} \qquad j = 1, 32$$

$$\left\{x_j^i\right\} = \left\{\left(\left|\frac{\Delta w}{\bar{w}}\right|\right)_{j-32}\right\} \qquad j = 33, 64$$

X^i, i = 4, 5

$$\left\{x_j^i\right\} = \left\{\frac{r_j}{\sum_{n=4}^{32} r_n}\right\} \qquad j = 1, 32$$

$$\left\{x_j^i\right\} = \left\{\left(\left|\frac{\Delta w}{\bar{w}}\right|\right)_{j-32}\right\} \qquad j = 33, 64$$

$$\left\{x_j^i\right\} = \left\{\left(\left|\frac{\Delta w}{(|\Delta w|)_{32}}\right|\right)_{j-64}\right\} \qquad j = 65, 96$$

'Figure 4-4c. (continued)

REFERENCES FOR SECTION 4

1. H. L. Kasdan, "A Distribution-Free Pattern Classification Procedure with Performance Monitoring Capability", Techniques of Optimization, ed. A.V. Balakrishnan, Academic Press, Inc., New York, 1972.

2. R.V. Hogg and A.T. Craig, Introduction to Mathematical Statistics, 2nd edition, The Macmillan Company, New York, 1967, Chapter 6.

5.0 QUANTITATIVE STATISTICAL EVALUATION OF DECISION RESULTS

5.1 Statistical Formulation of the Study Questions

The general question posed by this study is: What difference in terrain decision performance is there (if any) for optical power spectrum analysis of panchromatic, radar and thermal imagery? Referring to the experiment design (Figure 3-1), this broad question may be framed as several more specific questions:

1) Are the overall decision results different when comparing 2 mm sampled panchromatic to 2 mm sampled radar to 10 mm sampled thermal (equivalent to 2 mm when scale is taken into account)?

2) Considering the portion of the experiment design comparing panchromatic and radar imagery sampled with identical apertures:

   a) Is the overall decision performance different for panchromatic and radar imagery when all aperture sizes are taken into account?

   b) Is there a significant difference between the ability to recognize specific terrain types for panchromatic imagery compared to radar?

   c) Does aperture size affect overall decision performance or performance for any particular terrain type independent of imagery type.

3) Does aperture size affect the decision performance for panchromatic imagery? For radar imagery?

5.2 Statistical Framework

Two statistical tests can be used to answer all of the questions above. Questions 1 and 3 are answered by applying a form of the χ^2 Test[1] to test for the equality of two multinomial distributions with unknown subgroup probabilities. An analysis of variance based on a linear hypothesis model[2] is used to develop the answers to question 2.

5.2.1 Chi Square Test for Multinomial Equivalence

Considered two independent multinomial distributions with parameters given as follows:

$$n_j,\ p_{1j},\ p_{2j},\ \ldots,\ p_{kj},\quad j = 1,2$$

$$X_{ij},\quad i = 1, 2, \ldots, k\ ,\ j = 1, 2 \qquad (5\text{-}1)$$

the corresponding observed frequencies

If n_1 and n_2 are large, then the random variable

$$\widetilde{\chi^2} = \sum_{j=1}^{2} \sum_{i=1}^{k} \frac{(X_{ij} - n_j p_{ij})^2}{n_j p_{ij}} \qquad (5\text{-}2)$$

is a sum of two stochastically independent random variables each chi square with k-1 degrees freedom. Therefore in the limit as n_1 and n_2 approach infinity, $\widetilde{\chi^2}$ approaches a chi square random variable with 2k-2 degrees freedom.

5.2.1 --Continued.

The two multinomial distributions will be identical if $p_{11} = p_{12}$, $p_{21} = p_{22}$, and so on. Thus, the null hypothesis is given by

$$H_0: \quad p_{11} = p_{12}, \quad p_{21} = p_{22}, \ldots, p_{k1} = p_{k2}$$

$$\text{with each } p_{i1} = p_{i2} \tag{5-3}$$

$$i = 1, 2, \ldots, k \text{ unspecified.}$$

Since the subgroup probabilities are unknown, we may use a maximum likelihood estimate for $p_{i1} = p_{i2}$ given by

$$\hat{p}_i = (X_{i1} + X_{i2})/(n_1 + n_2)$$

$$i = 1, 2, \ldots, k \tag{5-4}$$

When this estimate is substituted into equation (5-2) we get the following statistic

$$\tilde{\chi}^2 = \sum_{j=1}^{2} \sum_{i=1}^{k} \frac{\left\{X_{ij} - n_j \left[(X_{i1} + X_{i2})/(n_1 + n_2)\right]\right\}^2}{n_j \left[(X_{i1} + X_{i2})/(n_1 + n_2)\right]} \tag{5-5}$$

This random variable approaches a chi square distribution with k-1 degrees of freedom. Notice that when $n_1 = n_2 = n$, the expression for χ^2 simplifies to

$$\tilde{\chi}^2 = 2 \sum_{i=1}^{k} \frac{\left\{X_{ij} - \frac{1}{2}(X_{i1} + X_{i2})\right\}^2}{(1/2)(X_{i1} + X_{i2})} \tag{5-6}$$

AD-A076 566 RECOGNITION SYSTEMS INC VAN NUYS CALIF F/G 5/8
FEASIBILITY OF USING OPTICAL POWER SPECTRUM ANALYSIS TECHNIQUES--ETC(U)
JUN 79 H L KASDAN DAAK70-78-C-0019
UNCLASSIFIED KS-77-370 ETL-0186 NL

2 OF 3
AD A076566

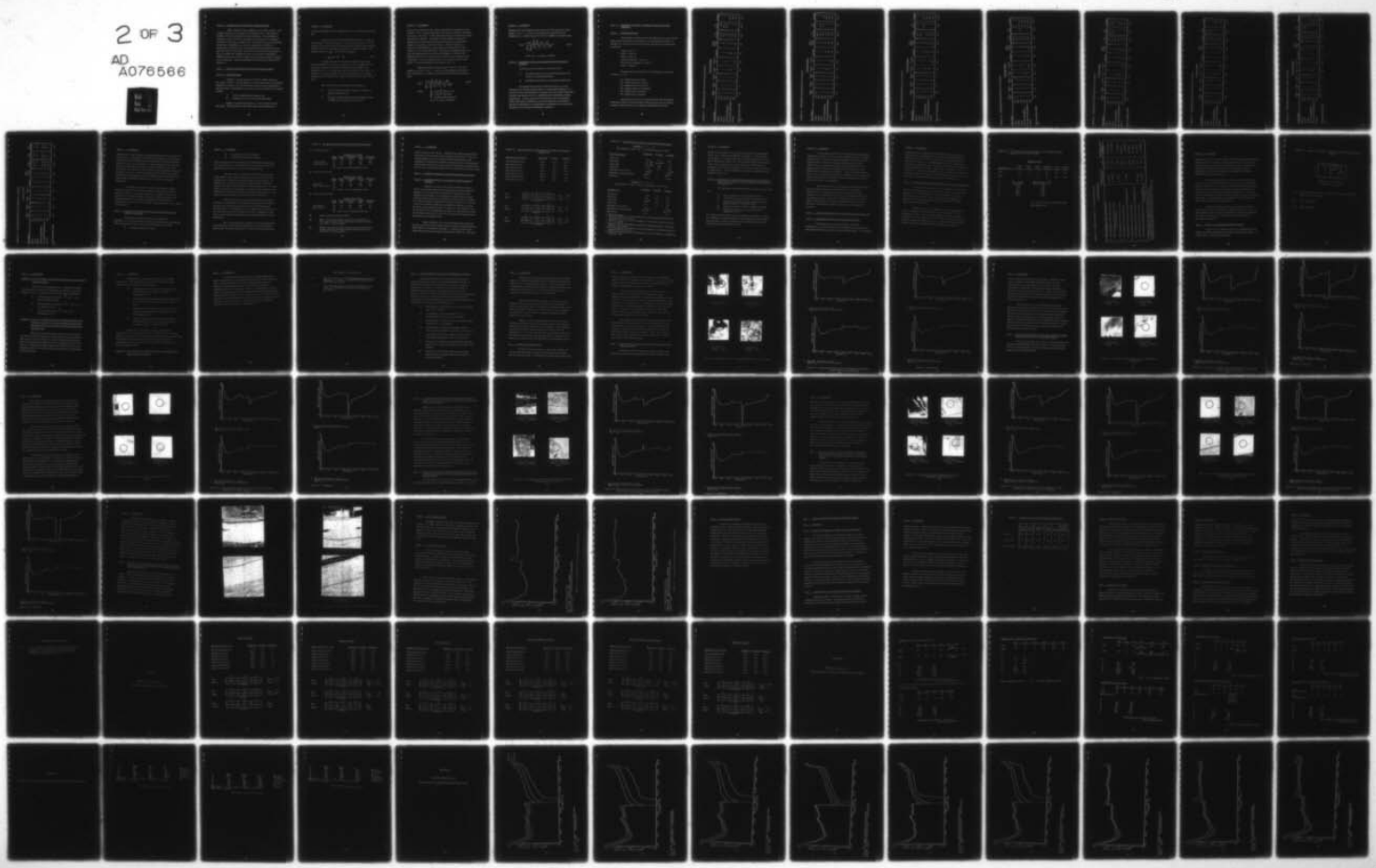

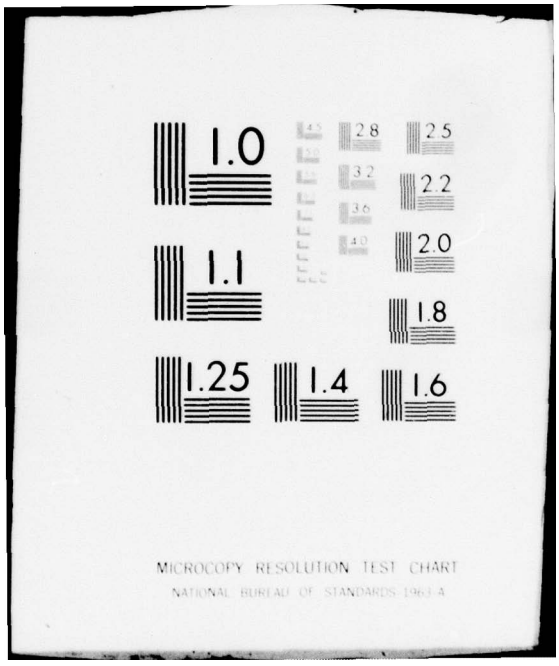
1.0
1.1
1.25
1.4
1.6
2.0
1.8
2.2
2.5
2.8
3.2
3.6
4.0
MICROCOPY RESOLUTION TEST CHART
NATIONAL BUREAU OF STANDARDS 1963-A

5.2.1.2 Applications of the Chi Square Multinomial Test

When a decision rule is applied to a set of data samples, each sample within the set is assigned to a particular class. This effects a partition of the data samples in various subgroups. The probability of observing a given number in each subgroup corresponds to a particular realization for the X_{ij} in equation (5-1). In general, the p_{ij} are determined by the prior probability of a given class occurring as well as the performance of decision rule. Assuming that the only effect on the true p_{ij} is the effect of the decision rule, then if we reject the null hypothesis, H_0, at a suitably low significance level, we have made a statistically significant statement that the results of the two decision making operations are not equivalent. Specific applications of this test will be discussed in Section 5.3.

5.2.2 Analysis of Variance for the Linear Hypothesis Model

5.2.2.1 Test Description

Consider a random process in which two effects operate on the random variable. For each effect, we wish to determine if a statistically significant variation in the observed value has been caused independent of the other effect. Specifically in our case, we have two effects on the decision results:

1) radar or panchromatic imagery, and
2) aperture size (2, 4 or 6 mm Gaussian beam).

Suppose we labeled the columns 2, 4 and 6 and the rows pan and radar. We could choose as the entries the overall probability of

5.2.2.1 --Continued.

correct classification for the specific case, i.e., 2mm pan, 4mm radar, etc.

In general, we may develop the following model. Assume a matrix with a rows and b columns. For each row one of the treatments is held constant and for each column the other treatment is held constant. Denote each entry in the table by X_{ij} and the mean value of these entry random variables as μ_{ij}. We may now write μ_{ij} as

$$\mu_{ij} = \mu + \alpha_i + \beta_i \qquad (5\text{-}7)$$

We thus basically wish to test the hypothesis that the α_i are all individually zero - or the results by row are not different. For the second treatment we wish to test whether or not the β_j are all individually zero - or results from column to column are the same. An analysis of variance procedure is used to compare the row or column variation to the variation of the entries with respect to the overall mean value.

This model assumes the following key properties:

1) The row effects and column effects are additive as shown in equation (5-7).

2) The X_{ij} are independent normally distributed random variables each with identical variance σ^2.

5.2.2.1 --Continued.

It is not clear exactly how the effects of aperture size and imagery type combine. Thus, at least at this stage of the game the additive assumption is as good as any other. A fairly strong case can be made that the second assumption is satisfied. The entries are the results of independent experiments so that in fact the decision results from one experiment should be independent of those for another. Since the entries are estimates of probabilities of error, correct or reject, they are the result of a sum of Bernoulli trials. This sum for sufficiently large N is very well approximated by the normal distribution. Under the null hypothesis that there is no column or row effect, all the variances will be identical. They are estimates of the same random variable which follows a binomial distribution with variance np (1 - p).

With the foregoing in mind, it can be shown that the null hypothesis H_0: $\beta_j = 0$ (j=1, ..., b) can be tested using the right tail of the F-distribution as a critical region where the following F-statistic is used.

$$F_{col} = \frac{(a-1)\sum_{i=1}^{a}\sum_{j=1}^{b}(\overline{X}_{.j} - \overline{\overline{X}})^2}{\sum_{i=1}^{a}\sum_{j=1}^{b}(X_{ij} - \overline{X}_{i.} - \overline{X}_{j.} + \overline{\overline{X}})^2} \qquad (5\text{-}8)$$

where, $\overline{X}_{.j}$ is the j^{th} column mean
$\overline{X}_{i.}$ is the i^{th} row mean
$\overline{\overline{X}}$ is the overall entry mean
$\nu_1 = b-1$ and $\nu_2 = (a-1)(b-1)$

5.2.2.1 --Continued.

Similarly, the null hypothesis that assumes the row means to be equal, $H_0: \alpha_i = 0$ (i=1, ..., a) may be tested using the right tail of the F-distribution as a critical region where the F-statistic is computed using

$$F_{row} = \frac{(b-1) \sum_{j=1}^{b} \sum_{i=1}^{a} (\bar{X}_{i.} - \bar{X})^2}{\sum_{i=1}^{a} \sum_{j=1}^{b} (X_{ij} - \bar{X}_{i.} - \bar{X}_{.j} + \bar{X})^2} \qquad (5\text{-}9)$$

where $\nu_1 = a-1$ and $\nu_2 = (a-1)(b-1)$

5.2.2.2 Applications of the Linear Hypothesis Model Analysis of Variance

In our case, the two effects we wish to test are:

1) the effect of the radar or panchromatic sensor data source on decision performance

2) the effect of aperture size on decision performance

By applying the analysis of variance procedure, we will determine if the results obtained differ in a statistically significant way for radar versus pan independent of aperture size and whether independent of sensor type aperture size is a significant factor influencing decision performance. Various measures of performance will be investigated. These will include probability of correct classification, probability of incorrect classification, and probability of abstaining from a decision for all classes and for classes individually considered.

5.3 Discussion of Results - Statistical Answers to the Study Questions

5.3.1 Confusion Matrices

The confusion matrices for the eight different cases represented in the experiment design tree of Figure 3-1 are presented in Tables 5-1 through 5-8. For the pan and radar imagery, the data was classified into six classes:

- Urban - class 10
- Water - class 15
- Water - class 60
- Plowed Agriculture - class 20
- Non-Plowed Agriculture - class 70
- Forest - class 40

Decision actions developed from the decision rule described in Section 4.2 were:

- 10 - decide in favor of urban
- 50 - decide in favor of water 50
- 60 - decide in favor of water 60
- 80 - decide in favor of agriculture
- 40 - decide in favor of forest
- 90 - abstain from a decision

Two classes of water were maintained both in the description of the data samples and for the decision actions because the two samples of water available in the data set appeared quite different visually.

TABLE 5-1. CONFUSION MATRIX 1MM PAN HARD CLIPPED

True Class		Decision Action: Urban 10	Water 50	Water 60	Agric. 80	Forest 40	Abstain	True Class Total	% Correct	% Error	Abstain
Urban	10	29	0	0	0	2	0	31	93.5	6.4	0
Water	50	0	5	0	6	0	0	11	45.4	54.5	0
Water	60	0	0	2	0	24	0	26	7.6	92.3	0
Plowed Agriculture	20	0	0	0	61	0	22	83	73.4	0	26.5
Non-plowed Agriculture	70	0	0	0	31	0	17	48	64.5	0	35.4
Forest	40	0	0	0	0	193	21	214	90.1	0	9.8
Decision Action Total		29	5	2	108	219	60	413	68.1	21.8	9.8

TABLE 5-2. CONFUSION MATRIX 2MM PAN GAUSSIAN

		Decision Action									
True Class		Urban 10	Water 50	Water 60	Agric. 80	Forest 40	Abstain	True Class Total	% Correct	% Error	Abstain
Urban	10	31	0	0	0	0	0	31	100.0	0	0
Water	50	0	9	0	2	0	0	11	81.8	18.1	0
Water	60	0	0	23	0	2	1	26	88.4	7.6	3.8
Plowed Agriculture	20	0	0	0	48	0	35	83	57.8	0	42.1
Non-plowed Agriculture	70	0	0	0	33	0	15	48	68.7	0	31.2
Forest	40	0	0	0	0	159	55	214	74.2	0	25.7
Decision Action Total		31	9	23	83	161	96	413	80.6	2.6	16.6

TABLE 5-3. CONFUSION MATRIX 4MM PAN GAUSSIAN

True Class		Decision Action: Urban 10	Water 50	Water 60	Agric. 80	Forest 40	Abstain	True Class Total	% Correct	% Error	Abstain
Urban	10	30	0	0	0	1	0	31	96.7	3.2	0
Water	50	0	11	0	0	0	0	11	100.0	0	0
Water	60	0	0	0	1	10	15	26	0	42.3	57.6
Plowed Agriculture	20	0	0	0	63	0	20	83	75.9	0	24.0
Non-plowed Agriculture	70	0	0	0	38	0	10	48	79.1	0	20.8
Forest	40	0	0	0	0	168	46	214	78.5	0	21.5
Decision Action Total		30	11	0	102	179	91	413	70.5	8.2	18.5

TABLE 5-4. CONFUSION MATRIX 6MM PAN GAUSSIAN

		Decision Action									
True Class		Urban 10	Water 50	Water 60	Agric. 80	Forest 40	Abstain	True Class Total	% Correct	% Error	Abstain
Urban	10	31	0	0	0	0	0	31	100.0	0	0
Water	50	0	11	0	0	0	0	11	100.0	0	0
Water	60	0	0	6	0	15	5	26	23.0	57.6	19.2
Plowed Agriculture	20	0	0	0	64	0	19	83	77.1	0	22.8
Non-plowed Agriculture	70	0	0	0	38	0	10	48	79.1	0	20.8
Forest	40	0	0	0	0	185	29	214	86.4	0	13.5
Decision Action Total		31	11	6	102	200	63	413	77.5	10.1	12.2

TABLE 5-5. CONFUSION MATRIX 2MM RADAR GAUSSIAN

True Class		Decision Action: Urban 10	Water 50	Water 60	Agric. 80	Forest 40	Abstain	True Class Total	% Correct	% Error	Abstain
Urban	10	20	0	0	0	4	2	26	76.9	15.3	7.6
Water	50	0	5	0	1	1	2	9	55.5	22.2	22.2
Water	60	0	0	19	0	0	0	19	100.0	0	0
Plowed Agriculture	20	0	0	0	60	0	12	72	83.3	0	16.6
Non-plowed Agriculture	70	0	0	0	45	0	8	53	84.9	0	15.0
Forest	40	0	0	0	0	199	12	211	94.3	0	5.6
Decision Action Total		20	5	19	106	204	36	390	85.2	5.6	9.0

TABLE 5-6. CONFUSION MATRIX 4MM RADAR GAUSSIAN

		Decision Action									
True Class		Urban 10	Water 50	Water 60	Agric. 80	Forest 40	Abstain	True Class Total	% Correct	% Error	Abstain
Urban	10	22	0	0	2	2	0	26	84.6	15.3	0
Water	50	0	6	0	3	0	0	9	66.6	33.3	0
Water	60	0	0	12	7	0	0	19	63.1	36.8	0
Plowed Agriculture	20	0	0	0	63	0	9	72	87.5	0	12.5
Non-plowed Agriculture	70	0	0	0	50	0	3	53	94.3	0	5.6
Forest	40	0	0	0	0	205	6	211	97.1	0	2.8
Decision Action Total		22	6	12	125	207	18	390	84.0	12.7	3.0

TABLE 5-7. CONFUSION MATRIX 6MM RADAR GAUSSIAN

		Decision Action									
True Class		Urban 10	Water 50	Water 60	Agric. 80	Forest 40	Abstain	True Class Total	% Correct	% Error	Abstain
Urban	10	23	0	0	1	2	0	26	88.4	11.5	0
Water	50	0	6	0	3	0	0	9	66.6	33.3	0
Water	60	0	0	19	0	0	0	19	100.0	0	0
Plowed Agriculture	20	0	0	0	65	0	7	72	90.2	0	9.7
Non-plowed Agriculture	70	0	0	0	50	0	3	53	94.3	0	5.6
Forest	40	0	0	0	0	202	9	211	95.7	0	4.2
Decision Action Total		23	6	19	119	204	19	390	91.3	5.5	3.0

TABLE 5-8. CONFUSION MATRIX 10MM THERMAL GAUSSIAN

True Class		Decision Action: Urban 10	Water 50	Agric. 80	Forest 40	Abstain	True Class Total	% Correct	% Error	% Abstain
Urban	10	59	0	4	1	0	64	92.19	7.8	0
Water	50	0	33	0	1	20	54	61.11	1.9	37.0
Other	30	21	2	13	14	12	62			
Plowed Agriculture	20	0	0	25	7	17	49	51.62	14.3	34.7
Non-plowed Agriculture	70	0	0	23	8	13	44	52.27	18.2	29.5
Forest	40	0	0	0	41	0	41	100.00	0	0
Decision Action Total		80	35	65	72	62	314	76.2	6.5	17.3

5.3.1 --Continued.

Initial decision results indicated significant differences in the two types of water involved. Both plowed and non-plowed agriculture were designated as separate classes initially in order to determine if accurate separation of these two classes was possible. For the panchromatic and radar data sets it was quite difficult visually to determine whether or not a field was plowed. Thus there was some question in the ground truth assignment for these two classes. Since the ground truth assignments were suspect and initial results indicated no clear distinctions between the two classes, only a single agriculture decision class was used in the subsequent experiments.

In addition to the number entries in the confusion matrix, summaries by class of the percent correct, percent error and percent abstain are listed. The overall percentages are obtained by averaging the values for each class equally. Thus, for example, in Table 5-1 the overall probability of correct percent equal to 68.1 is obtained by averaging 93.5, (45.4 X 11 + 7.6 X 26)/37 = 18.8, (73.4 X 83 + 64.5 X 48)/131 = 70.1 and 90.1.

5.3.2 Comparison of Panchromatic, Radar and Thermal Imagery Decision Performance

The chi square test for equivalence of multinomial distribution was used to compare the decision performance for panchromatic, radar and thermal imagery. Three pairs of comparisons are used:

1) 2 mm pan versus 2 mm radar

5.3.2 --Continued.

2) 2 mm pan versus 10 mm thermal

3) 2 mm radar versus 10 mm thermal

These comparisons are for aperture sizes that include approximately the same ground area. The comparisons are based on the number of samples the decision rule assigns to each decision class.

In order to allow a comparison with the thermal imagery which contains only a single water class, water 50 and water 60 are combined into a single class for both the pan and radar imagery. In addition, the number of samples in each decision class normalized relative to the number of true samples in that particular class. In order to get a comparable set of frequency observations, the percentages are multiplied by the number of samples in the class for pan imagery. Thus in this sense observations are normalized to the pan imagery.

Table 5-9 contains the normalized frequency observations for the three comparisons. Also indicated in each case is the value of the chi square variable computed from the data and how this value compares to the 1% significance level. We notice that in all three cases the value of the chi square variable exceeds the 1% significance level. Thus we can conclude that the performance is different for pan, radar and thermal.

If we use the chi square variable as a measure of closeness of performance, we note that the performance for pan and thermal is closest with a chi square value of 14.3. Next is radar versus thermal

Table 5-9. Pan/Radar/Thermal Decision Performance Comparison

a) Pan versus Radar

	Decision Class Label				
	Urban (10)	Water (50)	Agriculture (80)	Forest (40)	Ambiguous (90)
2 mm Pan (1)	31	32	83	161	106
2 mm Radar (2)	24	32	111	207	39

$\tilde{\chi}^2 = 41.19 > 13.3$ (1% significance level)

b) Pan versus Thermal

	Decision Class Label				
	Urban (10)	Water (50)	Agriculture (80)	Forest (40)	Ambiguous (90)
2 mm Pan	31	32	83	161	106
10 mm Thermal (3)	29	23	66	214	81

$\tilde{\chi}^2 = 14.31 > 13.3$ (1% significance level)

c) Radar versus Thermal

	Decision Class Label				
	Urban (10)	Water (50)	Agriculture (80)	Forest (40)	Ambiguous (90)
2 mm Radar	24	32	111	207	39
10 mm Thermal	29	23	66	214	81

$\tilde{\chi}^2 = 28.2 > 13.3$ (1% significance level)

(1) Actual number of decision samples.

(2) Number of decision samples chosen to be the fraction of Pan samples closest to the actual fraction of Radar samples, e.g. 20/26 ≈ 24/31 for Urban.

(3) Number of decision samples chosen to be the fraction of Pan samples closest to the actual fraction of Thermal samples, e.g. 59/64 ≈ 29/31 for Urban.

5.3.2 --Continued.

with a chi square value of 28.2. Finally the two which appear to differ the most are pan and radar with a chi square value of 41.2. Thus, in a semiquantitative way we can conclude that at least insofar as the application of optical power spectrum analysis for terrain classification, panchromatic and thermal imagery will have performance characteristics that are closer than panchromatic and radar or thermal and radar imagery.

5.3.3 Detailed Comparison of Panchromatic and Radar Imagery

5.3.3.1 Application of the Linear Hypothesis Model Analysis of Variance

Analysis of variance of the linear hypothesis model was used to examine the effect of sensor type (radar or panchromatic) and aperture size on the decision performance for all classes and for particular terrain types. For example, the decision action average percent correct, percent error and percent reject may be formed into 2 X 3 linear hypothesis model tables as shown in Table 5-10. The rows in each case contain the value for a particular sensor type at each of the three common aperture sizes 2, 4 and 6 mm. The column F-value is a measure of the variation due to aperture size independent of sensor. On the other hand, the row F-value is a measure of the effect of sensor type independent of aperture size.

Tables similar to 5-10 were constructed using the percent correct, percent error and percent reject for each of the terrain classes. These tables are presented in Appendix 1. A summary of the F test values obtained from these tables is presented in Table 5-11. Note that

Table 5-10. Linear Hypothesis Model Analysis of Variance for All Class Performance

Aperture/Type/Imagery	% Correct	% Error	% Abstain
1mm Hardclipped Pan	68.1	21.8	9.8
2mm Gaussian Pan	80.6	2.6	16.6
4mm Gaussian Pan	70.5	8.2	18.5
6mm Gaussian Pan	77.5	10.1	12.2
2mm Gaussian Radar	85.2	5.6	9.0
4mm Gaussian Radar	84.0	12.0	3.0
6mm Gaussian Radar	91.3	5.5	3.0

	2	4	6	
Pan	80.6	70.5	77.5	$F_{col} = 2.08$
Radar	85.2	84.0	91.3	$F_{row} = 12.4$

% Correct

	2	4	6	
Pan	2.6	8.2	10.1	$F_{col} = 1.7$
Radar	5.6	12.0	5.5	$F_{row} = 7.5$

% Error

	2	4	6	
Pan	16.6	18.5	12.2	$F_{col} = 1.6$
Radar	9.0	3.0	3.0	$F_{row} = 19.9$

% Abstain

Table 5-11. Linear Hypothesis Model Analysis of Variance Summary

F-Value ($\nu_1 = 1$, $\nu_2 = 2$)

(5% significance level = 18.5, 1% significance level = 98.4)

Pan versus Radar	% Correct	% Error	% Reject
All classes	12.4	7.5	19.9
Urban (10)	17.28[1]	120.86[2]	1.0
Water (50)	171.96[2]	5.86	1.0
Water (60)	6.5	1.9	2.8
Agriculture Plowed (20)	14.4[3]	-	14.2[3]
Agriculture Non-plowed (70)	2174[2]	-	2172[2]
Forest (40)	22.4	-	22.4

F-Value ($\nu_1 = 2$, $\nu_2 = 2$)

(5% significance level = 19.0, 1% significance level = 99.0)

Aperture Size	% Correct	% Error	% Reject
All classes	2.08	1.7	1.6
Urban (10)	0.8	2.9	1.0
Water (50)	17.0[4]	0.1	1.0
Water (60)	3.3	1.5	1.0
Agriculture Plowed (20)	3.4	-	3.4
Agriculture Non-plowed (70)	392.6[5]	-	392.2[5]
Forest (40)	1.4	-	1.3

1. Close to rejecting at the 5% significance level the hypothesis that Pan and Radar yield the same results.
2. Reject the hypothesis at the 1% significance level that Pan and Radar yield the same results.
3. Large F value but not sufficient to reject the hypothesis that Pan and Radar yield the same results.
4. Close to rejecting the hypothesis at the 5% significance level that results are independent of aperture size.
5. Reject the hypothesis at the 1% significance level that results are independent of aperture size.

5.3.3.1 --Continued.

for the row comparison, i.e., pan versus radar, the 5% significance level is 18.5 and the 1% significance level is 98.5. For the column comparison, i.e., aperture size, the 5% significance level is 19.0 and the 1% significance level is 99.0. Because of the form of the decision rule, it is impossible for an error to occur when the true class is agriculture or forest in the training set. Thus, the F value in this case is indeterminate. This is indicated by a dash in the appropriate entry position in Table 5-11.

5.3.3.2 Statistically Significant Differences Between Pan and Radar Independent of Aperture Size and of Aperture Size Independent of Pan or Radar

The statistically significant differences between pan and radar are:

1) urban-percent error (1% significance level)
2) water (50)-percent correct (1% significance level)
3) non-plowed agriculture (70)-percent correct and percent reject (1% significance level)
4) all classes-percent reject (5% significance level)
5) forest-percent correct and percent reject (5% significance level)

We may thus conclude that in general independent of aperture size there is a statistically significant difference in the performance using optical power spectrum analysis for the two cases: synthetic aperture radar sensor and panchromatic image sensor.

5.3.3.2 --Continued.

We also note from Table 5-11 that although not statistically significant at even the 5% level, a fairly substantial F value is obtained for urban percent correct and plowed agriculture percent correct and percent reject. On the other hand, even though there are large differences in mean performance values for water (60) between the panchromatic and radar sensor independent of aperture size, this difference is not statistically significant. This is due to the fact that there is also significant variation between aperture sizes for water (60). Thus in comparison to the variation between apertures, the variation due to sensor type is not significant.

From Table 5-11 the only statistically significant difference between apertures independent of sensor type is for non-plowed agriculture (70). The percent correct and percent reject values resulting in F-test values of 392.6 and 392.2 respectively differ at the 1% significance value. This result is intuitively appealing because it indicates that independent of sensor type, performance on a terrain type having relatively less texture is improved as the aperture size increases.

5.3.4 Effect of Aperture Size for Panchromatic and Radar Imagery

5.3.4.1 Application of the χ^2 Test for Multinomial Equality

The chi square test for the equality of multinomial distributions was used to test the effect of aperture size on performance for panchromatic imagery and radar imagery independently. For example,

5.3.4.1 --Continued.

to determine if the results for the 1 mm hard clipped aperture were different than the results for the 2 mm Gaussian aperture applied to panchromatic imagery, $\tilde{\chi}^2$ was computed using equation (5-6) and the data given in Table 5-12. The value obtained, 41.7, is greater than 15.1, the 1% significance level. Therefore we may reject the hypothesis that the distribution of decision actions is the same for the 1 mm and 2 mm cases. In other words, decision results are different for the 1 mm and 2 mm aperture cases at the 1% significance level. The remainder of the tables developed for the chi square test are in Appendix 2.

5.3.4.2 Statistically Significant Differences Depending on Aperture Size

A summary of the results from these tables is in Table 5-13. The six possible pairings of 1 mm, 2 mm, 4 mm and 6 mm panchromatic aperture cases were investigated. In certain situations as noted, a single decision class such as water 60 or a pair of decision classes such as forest 40 and abstain in combination caused the $\tilde{\chi}^2$ value to exceed the significance level.

In the case of the 1 mm aperture versus the 4 mm aperture, forest and abstain were combined in a single class and the $\tilde{\chi}^2$ value recomputed. In this case, no significant difference between the two aperture sizes is developed based on the $\tilde{\chi}^2$ value. Thus, the conclusion is that the difference between the 1 mm hard clip and the 4 mm Gaussian is due to the relative diffraction pattern signatures of forest and

Table 5-12. χ^2 Test Comparing Panchromatic 1mm Harclipped Aperture Results to 2mm Gaussian Results

	Decision Action					
Aperture Size	Urban 10	Water 50	Water 60	Agriculture 80	Forest 40	Abstain 90
1mm	29	5	2	98	219	60
2mm	31	9	23	83	161	106

i	$(X_{i1} + X_{i2})/2$	$\frac{1}{2}$(Contribution to $\tilde{\chi}^2$)
1	30.0	.03
2	7.0	.57
3	12.5	8.82
4	90.5	.62
5	190.0	4.42
6	83.0	6.37

$\chi^2 = 41.69 > 15.1$ (1% significance level)

(See Equation 5-6)

Table 5-13. Aperture Comparison - χ^2 Test Results Summary

Pan Aperture Sizes

	Significance Level Upper Bound	χ^2	Significance Level Exceeded
1. 1mm hardclipped versus 2mm Gaussian		41.69	15.1 (1%)
2. 1mm hardclipped versus 4mm Gaussian	15.1 (1%)	14.73	12.8 (2.5%)
1mm hardclipped versus 4mm Gaussian 40 and 90 combined	9.49 (5%)	4.50	0.711 (95%)
3. 1mm hardclipped versus 6mm Gaussian	11.1 (5%)	5.33	1.15 (95%)
4. 2mm Gaussian versus 4mm Gaussian		27.26	15.1 (1%)
2mm Gaussian versus 4mm Gaussian (Redistribute 60)*	11.1 (5%)	7.3	1.15 (50%)
5. 2mm Gaussian versus 6mm Gaussian		27.24	15.1 (1%)
2mm Gaussian versus 6mm Gaussian (Redistribute 60)**		18.04	15.1 (1%)
6. 4mm Gaussian versus 6mm Gaussian	15.1 (1%)	12.2	11.1 (5%)
4mm Gaussian (Redistribute 60) versus 6mm Gaussian (Redistribute 60)***	11.1 (5%)	3.16	1.15 (50%)

* Last two tests imply difference is Water (60) results

** Last two tests imply difference is not simply Water (60).

*** Last two tests imply 4mm and 6mm differ because of Water (60).

5.3.4.2 --Continued.

agriculture since these classes determine the decision boundaries between forest and abstain. A similar analysis for the 2 mm versus 4 mm and 4 mm versus 6 mm shows that assuming that all water 60 samples were correctly classified in one or both of the aperture cases yields a distribution of decision actions that is not statistically significantly different for the two aperture sizes.

The aperture comparisons are summarized in Table 5-14, which shows the comparisons between 1, 2, 4 and 6 mm apertures for panchromatic imagery. The entries in the table indicate the significance level at which the decision action distributions differ according to the chi square test for multinomial distribution comparison. In the case where no statistically significant difference exists, the entry none appears in the table. Where appropriate, an indication is made to denote the cause of the difference between apertures.

A similar analysis comparing 2, 4 and 6 mm results for radar imagery shows no statistically significant difference, even at the 5% significance level, between the distributions of decision actions for the various aperture sizes. The test tables for this analysis are presented in Appendix 3.

5.4 Summary of Statistically Significant Results

We are now in a position to answer in a statistically quantitative way the three questions posed at the beginning of this section. We do this next as a summary of the results.

Table 5-14. Aperture Performance Comparison Summary for Panchromatic Imagery

	1	2	4	6
1	-	1%	2.5%(1)	None
2		-	1%(2)	1%
4			-	5%(3)
6				-

χ^2 Significance Level Indicating Performance Difference

(1) Because distinction between Agriculture and Forest is not as well defined for 4mm aperture.

(2) Due to Water (60).

(3) Due to Water (60).

5.4 --Continued.

Question 1: Are the decision results for panchromatic, radar and thermal imagery different?

The answer to this question is yes. Specifically using the chi square test for multinomial distribution equivalence, we have the following based on a comparison of the decision action distributions:

1) Panchromatic versus radar - $\tilde{\chi}^2 = 41.2 > 13.3 =$ the 1% significance level

2) Panchromatic versus thermal - $\tilde{\chi}^2 = 14.3 > 13.3 =$ 1% significance value

3) Radar versus thermal - $\tilde{\chi}^2 = 28.2 > 13.3 =$ 1% significance level

Question 2: What does a detailed comparison of panchromatic and radar imagery show insofar as: (1) overall decision performance, (2) discrimination between various terrain types, (3) effect of aperture size

With respect to overall decision performance, the analysis of variance of the linear hypothesis model comparing panchromatic and radar imagery across aperture sizes shows that the percent reject for radar and panchromatic is different at the 5% significance level. Thus, there is a statistically significant difference, although not as strong as it might be, between the overall decision performance for panchromatic and radar imagery.

5.4 --Continued.

The difference in performance is stronger for specific terrain types. In particular, the analysis of variance for the linear hypothesis model yields the following results:

1) Urban-percent error differs from panchromatic to radar independent of aperture size at the 1% significance level.

2) Water (50)-percent correct differs from panchromatic to radar imagery independent of aperture at the 1% level.

3) Agriculture (70)-percent correct and percent reject differ from panchromatic to radar imagery at the 1% significance level.

4) Forest-percent correct and percent reject differ from panchromatic to radar imagery independent of aperture at the 5% significance level.

Examination of the effect of aperture independent of panchromatic or radar sensor type shows a significant difference using analysis of variance on the linear hypothesis model only for agriculture (70). In particular the percent correct and percent reject are different independent of panchromatic or radar as a function of aperture size at the 1% significance level.

Question 3: Does aperture size affect performance of panchromatic and radar imagery individually?

5.4 --Continued.

As shown in Table 5-14, there are significant differences between the performance on panchromatic imagery for different aperture sizes. In three of the five cases where such differences exist, the difference is attributable primarily to the decision results for a particular class or pair of classes. There is no statistically significant (at the 5% significance level or better) difference between the performance utilizing different aperture sizes on radar imagery. We shall see however in the next section that although the number of decisions remains unchanged for radar when comparing the 2 mm to 6 mm case for water (60), the diffraction pattern signatures are quite different.

REFERENCES FOR SECTION 5

1. R.V. Hogg and A.T. Craig, Introduction to Mathematical Statistics, 2nd Edition, The MacMillan Company, New York 1967, pp. 303-304.

2. P.G. Hoel, Introduction to Mathematical Statistics, 4th Edition, John Wiley and Sons, Inc., New York, 1971, pp. 285-293.

6.0 COMPARISON OF RESULTS FOR INDIVIDUAL SAMPLES

The quantitative discussion in the last section treats the decision performance from a macroscopic statistical viewpoint. In this section individual OPS samples will be compared in order to point out in a qualitative way differences that may be expected in diffraction pattern signatures when different sensors are used. Because samples were taken over identical areas using the panchromatic and radar sensors, we will limit the discussion in this section to comparisons of results obtained using radar and panchromatic imagery. The specific comparisons we will consider are:

1) classification of urban using radar and panchromatic with a 2 mm aperture

2) classification of water (50) using radar and panchromatic imagery and a 2 mm aperture

3) classification of forest using radar and panchromatic imagery with a 2 mm aperture

4) classification of non-plowed agriculture utilizing radar and panchromatic imagery with a 2 mm aperture

5) classification of plowed agriculture utilizing radar and panchromatic imagery with a 2 mm aperture

6) comparison of decisions for water (60) and agriculture utilizing radar and panchromatic imagery with a 2 mm aperture

7) comparison of the results obtained for water (60) utilizing radar and panchromatic imagery with 2, 4 and 6 mm apertures.

6.0 --Continued.

The first four comparisons correspond to cases for which there is a statistically significant difference between the performance utilizing radar and panchromatic imagery. In the fifth case there is no statistically significant difference between decisions utilizing radar and panchromatic imagery. We present this case to compare a statistically significant difference to one that is not.

The confusion matrices in Tables 5-1 through 5-8 show a distinct trend of overlap between the water classes, agriculture, forest and abstention actions. (Recall that the abstention action region is the intersection of the region in which both forest and agriculture are accepted.) Thus, we show one example illustrating how this confusion can come about.

Finally, we show specific examples comparing the water detection performance of radar and panchromatic imagery as larger aperture sizes include varying degrees of shoreline. This particular example shows how the specular return present in the radar is implicitly used as a feature while the lack of the specular return from the shoreline in the panchromatic imagery yields an aperture sample containing on-shore terrain and water that is not classified as water.

6.1 Urban Sample Comparison

For the 2 mm case, 20 of the 26 radar urban samples are correctly classified while 31 of the 31 urban panchromatic samples were correctly classified. To illustrate why errors occur in the radar

6.1 --Continued.

based decisions, we have chosen two samples: one for which both radar and pan based decisions are urban (shown in Figure 6-1a and b), and the second for which the radar decision is forest while the pan decision is urban (shown in Figure 6-1c and d).

Examining the wedge feature plots in Figure 6-2 for these two cases, we observe that the incorrectly classified radar sample does not exhibit the characteristic peak between wedges 14 and 18. This peak which is due to the specular return in the radar samples is in fact what enables us to distinguish urban from non-urban terrain types. Observing the pictures in Figure 6-1 of the specific aperture samples, we see that while a building is visible in the panchromatic imagery, orientation of the building is such that there is no specular return in the radar sample.

This single example illustrates the difference between the urban detection diffraction feature used for panchromatic imagery and the feature used for radar imagery. The panchromatic feature is simply a relative increase in high spatial frequency content due to the line structure of man-made objects. On the other hand, the radar feature is the specular cross pattern which causes a similar cross pattern in the diffraction plane.

6.2 Representative Samples Comparing Water 50 Panchromatic and Radar Results

For the case of water (50), nine of eleven samples were correctly classified using panchromatic data while only five of nine

a. 10236 (Urban)
Decision = Urban
Pan

b. 10236 (Urban)
Decision = Urban
Radar

c. 20214 (Urban)
Decision = Urban
Pan

d. 20214 (Urban)
Decision = Forest
Radar

Figure 6-1. Comparison of Urban Areas in Panchromatic and Radar Imagery
2mm

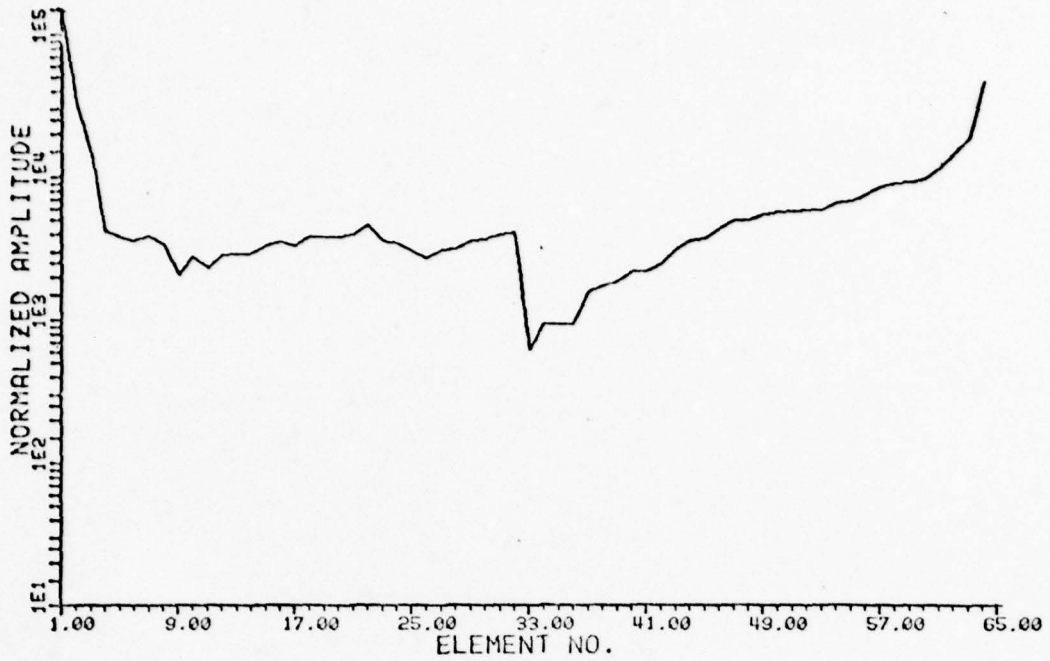

a. 10236 (URBAN) DECISION = URBAN 2KM PAN
FILE D1.NLK5 .NVD103- /NVD003/DECISIONS USING NVN503-NVN603
05/01/79 09:51

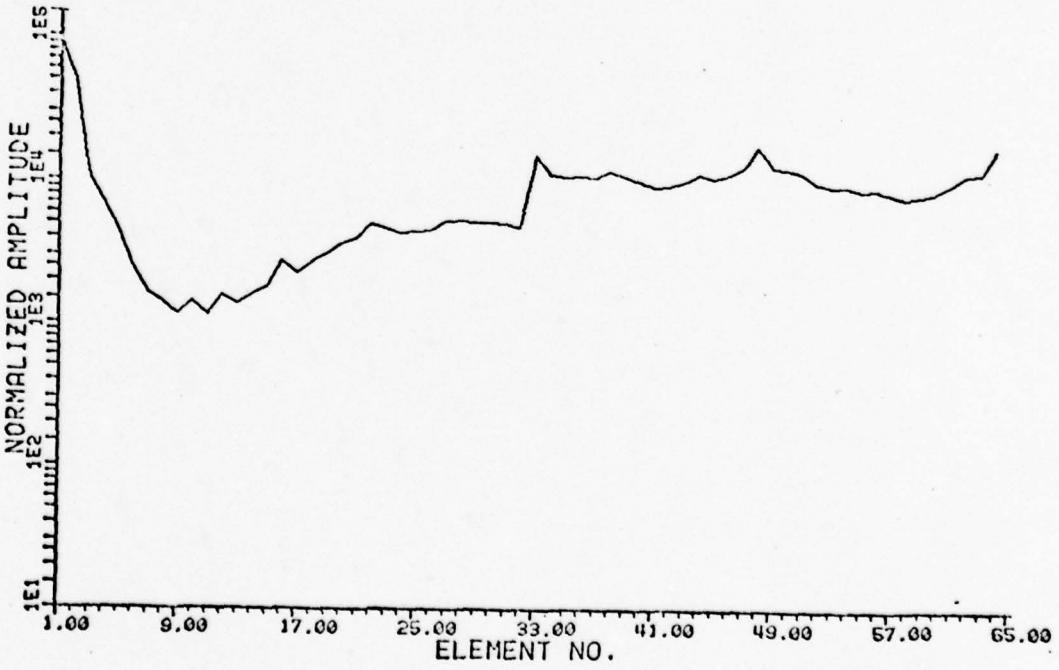

b. 10236 (URBAN) DECISION = URBAN 2KM RADAR
FILE D1.NLK5 NVD008- /NVD008/DECISIONS USING NVN008-NVN108
05/01/79 09:20

Figure 6-2. Comparison of Features for Urban Samples Derived from Panchromatic and Radar Imagery

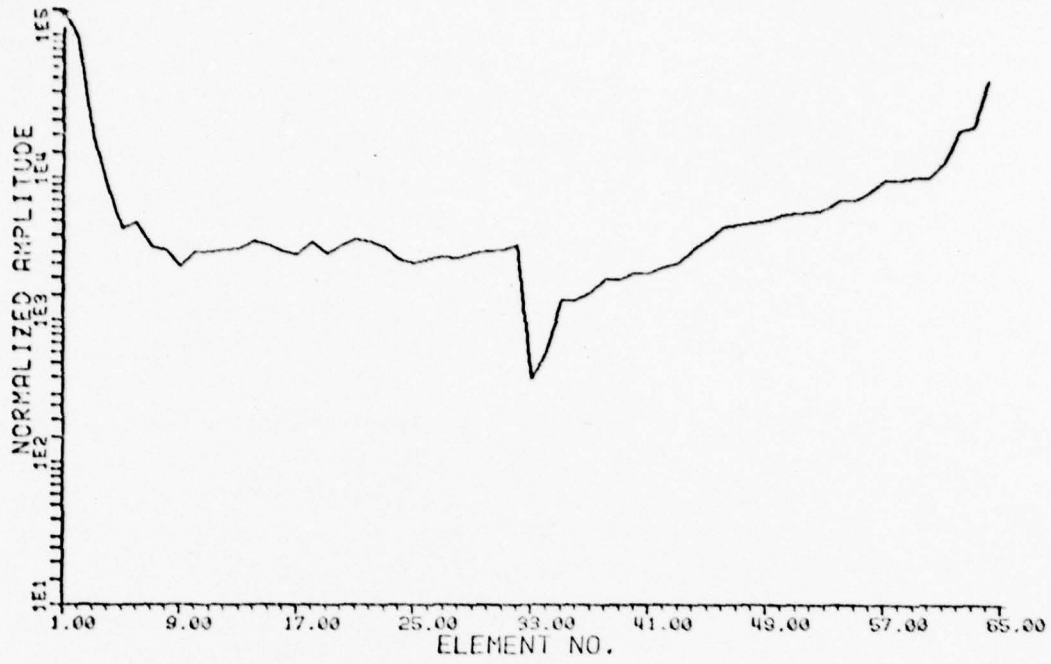

c. 20214 <URBAN> DECISION = URBAN 2MM PAN
FILE D1.IK.KS .NVD103- /NVD003/DECISIONS USING NVN503-NVN603
05/01/79 09:53

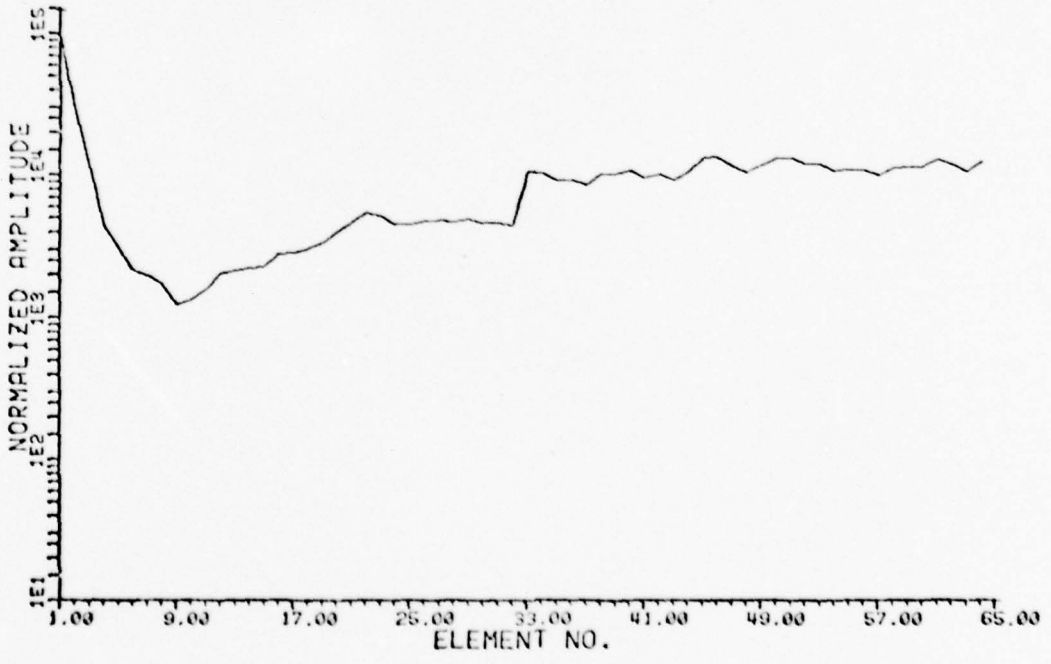

d. 20214 <URBAN> DECISION = FOREST 2MM RADAR
FILE D1.IK.KS NVD008- /NVD008/DECISIONS USING NVN008-NVN108
05/01/79 09:27

Figure 6-2. (Continued)

6.2 --Continued.

were correctly classified from the radar data. Figure 6-3a and b shows a sample area correctly classified for both radar and panchromatic data, while Figure 6-3c and d shows a sample correctly classified using panchromatic data but assigned to the abstention region when radar data is used. Figure 6-4 contains the feature plots for both of these samples which should be compared to the feature statistical limit plots for water (50), agriculture and forest in Appendix 4.

There appears to be no significant difference in the diffraction pattern feature signatures or in the imagery itself between the sample correctly classified by both sensors and the other sample which is correctly classified only using the diffraction pattern data from the panchromatic imagery. Examination of other samples appears to substantiate the conclusion that diffraction pattern signature difference causing the performance difference between radar and pan is more complex than can be seen by a simple examination of the feature plots and imagery samples.

6.3 Comparison of Results for Forest Using Diffraction Pattern Samples from Radar and Panchromatic Imagery

For the 2 mm aperture case, 199 of 211 forest samples were correctly classified utilizing the radar imagery. On the other hand, for the 2 mm aperture only, 159 of 214 samples from panchromatic imagery were correctly classified.

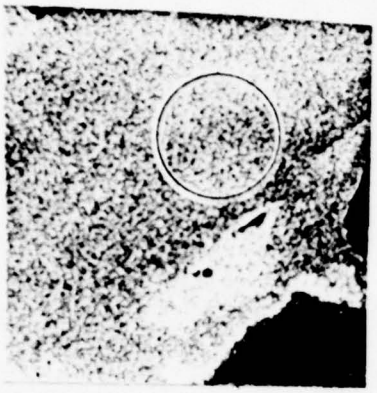

a. 10505 (Water)
Decision = Water
Pan

b. 10505 (Water)
Decision = Water
Radar

c. 10321 (Water)
Decision = Water
Pan

d. 10321 (Water)
Decision = Ambiguous
Radar

Figure 6-3. Comparison of Water (50) Areas in Panchromatic and Radar Imagery
2mm

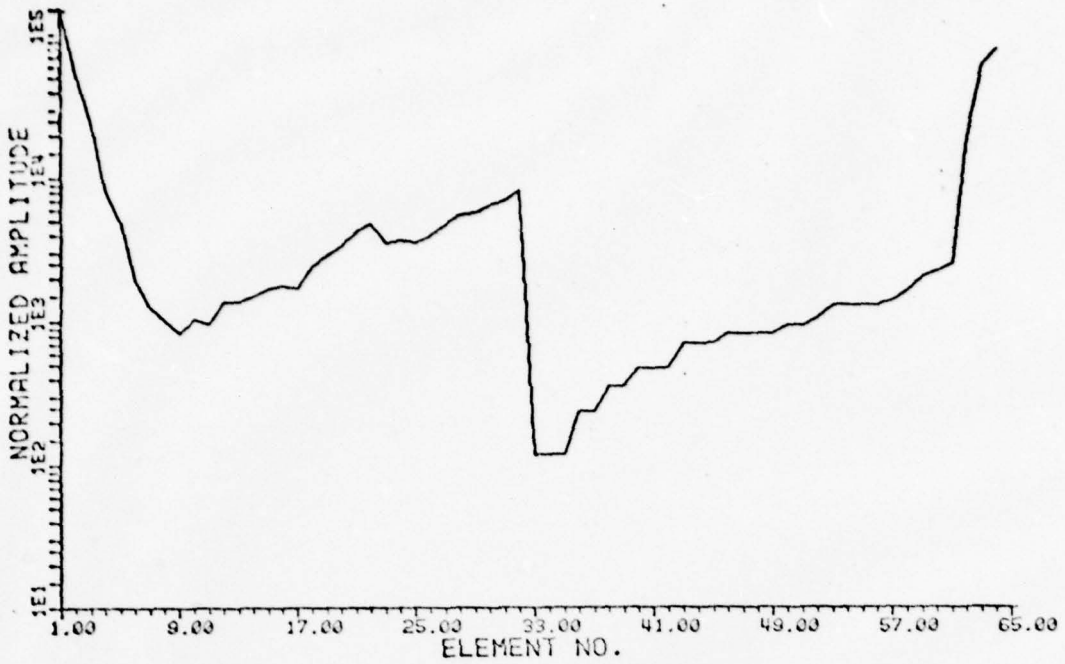

a. 10505 <WATER> DECISION = WATER 2MM PAN
FILE D1.HLKS .NVD103- /NVD003/DECISIONS USING NVN503-NVN503
05/01/79 09:55

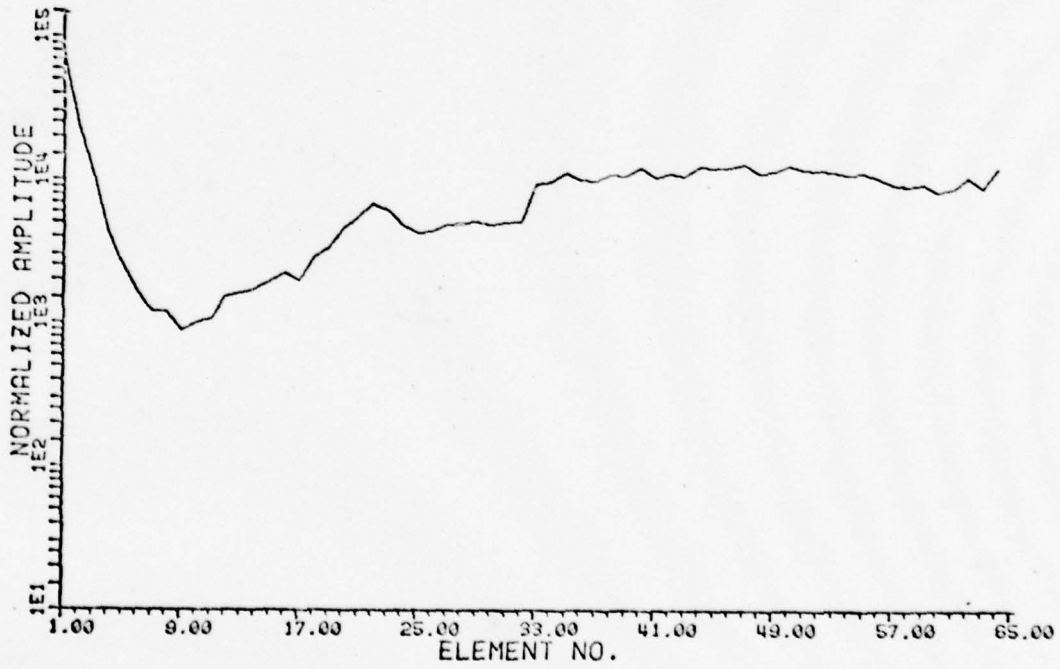

b. 10505 <WATER> DECISION = WATER 2MM RADAR
FILE D1.HLKS .NVD308- /NVD008/DECISIONS USING NVN308-NVN108
05/01/79 09:29

Figure 6-4. Comparison of Features for Water (50) Samples Derived from Panchromatic and Radar Imagery

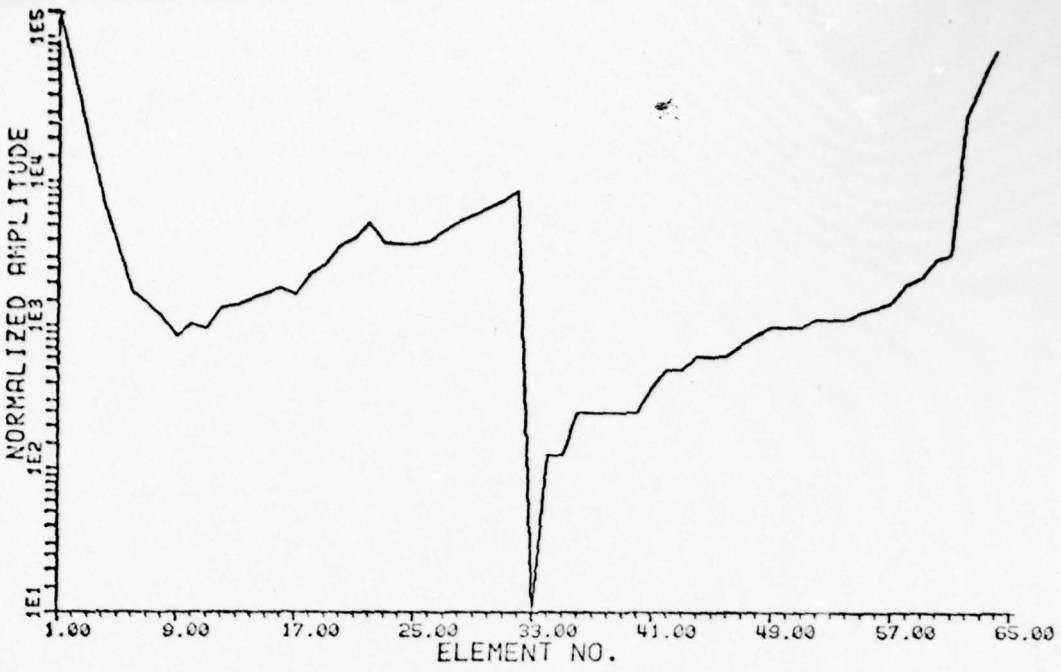

c. 10321 (WATER) DECISION = WATER 2MM PAN
FILE D1.HLKS .NVD103- /NVD003/DECISIONS USING NVN503-NVN603
05/01/79 09:57

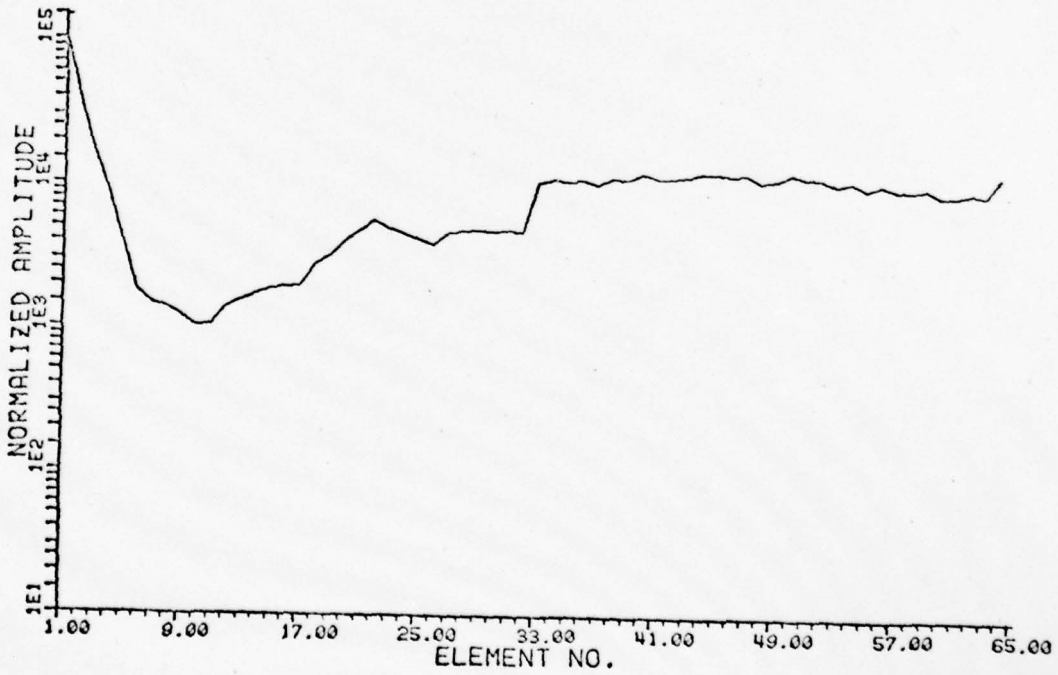

d. 10321 (WATER) DECISION = AMBIGUOUS 2MM RADAR
FILE D1.HLKS .NVD026- /NVD003/DECISIONS USING NVN003-NVN108
05/01/79 09:91

Figure 6-4. (Continued)

6.3 --Continued.

Once again, two specific sample areas were chosen to illustrate the qualitative differences between the results for radar and panchromatic imagery. The sample area correctly classified utilizing either panchromatic or radar derived data is shown in Figure 6-5a and b. The area correctly classified from radar but incorrectly classified from pan is shown in Figure 6-5c and d. Corresponding feature plots that may be compared to class feature statistics for forest and agriculture are shown in Figure 6-6.

Observing the pictures in Figure 6-5 we conjecture that the superior performance of the OPS measurement data derived from radar imagery is due to tree crown and branch induced texture which is more pronounced and consistent in radar imagery than in panchromatic imagery. The texture associated with forest in panchromatic imagery is quite often duplicated in non-forest agricultural regions. This is consistent with the decision results shown in the confusion matrices (Tables 5-1 through 5-8) where a significant ambiguity between forest and agriculture exists for the panchromatic samples.

The difference in texture appearance is obviously due to the different sensor wavelengths. The appearance of the forest areas in the radar reconstruction is very similar to the speckle pattern observed in photographs when a rough surface is illuminated by coherent visible wavelength light. The relationship between the radar illumination wavelength and the surface height structure in the forest areas is undoubtedly quite similar to the wavelength and height profile relationship for a visible wavelength and typical optical diffuser.

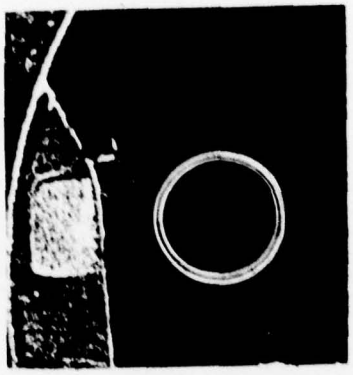

a. 40226 (Forest)
Decision = Forest
Pan

b. 40226 (Forest)
Decision = Forest
Radar

c. 40231 (Forest)
Decision = Ambiguous
Pan

d. 40231 (Forest)
Decision = Forest
Radar

Figure 6-5. Comparison of Forest Areas in Panchromatic and Radar Imagery
2mm

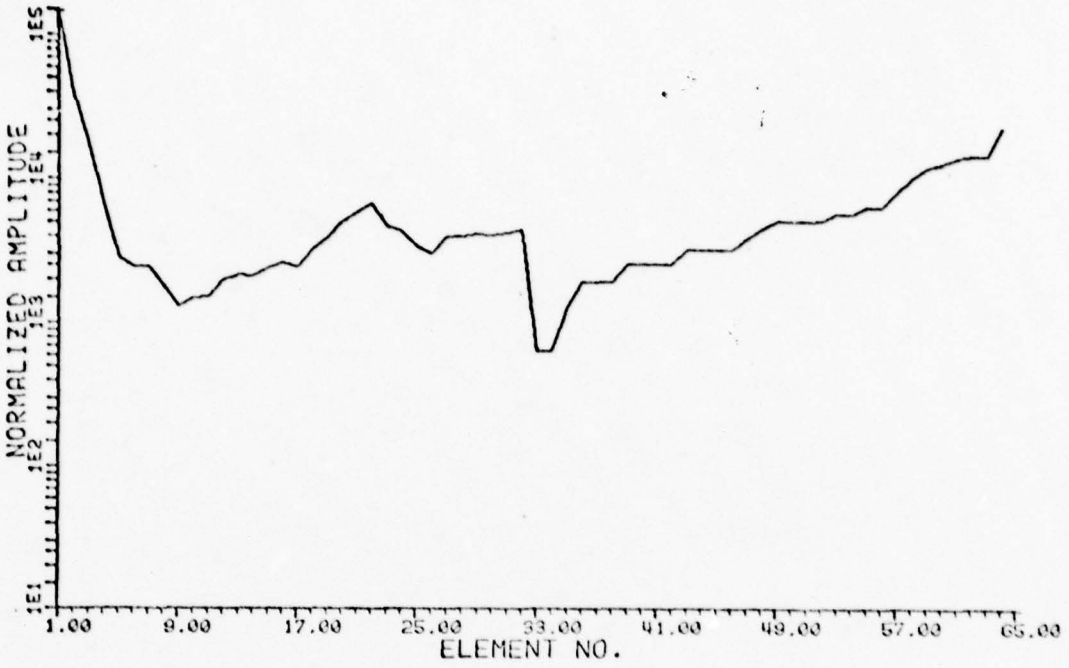

a. 40226 <FOREST> DECISION = FOREST 2MM PAN
FILE D1.HLKS .NVD103- /NVD003/DECISIONS USING NVN503-NVN603
05/01/79 09:59

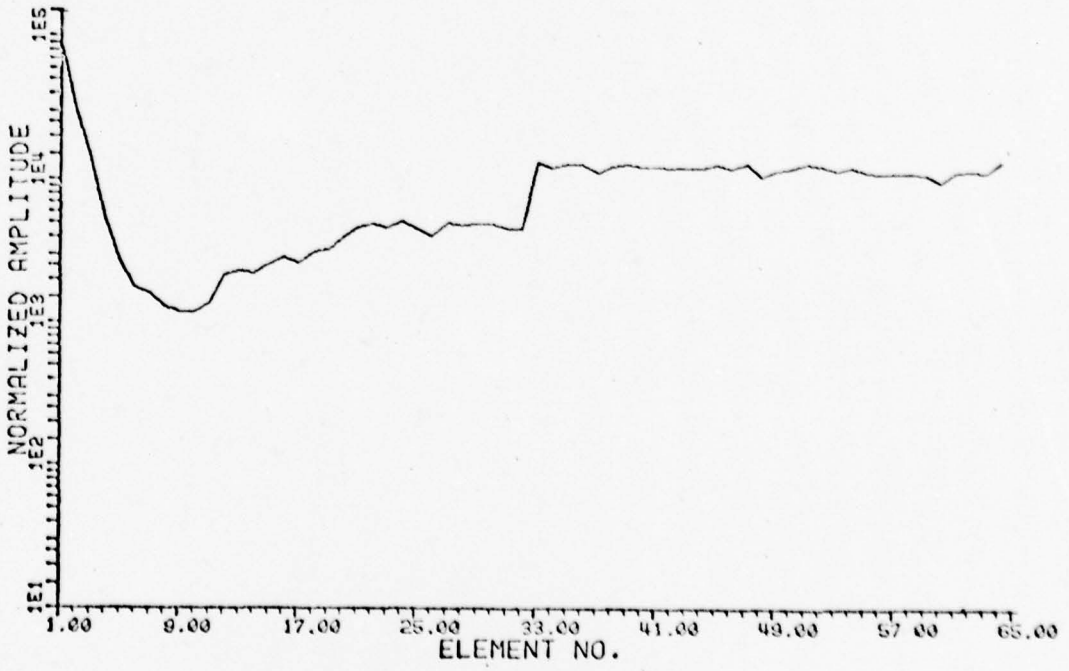

b. 40226 <FOREST> DECISION = FOREST 2MM RADAR
FILE D1.HLKS .NVD208- /NVD008/DECISIONS USING NVN008-NVN108
05/01/79 09:33

Figure 6-6. Comparison of Features for Forest Samples Derived from Panchromatic and Radar Imagery

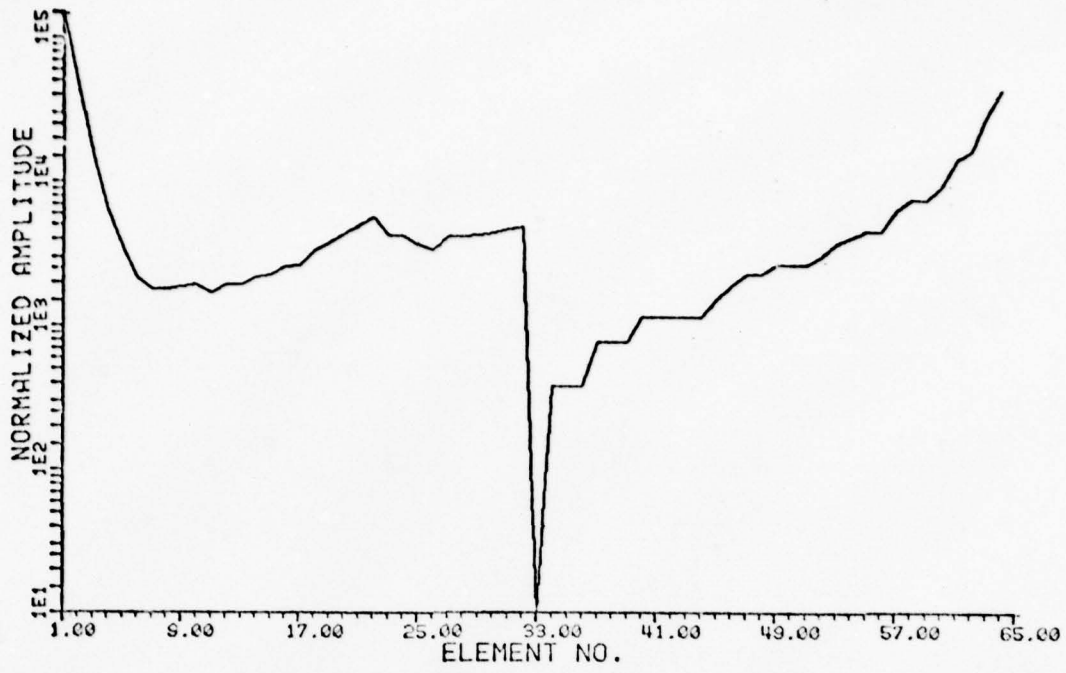

c. 40231 (FOREST) DECISION = AMBIGUOUS 2MM PAN
FILE D1.HLK5 .NVD103- /NVD003/DECISIONS USING NVN303-NVN603
05/01/79 10:02

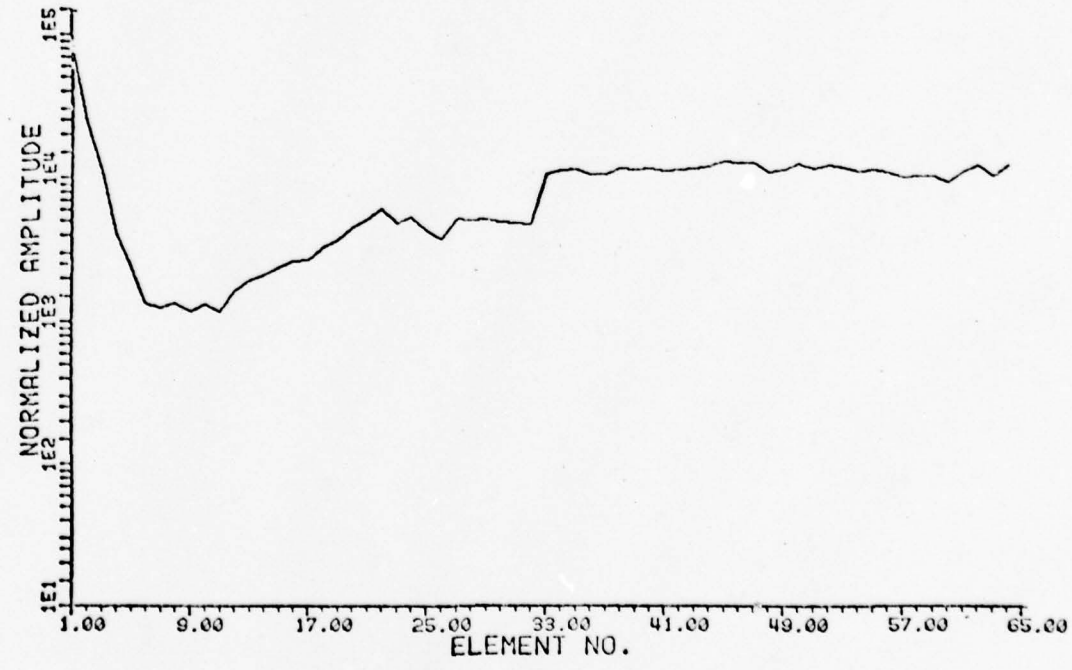

d. 40231 (FOREST) DECISION = FOREST 2MM RADAR
FILE D1.HLK5 .NVD008- /NVD008/DECISIONS USING NVN008-NVN108
05/01/79 00:36

Figure 6-6. (continued)

6.4 Comparison of Non-Plowed Agriculture (70) Performance Utilizing OPS Samples Derived from Radar and Panchromatic Imagery (2 mm aperture)

In this case, 45 of 53 non-plowed agriculture samples identified utilizing OPS measurements from radar imagery were correctly identified. The corresponding number for samples derived from panchromatic imagery was 33 of 48 samples. Once again, we compare samples correctly identified in both cases and a sample correctly identified for the radar case but incorrectly identified for the panchromatic case. Pictures of these samples are shown in Figure 6-7. The corresponding feature plots which can be compared to the feature statistic plots for agriculture and forest in Appendix 4 are shown in Figure 6-8.

The only observed difference in this case between the radar imagery and the pan is that the field boundaries are not as visible in the panchromatic imagery as they are in the radar. Also, as noted previously, the forest texture is much more pronounced and different from the agriculture texture in radar imagery than it is in the pan imagery. Since the correct classification is based on distinguishing agriculture from forest we conjecture that the combination of poor texture differentiation in pan between radar and agriculture as well as the absence of field boundary lines in pan accounts for the difference in performance.

6.5 Comparison of Plowed Agriculture (20) Decision Performance Utilizing OPS Samples from Radar and Panchromatic Imagery (2 mm aperture)

Overall results for radar are 60 of 72 agriculture (70) samples correctly classified while for panchromatic only 48 of 83 are correctly

a. 20317 (Non-Plowed)
Decision = Agriculture
Pan

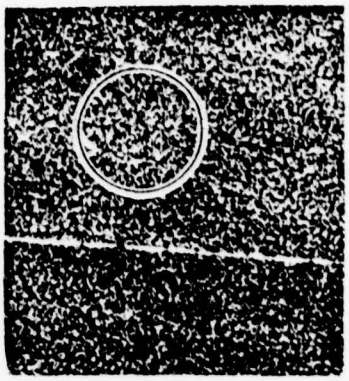

b. 20317 (Non-Plowed)
Decision = Agriculture
Radar

c. 20310 (Non-Plowed)
Decision = Ambiguous
Pan

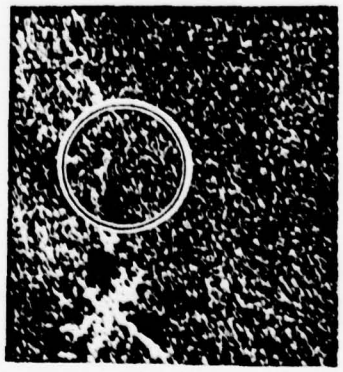

d. 20310 (Non-Plowed)
Decision = Agriculture
Radar

Figure 6-7. Comparison of Non-Plowed Agriculture (70) Areas in Panchromatic and Radar Imagery
2mm

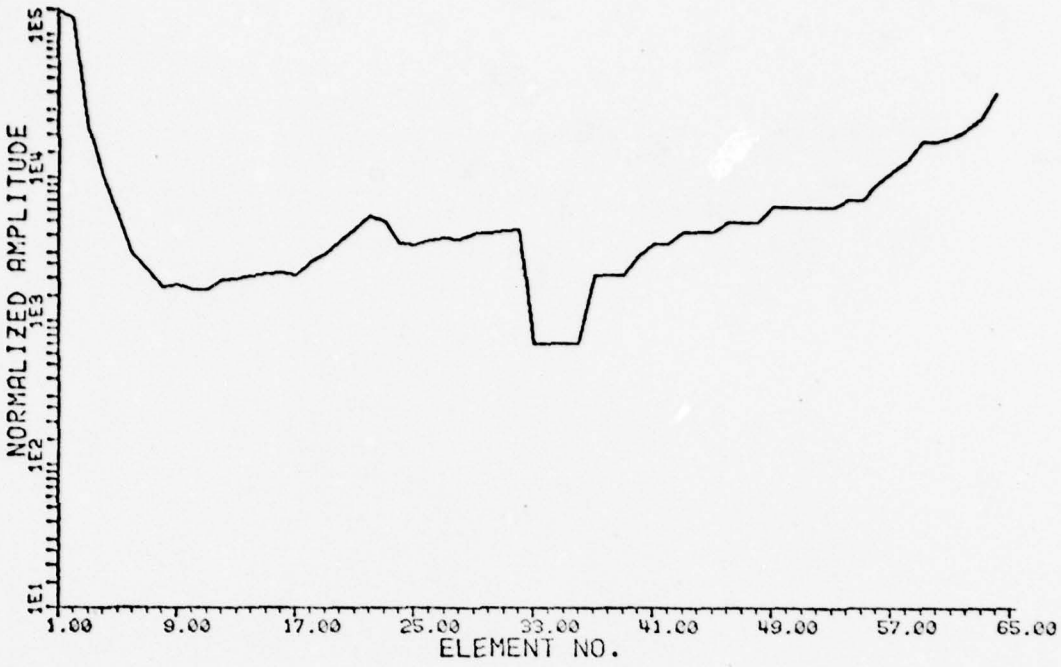

a. 20317 <NON-PLOWED> DECISION = AGRICULTURE 2MM PAN
FILE D1.HLKS .NVD103- /NVD003/DECISIONS USING NVN503-NVN603
05/01/79 10:04

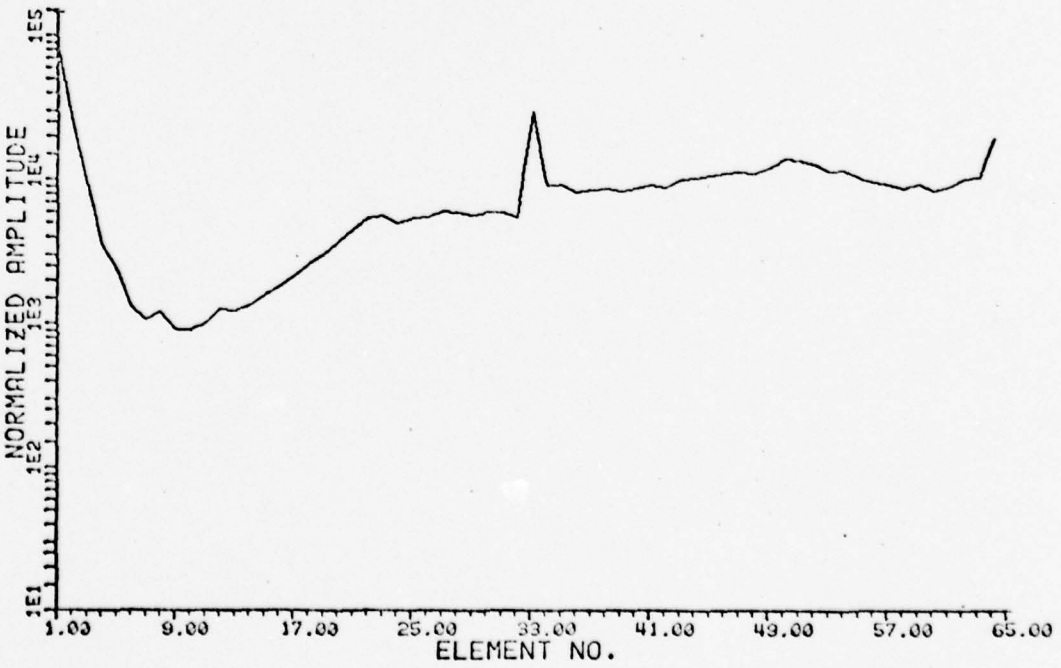

b.. 20317 <NON-PLOWED> DECISION = AGRICULTURE 2MM RADAR
FILE D1.HLKS .NVD003- /NVD003/DECISIONS USING NVN008-NVN108
05/01/79 09:38

Figure 6-8. Comparison of Features for Non-Plowed Agriculture Samples Derived from Panchromatic and Radar Imagery

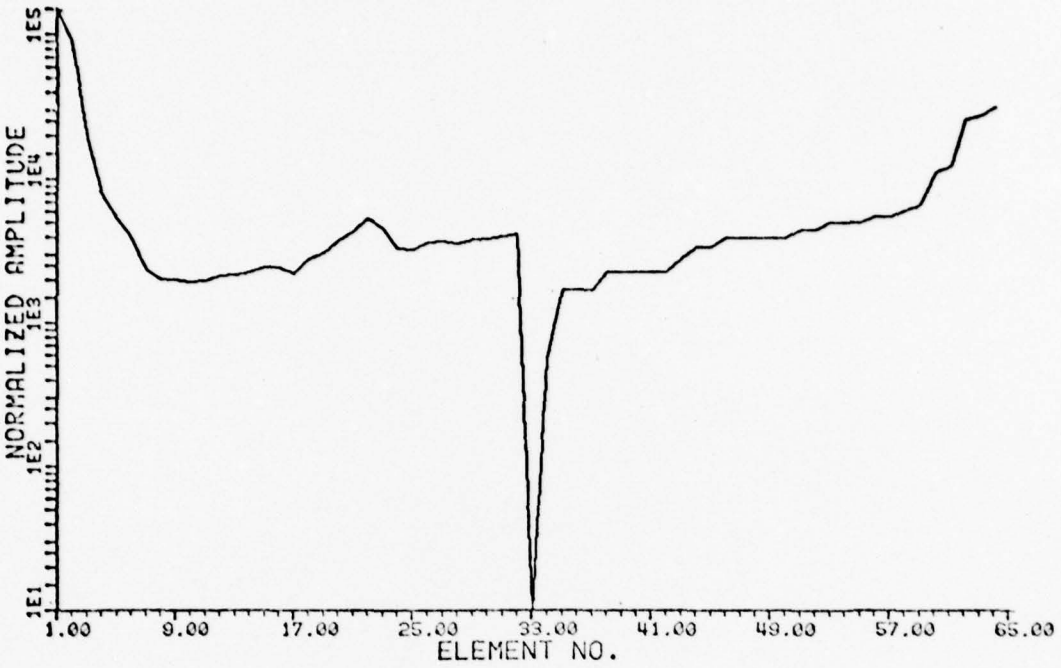

c. 20310 <NON-PLOWED> DECISION = AMBIGUOUS 2MM PAN
FILE D1.HLKS .NVD103- /NVD003/DECISIONS USING NVN503-NVN603
05/01/79 10:07

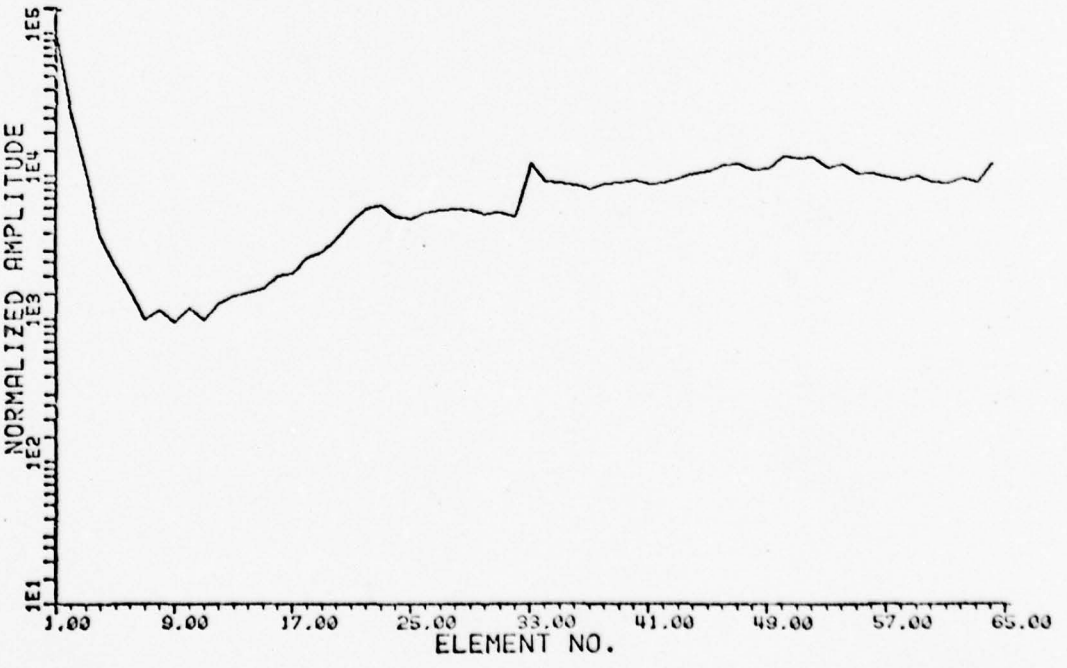

d. 20310 <NON-PLOWED> DECISION = AGRICULTURE 2MM RADAR
FILE D1.HLKS .NVD008- /NVD003/DECISIONS USING NVN303-NVN103
05/01/79 09:40

Figure 6-8. (continued)

6.5 --Continued.

classified. Photographs of the samples correctly identified in both cases are shown in Figure 6-9a and b while the samples correctly classified from radar and incorrectly classified from pan samples are shown in Figure 6-9c and d. The corresponding feature plots are shown in Figure 6-10. These should be compared to the statistics for the feature families shown in Appendix 4.

Comments concerning the plowed agriculture samples in this case are essentially the same as those in the previous section concerning non-plowed agriculture. In general, in the samples available, it was extremely difficult to discern any visual difference between samples classified as plowed and samples classified as non-plowed. Wherever some degree of directed line structure was present in a field, the sample was classified as plowed. However, quite often this line structure did not have sufficient contrast to form the characteristic diffraction pattern of a grating.

6.6 Comparison of Results for Water (60) and Agriculture Utilizing Optical Power Spectrum Measurements from Radar and Panchromatic Imagery with a 2 mm Sampling Aperture

In this case we wish to compare a sample area in the water (60) region to another in agriculture that appear to have identical texture in the panchromatic format, but markedly different texture in the radar reconstruction. The two areas are pictured in Figure 6-11. The corresponding optical power spectrum feature plots should be compared to the class feature statistics for water, agriculture and forest in Appendix 4 as shown in Figure 6-12.

a. 30516 (Plowed)
Decision = Agriculture
Pan

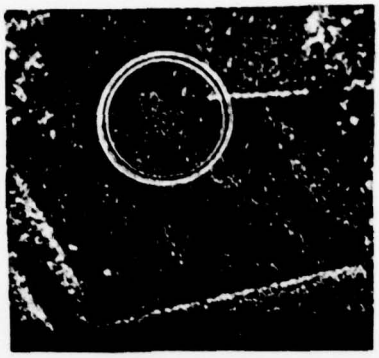

b. 30516 (Plowed)
Decision = Agriculture
Radar

c. 30532 (Plowed)
Decision = Ambiguous
Pan

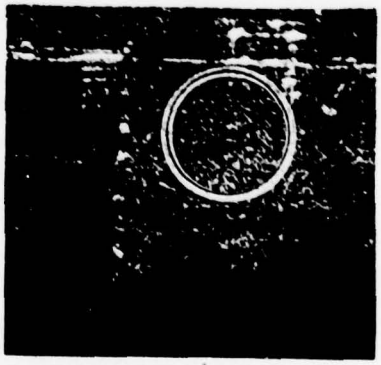

d. 30532 (Plowed)
Decision = Agriculture
Radar

Figure 6-9. Comparison of Plowed Agriculture (20) Areas in Panchromatic and Radar Imagery
2mm

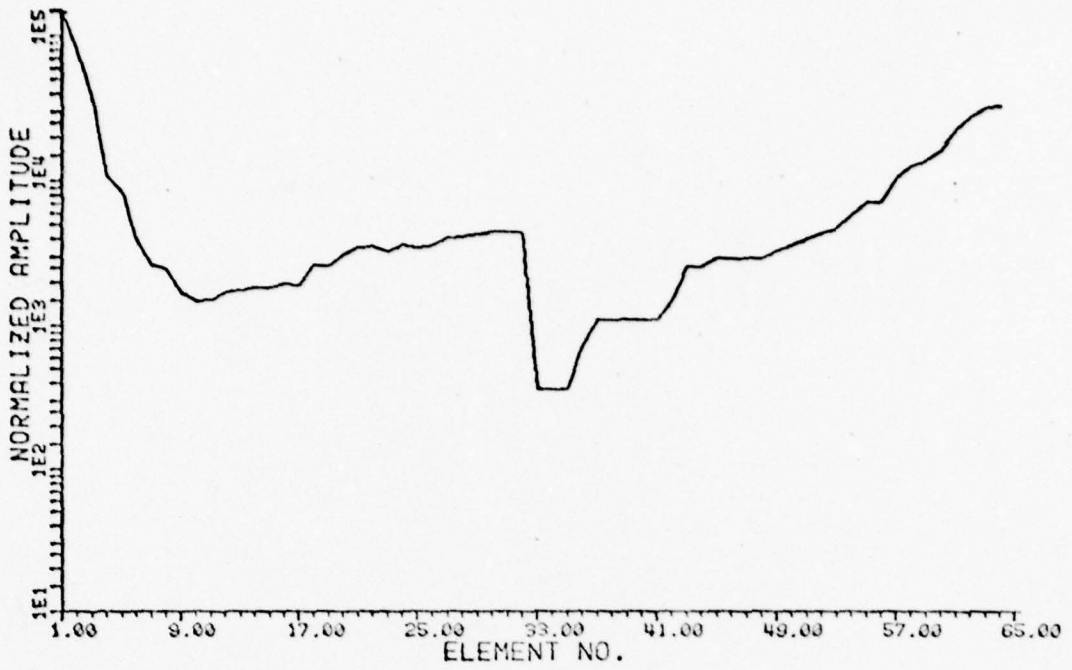

a. 30516 (PLOWED) DECISION = AGRICULTURE 2MM PAN
FILE D1.HLK5 .NVD103- /NVD003/DECISIONS USING NVN503-NVN603
05/01/79 10:10

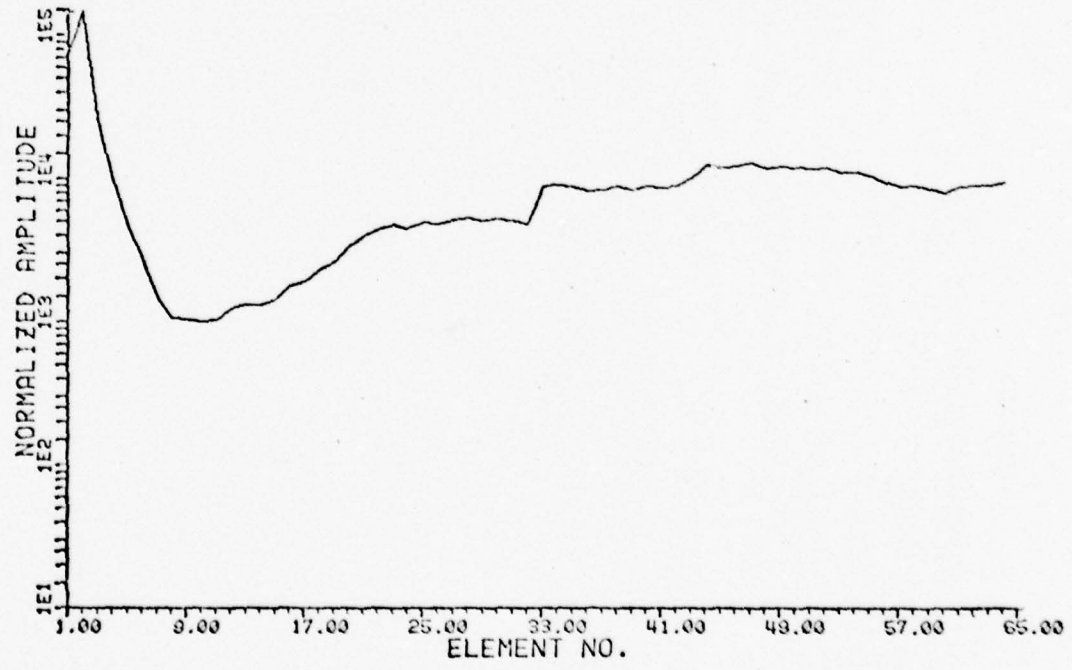

b. 30516 (PLOWED) DECISION = AGRICULTURE 2MM RADAR
FILE D1.HLK5 .NVD308- /NVD008/DECISIONS USING NVN008-NVN108
05/01/79 09:42

Figure 6-10. Comparison of Features for Plowed Agriculture Samples Derived from Panchromatic and Radar Imagery

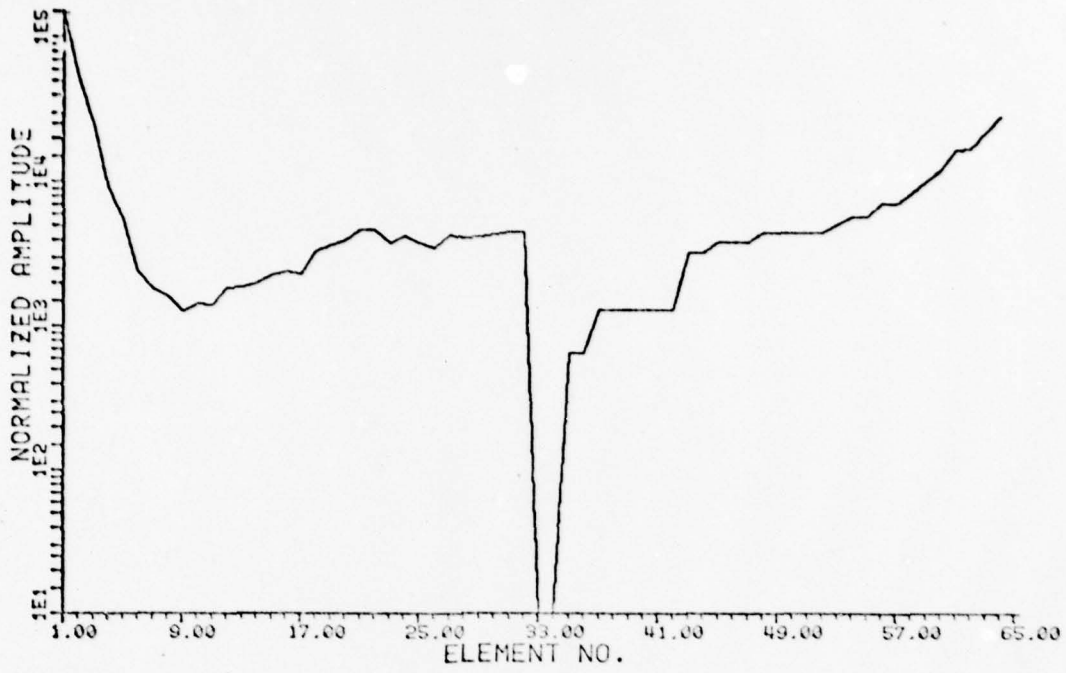

c. 30532 (PLOWED) DECISION = AMBIGUOUS 2MM PAN
FILE D1.HLK5 .NVD103- /NVD003/DECISIONS USING NVN503-NVN603
05/01/79 10:12

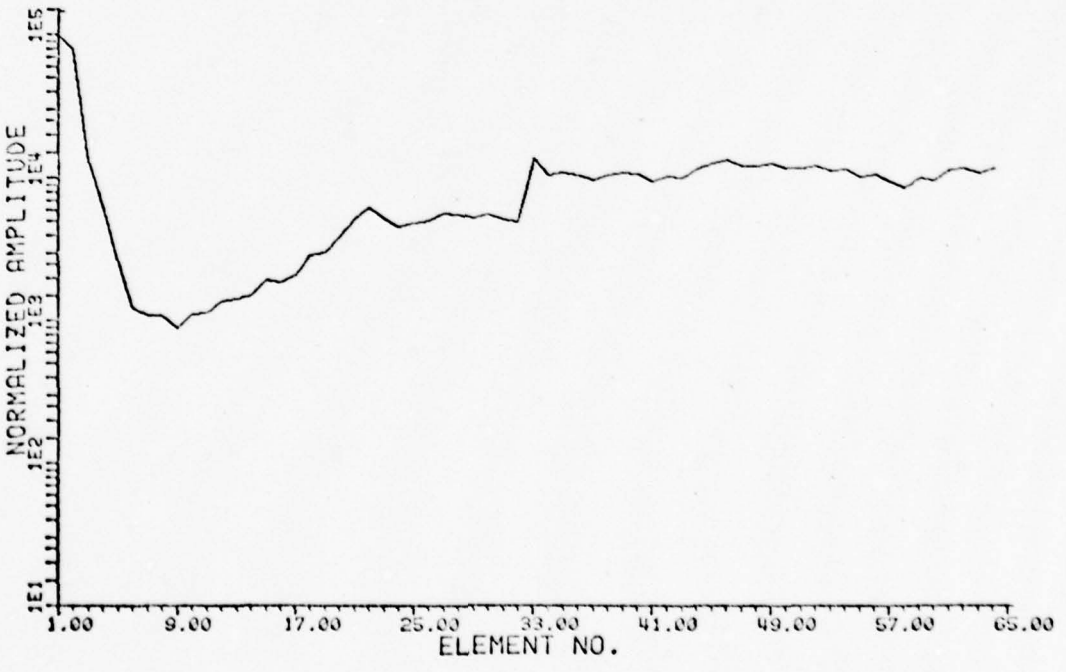

d. 30532 (PLOWED) DECISION = AGRICULTURE 2MM RADAR
FILE D1.HLK5 .NVD003- /NVD003/DECISIONS USING NVN003-NVN103
05/01/79 03:45

Figure 6-10. (Continued)

a. 20310 (Non-Plowed)
Decision = Ambiguous
Pan

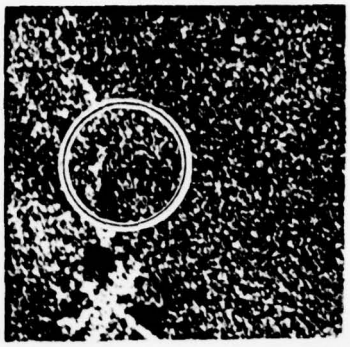

b. 20310 (Non-Plowed)
Decision = Agriculture
Radar

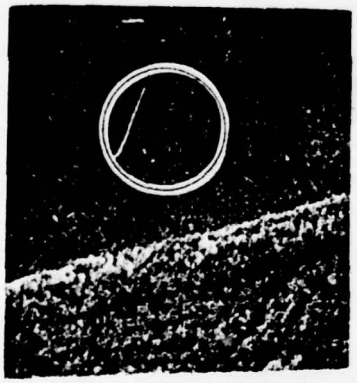

c. 20426 (Water)
Decision = Forest
Pan

d. 20426 (Water)
Decision = Water
Radar

Figure 6-11. Comparison of Water (60) and Agriculture Areas in Panchromatic and Radar Imagery
2mm

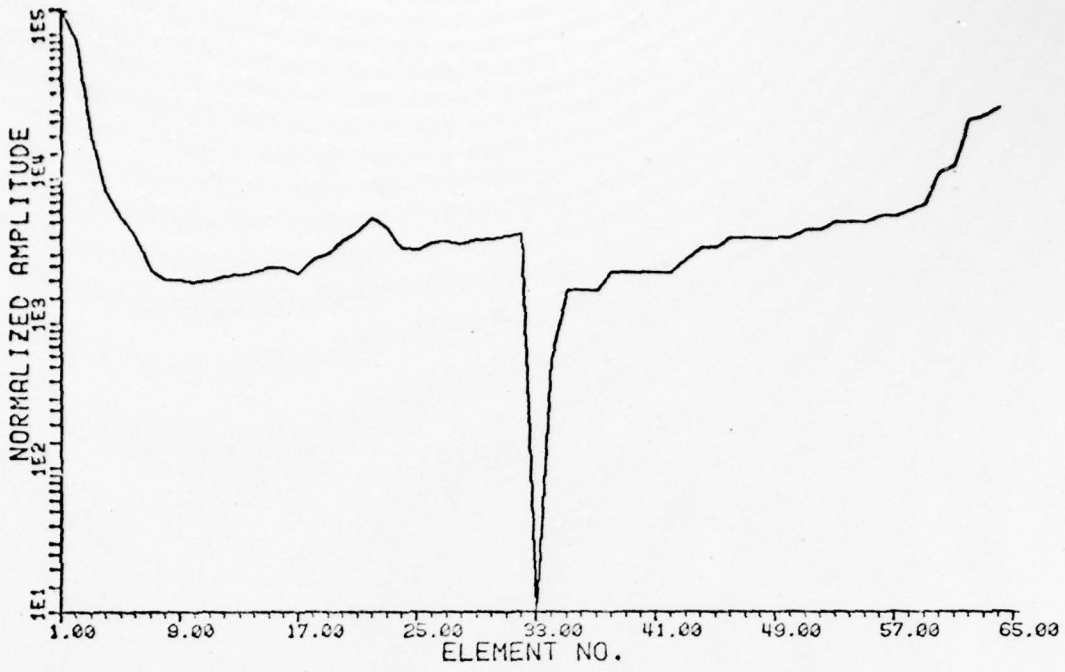

a. 20310 <NON-PLOWED> DESICION = AMBIGUOUS 2MM PAN
FILE D1.HLK5 .NVD103- /NVD003/DECISIONS USING NVN503-NVN603
05/01/79 10:16

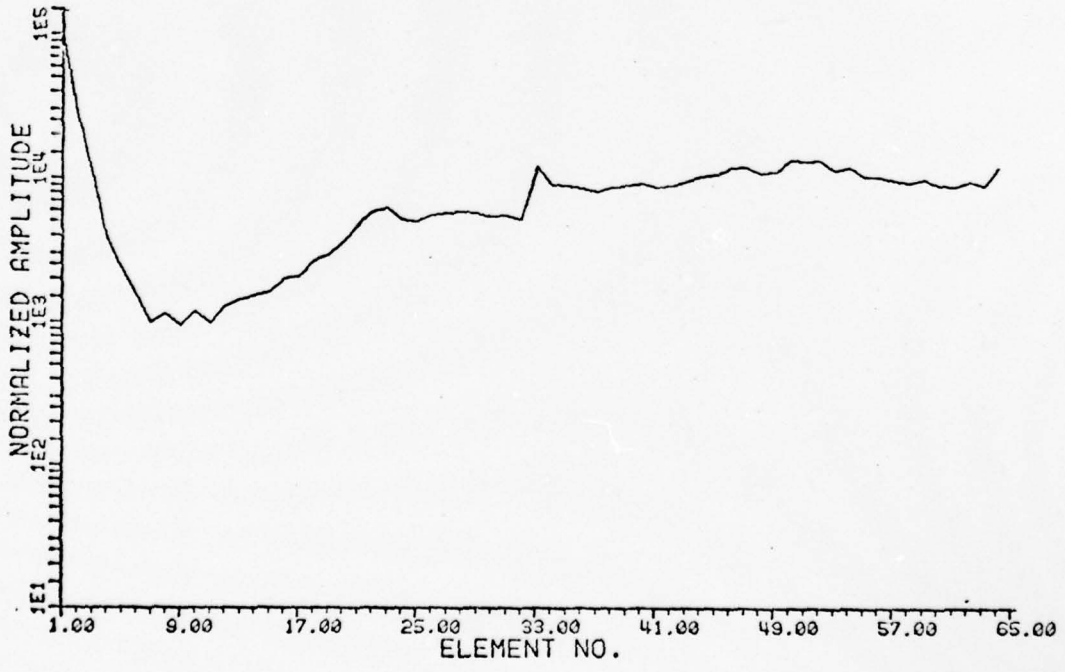

b. 20310 <NON-PLOWED> DESICION = AGRICULTURE 2MM RADAR
FILE D1.HLK5 .NVD008- /NVD008/DECISIONS USING NVN008-NVR108
05/01/79 09:40

Figure 6-12. Comparison of Features for Water (60) and Agriculture Samples Derived from Panchromatic and Radar Imagery

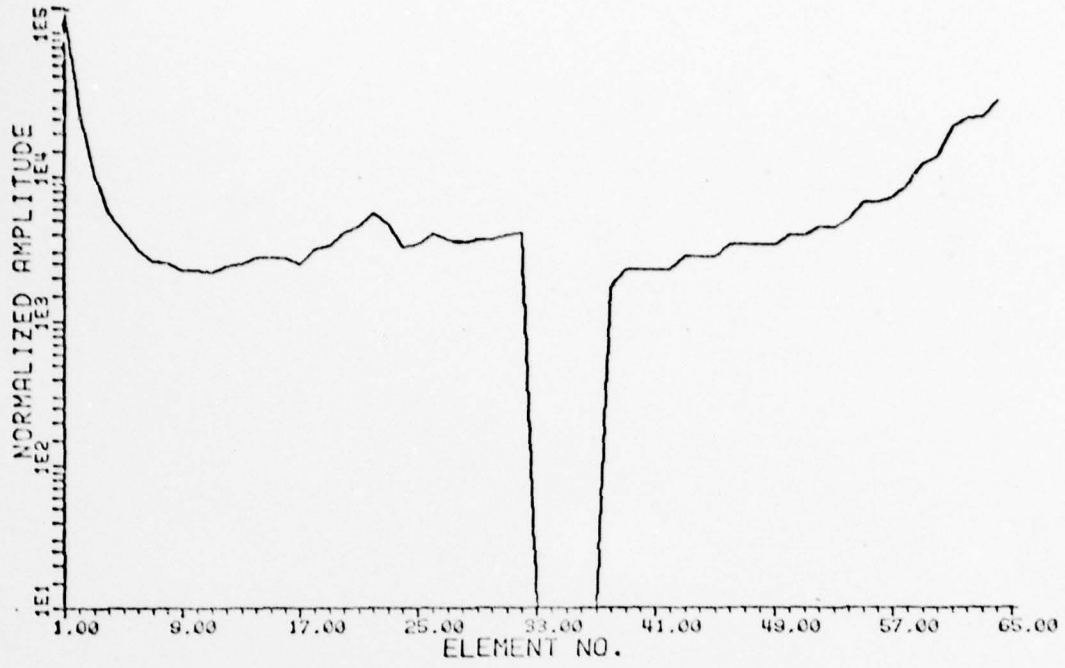

c. 20426 <WATER> DESICION = FOREST 2MM PAN
FILE D1.HLKS .NVD103- /NVD003/DECISIONS USING NVN503-NVN603
05/01/79 10:14

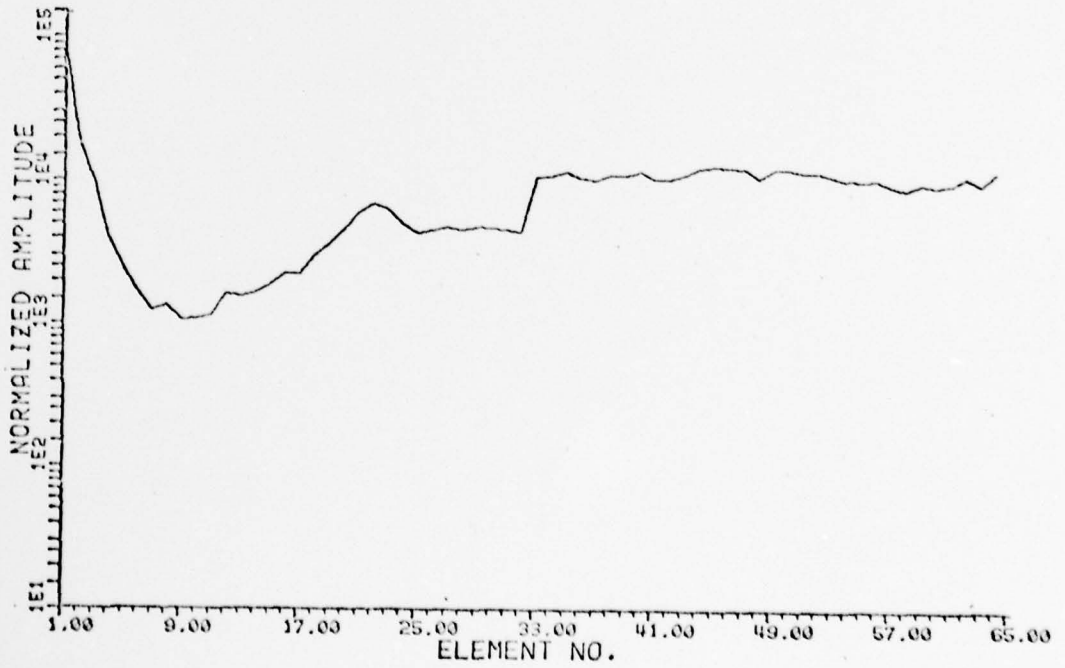

d. 20426 <WATER> DESICION = WATER 2MM RADAR
FILE D1.HLKS .NVD008- /NVD003/DECISIONS USING NVN808-NVN108
05/01/79 09:47

Figure 6-12. (continued)

6.6 --Continued.

For the panchromatic imagery, the water sample is incorrectly classified as forest while the agriculture sample is assigned an abstention action. (Recall that an abstention in this case is due to the fact that the sample falls in the region of acceptance for both forest and agriculture.) For the radar case, the water sample is correctly identified as water (60) and the agriculture correctly identified as agriculture. This points out once again that optical power spectrum analysis essentially provides a measure of texture. When the sensor type is such that unambiguous texture differences correspond to different terrain types as is the case here for radar, the correct decision will result. On the other hand, when no apparent texture difference can be associated with different terrain types, as is the case here for the panchromatic imagery, an incorrect or abstention action will result.

6.7 Qualitative Examination of the Results for Water (60) When 2, 4 and 6 mm Aperture Samples are Taken from Radar and Panchromatic Imagery

This example examines what may at first appear to be a strange result in the classification of water (60) for 2, 4 and 6 mm apertures. For the radar sensor, the results for 2, 4 and 6 mm apertures are respectively 19 of 19, 12 of 19 and 19 of 19 correctly classified. On the other hand, for panchromatic imagery the corresponding results are 23 of 26, 0 of 26 and 6 of 26 correctly classified. Figure 6-13 shows the radar samples that will be considered, while Figure 6-14 shows the panchromatic samples.

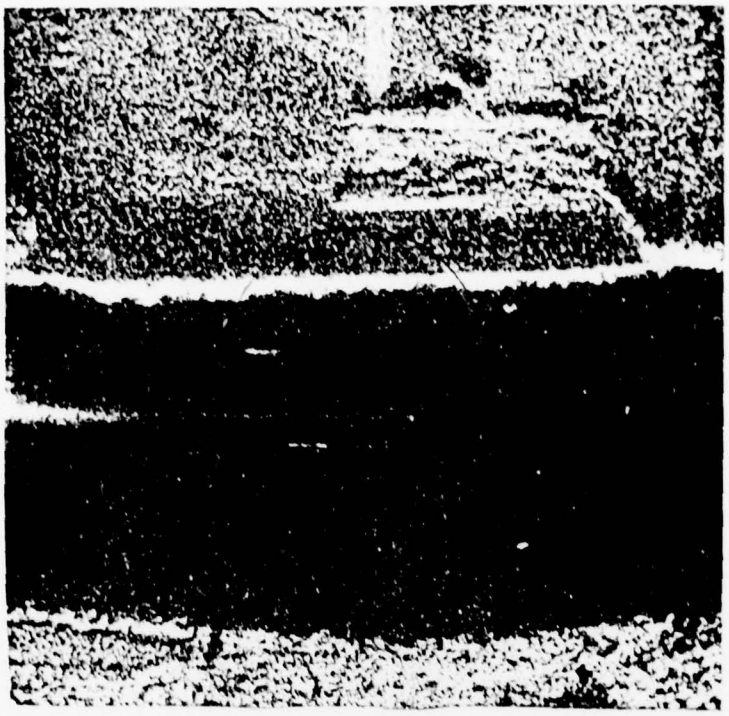

a. 20417 (Water)
Decision = Water

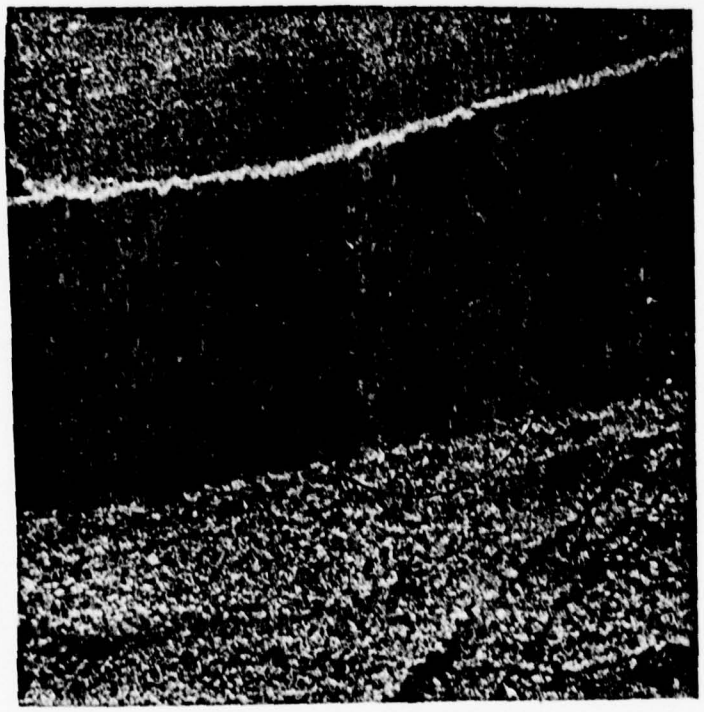

b. 20426 (Water)
Decision = Agriculture

Figure 6-13. Comparison of Water (60) Areas in 4mm Radar Imagery

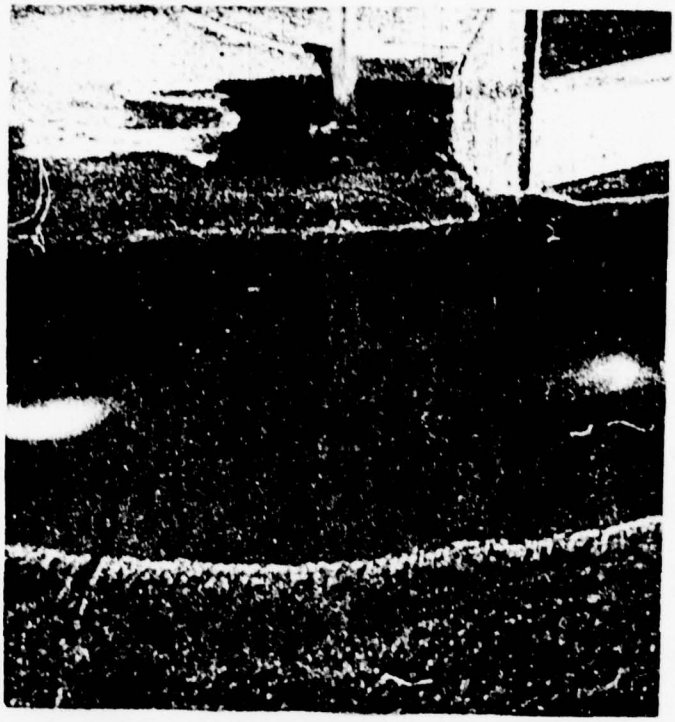

a. 20417 (Water)
Decision = Ambiguous

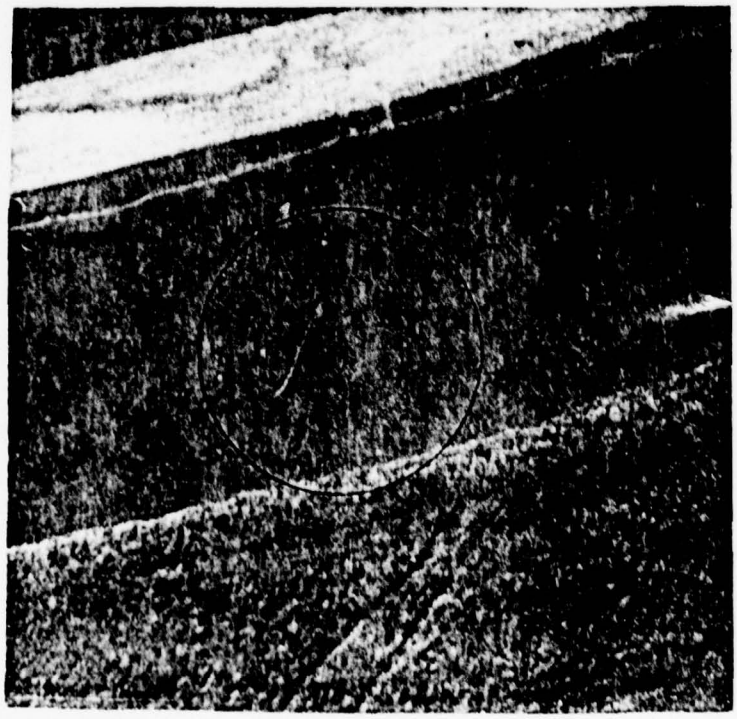

b. 20426 (Water)
Decision = Ambiguous

Figure 6-14. Comparison of Water (60) Areas in 4mm Panchromatic Imagery

6.7.1 2 mm Aperture Results

Basically we observe that in the 2 mm case, all of the radar samples are solidly within the water and no shoreline is present. On the other hand, a few of the panchromatic samples include a portion of the lower shore and are classified as Forest or are assigned an abstention action. Thus, in the 2 mm case, both radar and pan will correctly classify all samples which are completely within the water area.

6.7.2 4 mm Aperture Results

For the 4 mm aperture, the 12 of 19 radar samples correctly classified all contain a strong specular reflection from the upper shoreline. The other samples not containing the specular return are all classified as agriculture. Thus, in effect the system has trained itself to recognize this river water on the basis of the specular return from the shoreline. (Figure 6-15 shows the wedge clue comparison.)

On the other hand, all panchromatic samples are incorrectly identified because some shoreline is present in all samples. The shoreline near the river basically contains trees and appears as forest. As one moves further inland from the shoreline, the shoreline trees thin out and a more agricultural type terrain is present. This in fact corresponds to the decisions obtained. Those samples with relatively little shoreline are classified as forest, while those that contain more shoreline are typically assigned the abstention action corresponding to a mixture of forest and agriculture.

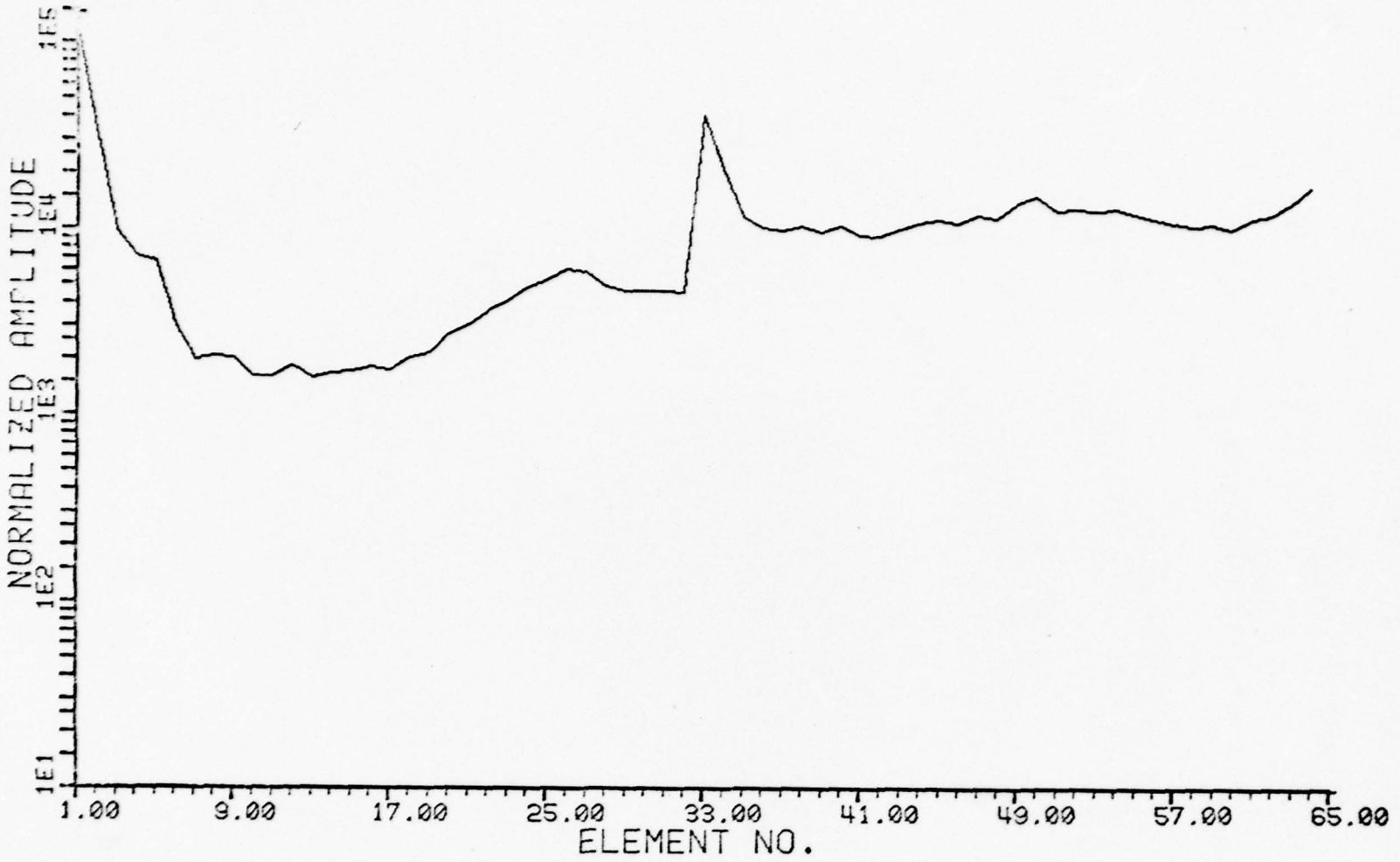

a. Specular component visible

20417 <WATER> DECISION = WATER 4MM RADAR
FILE D1.HLK5 .NVD011- /NVD011/DECISIONS USING NVN011-NVN111
05/01/79 10:34

Figure 6-15 Radar Imagery Wedge Clue Comparison for Water (60)

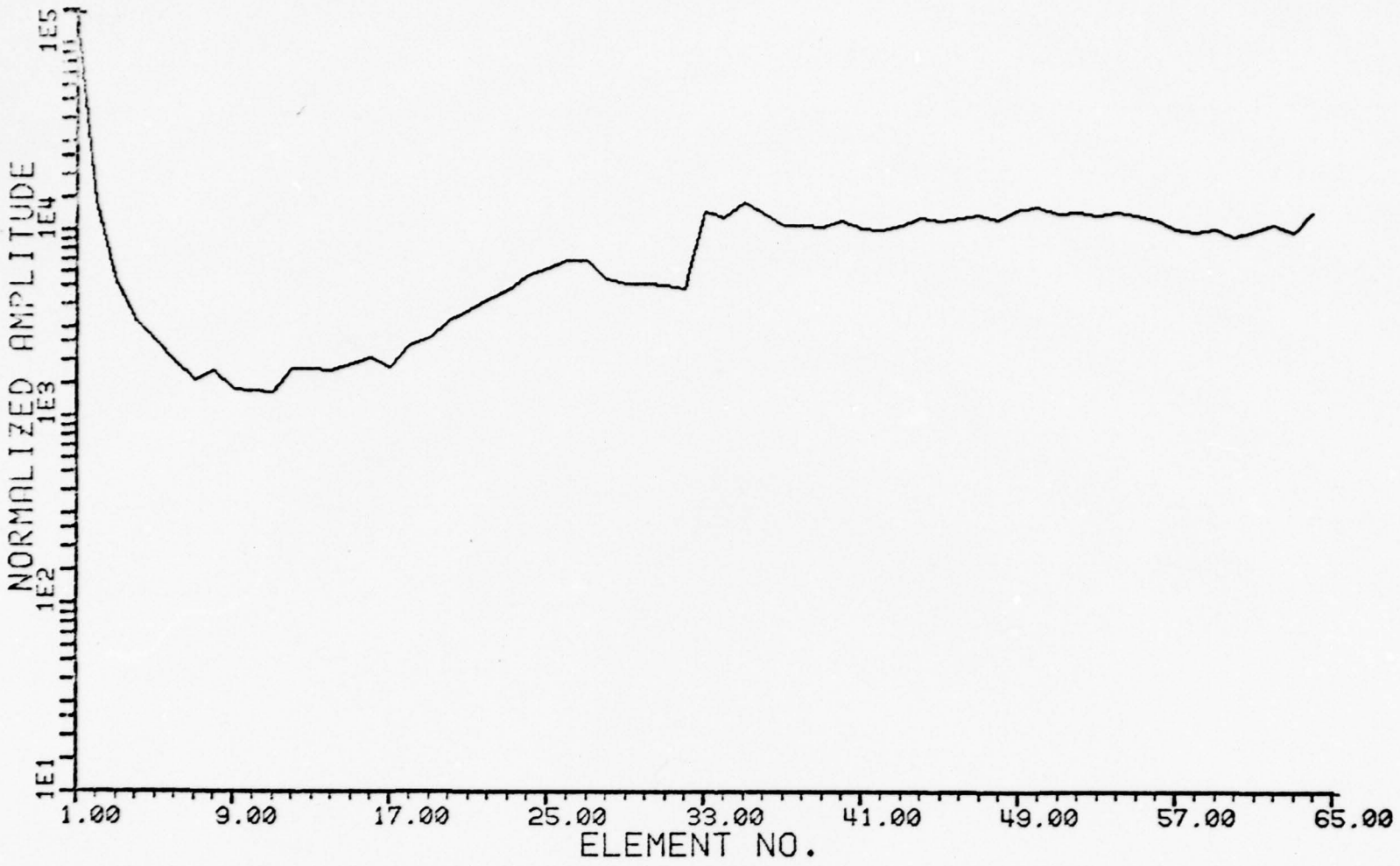

b. No specular component visible

20426 <WATER> DECISION = AGRICULTURE 4MM RADAR
FILE D1.HLK5 .NVD011- /NVD011/DECISIONS USING NVN011-NVN111
05/01/79 10:54

Figure 6-15 Radar Imagery Wedge Clue Comparison for Water (60)

6.7.3 6 mm Aperture Results

For the 6 mm aperture, all samples had at least one shoreline in view. Thus, a specular shoreline return was present in all 19 of the radar samples and all were correctly classified. On the other hand, only 6 of the 26 pan samples were correctly identified. For the most part, these were samples in the middle of the river containing mainly water with relatively small amounts of shoreline. Where both shorelines were present a decision was forest, and where only a single shoreline was present both forest decisions and abstention actions resulted. In this case once again, the radar specular return was implicitly recognized in the training algorithm as an indicator of shoreline implying a river sample. On the other hand, the lack of a specular return and the inclusion of forest and/or agriculture terrain in the panchromatic sample caused a correct, incorrect or abstention decision to be made depending on the amount and position of each terrain type.

7.0 CONCLUSIONS AND SUGGESTED FURTHER STUDY

7.1 Conclusions

7.1.1 Overall Performance for Different Sensor Types Differ

The major conclusion drawn from this study is that while optical power spectrum analysis can be applied to imagery derived from panchromatic visual sensors, synthetic aperture radar sensors and scanning thermal imagers, the detection capability in general and for specific terrain types is influenced by the sensor. This is primarily due to the fact that optical power spectrum signatures are strongly influenced by image texture so that the variation of terrain texture as a function of sensor strongly influences automatic detection capability.

It is not surprising that the different sensors will produce imagery with different texture characteristics. The radar sensor uses a wavelength considerably longer than either the thermal or the panchromatic imager. Furthermore, the radar "illumination" is coherent. Therefore, speckle and specular reflection characteristics appear in the reconstructed imagery for this sensor type. In fact, as noted in Section 6, the computed chi square value indicates that radar differs to a greater extent from either panchromatic or thermal imagery than panchromatic differs from thermal imagery.

7.1.2 Certain Sensors are Better for Specific Terrain Types

While the results do differ by sensor type, no single sensor is uniformly better than the other. In particular, urban area detection performance is better using panchromatic samples than using radar or

7.1.2 --Continued.

thermal samples. A detailed comparison of panchromatic and radar images indicates that this is because the urban line structure texture in panchromatic imagery presents a strong signature in the corresponding diffraction patterns. On the other hand, radar imagery causes a unique signature in the optical power spectrum whenever a specular return occurs from a man-made object acting as a cornercube reflector. In some urban areas, the specular return does not occur even when a strong line structure texture is present in the panchromatic imagery.

On the other hand, optical power spectrum samples from radar imagery generally provide better results than corresponding samples from panchromatic imagery for detection of agriculture and forest. This appears to be due to the fact that the textural differences associated with these classes are more distinct in the radar imagery than in the panchromatic.

Finally, it would appear by examining Table 7-1 that the best situation would be to use panchromatic imagery to detect urban areas and water, radar to detect agriculture, and thermal to detect forest. One would not do very much worse utilizing radar to detect water and forest as well. In fact, were a single sensor to be chosen, the choice would most likely be radar.

Table 7-1. Sensor Percent Correct Performance Comparison

	Urban (10)	Water (50)	Agriculture (80)	Forest (40)	Abstain	Average Correct Percent
2 mm Pan	100.0	86.44	61.79	74.2	25.7	80.6
2 mm Radar	76.9	85.69	83.98	94.3	9.2	85.2
10 mm Thermal	92.19	61.11	51.60	100.0	19.75	76.2

7.1.3 Aperture Size Effect

The effect of aperture size on the sampled imagery is not uniform for panchromatic and radar imagery. No statistically significant effect was observed for different size apertures insofar as their influence on detection performance for the radar imagery. One should of course take into account the discussion of the river water recognition in Section 6 that ostensibly does not change as a function of aperture size. This of course is true insofar as the statistics are concerned, but the closer analysis in Section 6 shows that the mechanism causing the decisions does in fact change.

For panchromatic imagery, the decision results are statistically different as the aperture size is changed. However, there appears to be no specific trend relating aperture size to improved decision performance. In fact, the differences appear to be due primarily to the river water/shoreline effect discussed in Section 6 and the forest/agriculture decision partition. In effect then, changing the aperture size affects decision performance because of changes in the number of terrain types present in an aperture. This is really a manifestation of the problem of unambiguously defining terrain boundaries that run through individual optical power spectrum sample apertures.

7.1.4 Conclusion Generality

Finally, we should point out that the results obtained here, although involving a substantial number of samples for certain classes, must still be considered tentative and preliminary. Even assuming that our results for the panchromatic and radar imagery are statistically valid, the

7.1.4 --Continued.

samples included in this study are from a very small region around Huntsville, Alabama. Without considering a broader range of geographical locations, one could not assume that these results would hold in a general setting. Also, since the region over which the thermal imagery was acquired was geographically remote from the Huntsville area, our comparisons of thermal results to results for panchromatic and radar involve the assumption that although the terrain was not identical the terrain characteristics were similar.

7.2 Areas for Further Study

In a certain sense this study has raised more questions than it has answered. But, this is the purpose of an initial study.

7.2.1 Expanded and Generalized Experiment

An obvious area for additional work is to broaden the range of the data base to include more samples reflecting more general terrain types and test the results obtained in this study in a more general setting.

7.2.2 Terrain Boundary Determination

In the context of the decision rule, we have raised, but not significantly considered, the question of how to treat boundary determination. This is clearly a key question for any automatic topographic classification system. Our results with samples not included in the training class because they were on a boundary being assigned the abstention action indicates that it may in fact be possible to automatically identify areas that include a

7.2.2 --Continued.

boundary between two terrain types. Obviously additional processing techniques, perhaps some combination of digital image processing and optical power spectrum analysis, will be required in order to correctly identify boundaries.

The ability to identify boundaries is important for another reason as well. Individual aperture sample decisions are based on local texture. We have seen examples in which local texture is not sufficient to unambiguously identify terrain type. On the other hand knowledge of boundaries provides a contextual framework within which a more "intelligent" decision can be made about a particular sample. For example, it is unlikely that a 200 foot square lake will exist in the middle of a plowed agricultural field.

7.2.3 Decision Rule Improvement

Finally, in the course of this study we have developed a decision rule and an approach to the development of similar decision rules that appears useful for multiclass problems with numerous classes and relatively few samples from each class. The rule is basically a threshold decision rule, similar to the one utilized in MISTIC. However, the threshold is not based on a comparison of the posterior probability estimate to a threshold. It would be worthwhile to consider how the rule structure developed during the course of this study can be extended so that it is based on the posterior probability. If this can be done, we can directly evaluate how close the decision rule performance is to the Bayes Rule by examining the percentage of ambiguous decisions[1].

REFERENCES FOR SECTION 7

1. H. L. Kasdan, "A Distribution-Free Pattern Classification Procedure with Performance Monitoring Capability", Techniques of Optimization, ed. A. V. Balakrishnan, Academic Press, Inc., New York, 1972.

APPENDIX I

LINEAR HYPOTHESIS MODEL

ANALYSIS OF VARIANCE TEST RESULTS

Class 10 - Urban

Aperture/Type/Imagery	% Correct	% Error	% Abstain
1mm Hardclipped Pan	93.5	6.4	0
2mm Gaussian Pan	100.0	0.0	0
4mm Gaussian Pan	96.7	3.2	0
6mm Gaussian Pan	100.0	0.0	0
2mm Gaussian Radar	76.9	15.3	7.6
4mm Gaussian Radar	84.6	15.3	0
6mm Gaussian Radar	88.4	11.5	0

	2	4	6
Pan	100	96.7	100
Radar	76.9	84.6	88.4

% Correct

$F_{col} = 0.79$

$F_{row} = 17.28$

	2	4	6
Pan	0.0	3.2	0.0
Radar	15.3	15.3	11.5

% Error

$F_{col} = 2.94$

$F_{row} = 120.86$

	2	4	6
Pan	0	0	0
Radar	7.6	0	0

% Abstain

$F_{col} =$

$F_{row} =$

Class 50 - Water

Aperture/Type/Imagery	% Correct	% Error	% Abstain
1mm Hardclipped Pan	45.4	54.5	0.0
2mm Gaussian Pan	81.8	18.1	0.0
4mm Gaussian Pan	100.0	0.0	0.0
6mm Gaussian Pan	100.0	0.0	0.0
2mm Gaussian Radar	55.5	22.2	22.2
4mm Gaussian Radar	66.6	33.3	0.0
6mm Gaussian Radar	66.6	33.3	0.0

	2	4	6
Pan	81.8	100.0	100.0
Radar	55.5	66.6	66.6

% Correct

$F_{col} = 17.03$

$F_{row} = 171.96$

	2	4	6
Pan	18.1	0.0	0.0
Radar	22.2	33.3	33.3

% Error

$F_{col} = .06$

$F_{row} = 5.86$

	2	4	6
Pan	0	0	0
Radar	22.2	0	0

% Abstain

$F_{col} =$

$F_{row} =$

Class 60 - Water

Aperture/Type/Imagery	% Correct	% Error	% Abstain
1mm Hardclipped Pan	7.6	92.3	0
2mm Gaussian Pan	88.4	7.6	3.8
4mm Gaussian Pan	0.0	42.3	57.6
6mm Gaussian Pan	23.0	57.6	19.2
2mm Gaussian Radar	100.0	0.0	0.0
4mm Gaussian Radar	63.1	36.8	0.0
6mm Gaussian Radar	100.0	0.0	0.0

	2	4	6
Pan	88.4	0.0	23.0
Radar	100.0	63.1	100.0

% Correct

$F_{col} = 3.3$

$F_{row} = 6.5$

	2	4	6
Pan	7.6	42.3	57.6
Radar	0.0	36.8	0.0

% Error

$F_{col} = 1.5$

$F_{row} = 1.9$

	2	4	6
Pan	3.8	57.6	19.2
Radar	0.0	0.0	0.0

% Abstain

$F_{col} = 1.0$

$F_{row} = 2.8$

Class 20 Agriculture (Plowed)

Aperture/Type/Imagery	% Correct	% Error	% Abstain
1mm Hardclipped Pan	73.4	0.0	26.5
2mm Gaussian Pan	57.8	0.0	42.1
4mm Gaussian Pan	75.9	0.0	24.0
6mm Gaussian Pan	77.1	0.0	22.8
2mm Gaussian Radar	83.3	0.0	16.6
4mm Gaussian Radar	87.5	0.0	12.5
6mm Gaussian Radar	90.2	0.0	9.7

	2	4	6
Pan	57.8	75.9	77.1
Radar	83.3	87.5	90.2

% Correct

$F_{col} = 3.4$

$F_{row} = 14.4$

	2	4	6
Pan	0.0	0.0	0.0
Radar	0.0	0.0	0.0

% Error

$F_{col} =$

$F_{row} =$

	2	4	6
Pan	42.1	24.0	22.8
Radar	16.6	12.5	9.7

% Abstain

$F_{col} = 3.4$

$F_{row} = 14.2$

Class 70 Agriculture (Non-Plowed)

Aperture/Type/Imagery	% Correct	% Error	% Abstain
1mm Hardclipped Pan	64.5	0.0	35.4
2mm Gaussian Pan	68.7	0.0	31.2
4mm Gaussian Pan	79.1	0.0	20.8
6mm Gaussian Pan	79.1	0.0	20.8
2mm Gaussian Radar	84.9	0.0	15.0
4mm Gaussian Radar	94.3	0.0	5.6
6mm Gaussian Radar	94.3	0.0	5.6

	2	4	6
Pan	68.7	79.1	79.1
Radar	84.9	94.3	94.3

% Correct

$F_{col} = 392.6$

$F_{row} = 2174.8$

	2	4	6
Pan	0.0	0.0	0.0
Radar	0.0	0.0	0.0

% Error

$F_{col} =$

$F_{row} =$

	2	4	6
Pan	31.2	20.8	20.8
Radar	15.0	5.6	5.6

% Abstain

$F_{col} = 392.2$

$F_{row} = 2172.4$

Class 40 - Forest

Aperture/Type/Imagery	% Correct	% Error	% Abstain
1mm Hardclipped Pan	90.1	0.0	9.8
2mm Gaussian Pan	74.2	0.0	25.7
4mm Gaussian Pan	64.8	0.0	35.1
6mm Gaussian Pan	86.4	0.0	13.5
2mm Gaussian Radar	94.3	0.0	5.6
4mm Gaussian Radar	97.1	0.0	2.8
6mm Gaussian Radar	95.7	0.0	4.2

	2	4	6
Pan	74.2	78.5	86.4
Radar	94.3	97.1	95.7

% Correct

$F_{col} = 9.58$

$F_{row} = 22.4$

	2	4	6
Pan	0.0	0.0	0.0
Radar	0.0	0.0	0.0

% Error

$F_{col} =$

$F_{row} =$

	2	4	6
Pan	25.7	21.5	13.5
Radar	5.6	2.8	4.2

% Abstain

$F_{col} = 9.58$

$F_{row} = 22.4$

APPENDIX 2

χ^2 TEST RESULTS FOR

PANCHROMATIC APERTURE PERFORMANCE COMPARISON

Hardclip 1mm versus 4mm Gaussian Pan

	10	50	60	80	40	90	
					279		
1mm	29	5	2	98	219	60	413
4mm	30	11	0	102	179	91	413
					270		

i		
1	29.5	.01
2	8.0	1.13
3	1.0	1.00
4	100.0	.04
5	199.0	2.01
6	75.5	3.18

(1% significance level) $15.1 > 14.73 > 12.8$ (2.5% significance level)

If 40 and 90 combined

	10	50	60	80	40-90
1mm	29	5	2	98	279
4mm	30	11	0	102	270

i		
1	29.5	.01
2	8.0	1.13
3	1.0	1.00
4	100.0	.04
5	274.5	.07

(5% significance level) $9.49 > 4.50 > 0.711$ (50% significance level)

Hardclip 1mm versus 6mm Gaussian Pan

	10	50	60	80	40	90
1mm	29	5	2	98	219	60
6mm	31	11	6	102	200	63

i		
1	30	.03
2	8	1.125
3	4	1.0
4	100	.04
5	209.5	.43
6	61.5	.04

(95% significance level) 11.1 > 5.33 > 1.15 (50% significance level)

2mm versus 4mm Gaussian

	10	50	60	80	40	90
2mm	31	9	23	83	161	106
				(20 from 50)		
4mm	30	11	0	102	179	91
				(1 from 60)	(10 from 60)	(15 from 60)

i		
1	30.5	.008
2	10	.1
3	11.5	11.5
4	92.5	.976
5	170.0	.476
6	98.5	.571

27.26 > 15.1 (1% significance level)

Redistribute class 60 for 4mm

	10	50	60	80	40	90
2mm	31	9	23	83	161	106
4mm (Redistribute 60)	30	11	26	101	169	76

i		
1	30.5	.008
2	10	.1
3	24.5	.09
4	92	.88
5	165	.10
6	91	2.47

(5% significance level) 11.1 > 7.3 > 1.15
(50% significance level)

2mm versus 6mm Gaussian

	10	50	60	80	40	90
2mm	31	9	23	83	161	106
6mm	31	11	6	102	200 15(60)	63 5(60)

i	
1	31 0
2	10 .1
3	14.5 4.98
4	92.5 .98
5	180.5 2.10
6	84.5 5.47

27.24 > 15.1 (1% significance level)

2mm versus 6mm Redistribute 60 for 6mm

	10	50	60	80	40	90
2mm	31	9	23	83	161	106
6mm (Redistribute 60)	31	11	26	102	185	58

doing better on agriculture and forest

i	
1	31 0
2	10 .1
3	24.5 .09
4	92.5 .98
5	173 .83
6	82 7.02

18.04 > 15.1 (1% significance level)

4mm versus 6mm Gaussian

	10	50	60	80	40	90
4mm	30	11	0	102	179	91
6mm	31	11	6	102	200	63

i		
1	30.5	.008
2	11	0
3	3	3.0
4	102	0
5	189.5	.58
6	77	2.55

(1% significance level) 15.1 > 12.2 > 11.1
(5% significance level)

4mm versus 6mm Redistribute 60 for both

	10	50	60	80	40	90
4mm (Redistribute 60)	30	11	26	101	169	76
6mm (Redistribute 60)	31	11	26	102	185	58

i		
1	30.5	.008
2	11	0
3	26	0
4	101.5	.005
5	177	.361
6	67	1.2

(5% significance level) 11.1 > 3.16 > 1.15
(50% significance level)

APPENDIX 3

χ^2 TEST RESULTS FOR RADAR APERTURE PERFORMANCE COMPARISON

I	ROW 1	ROW 2	PI	CHI-SQ(I)
1	20	22	21	4.7619E-02
2	5	6	5.5	4.54545E-02
3	19	12	15.5	0.790323
4	106	125	115.5	0.781385
5	204	207	205.5	1.09489E-02
6	36	18	27	

CHI SQUARE = 9.35146 WITH 5 DEGREES OF FREEDOM
ENTER NO. OF COLUMNS
3

2mm Gaussian versus 4mm Gaussian

I	ROW 1	ROW 2	PI	CHI-SQ(I)
1	20	23	21.5	0.104651
2	5	6	5.5	4.54545E-02
3	19	19	19	0
4	106	119	112.5	0.375556
5	204	204	204	0
6	36	19	27.5	2.62727

CHI SQUARE = 6.30587 WITH 5 DEGREES OF FREEDOM
ENTER NO. OF COLUMNS

2mm Gaussian versus 6mm Gaussian

I	ROW 1	ROW 2	PI	CHI-SQ(I)
1	22	23	22.5	1.11111E-02
2	6	6	6	0
3	12	19	15.5	0.790323
4	125	119	122	7.37705E-02
5	207	204	205.5	1.09489E-02
6	18	19	18.5	1.35135E-02

CHI SQUARE = 1.79933 WITH 5 DEGREES OF FREEDOM
ENTER NO. OF COLUMNS

4mm Gaussian versus 6mm Gaussian

APPENDIX 4

CLASS STATISTICS PLOTS -

2MM APERTURE PANCHROMATIC AND RADAR CASES

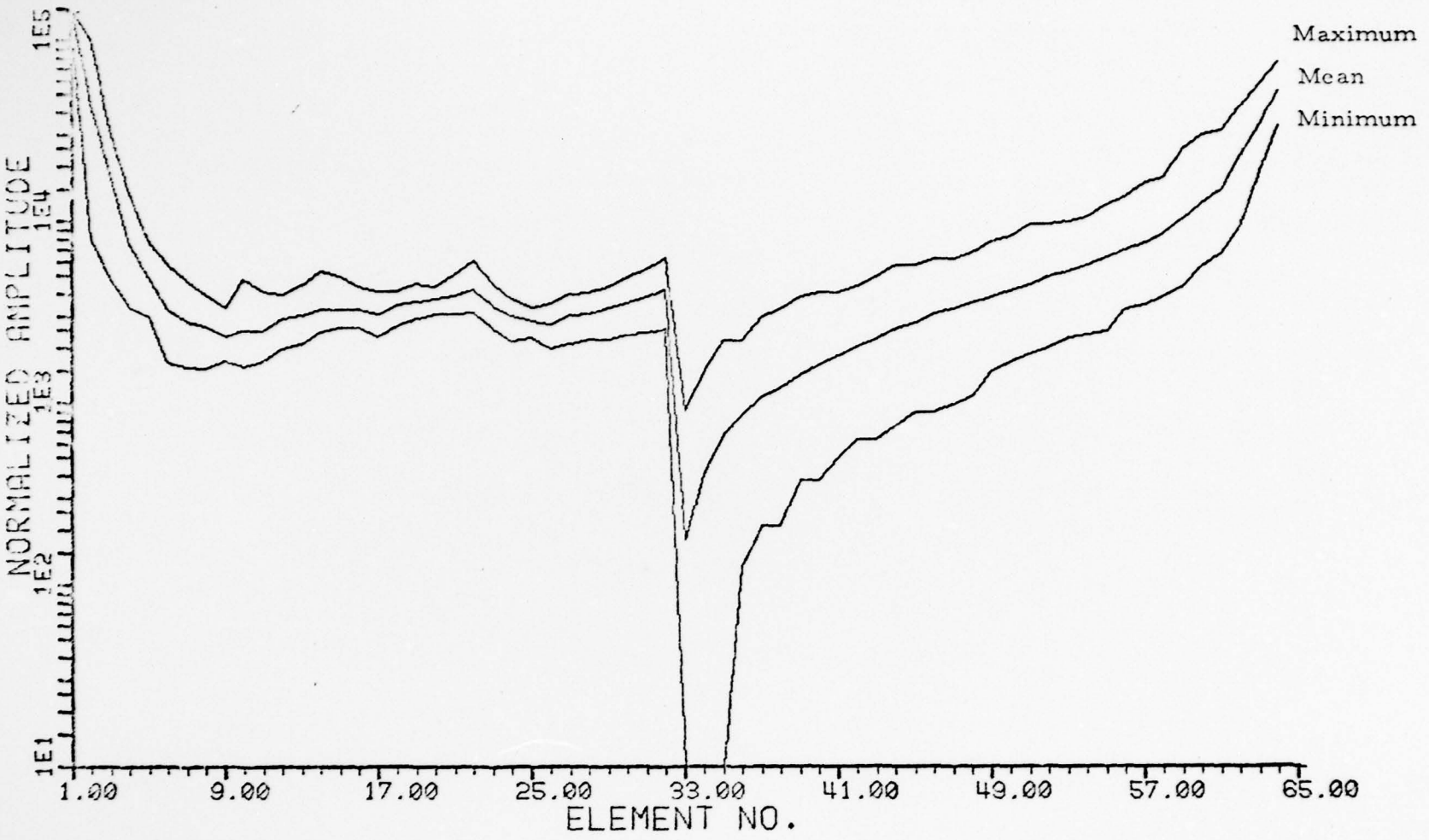

171

FILE D1.HLK5 .NS1503- STATISTICS FROM NVN503-CLASS10
0 ASS 10. <URBAN> 2MM PAN STATISTICS
04/3[illegible]9 10:31

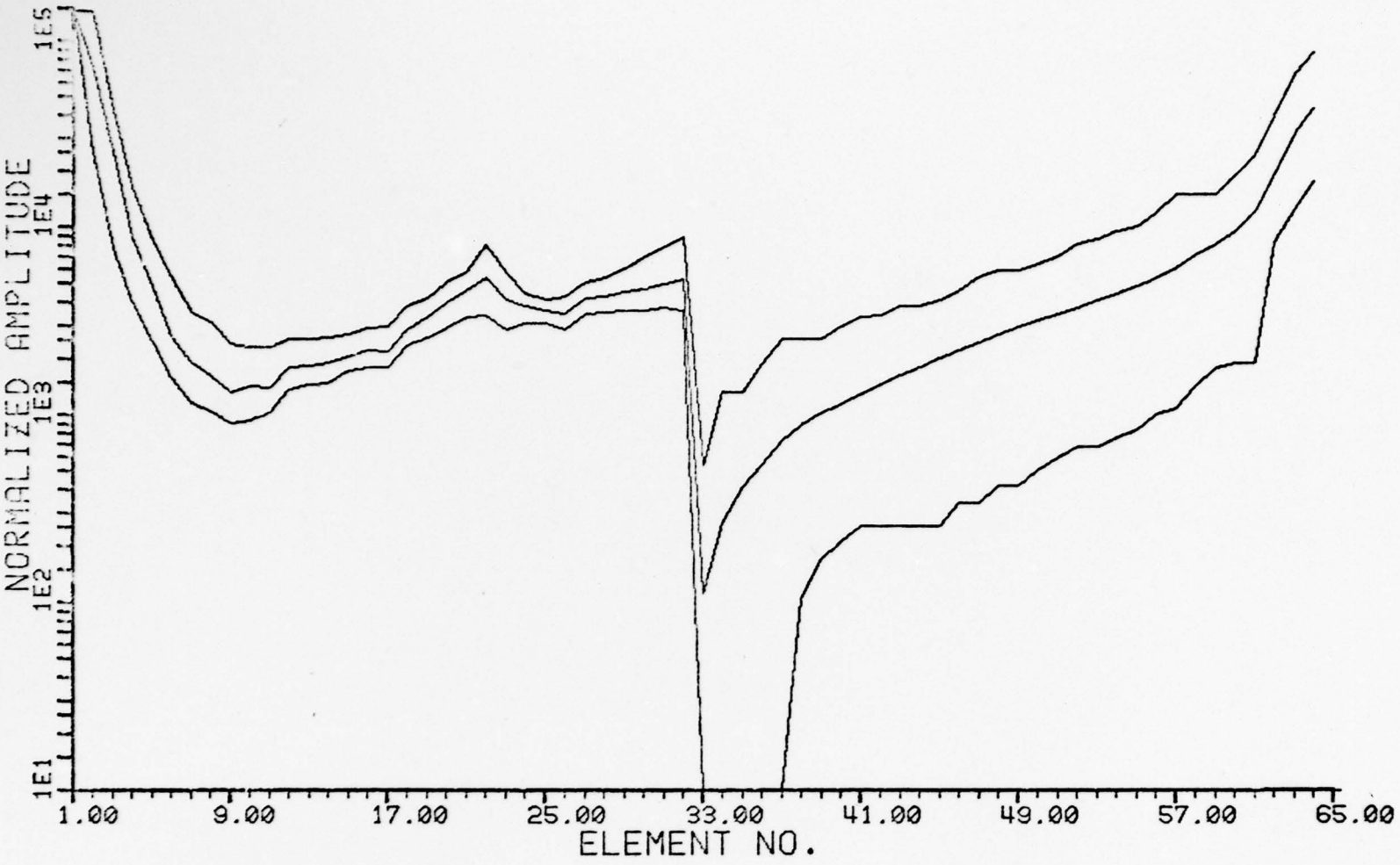

172

FILE D1.HLK5 .NS2503- STATISTICS FROM NVN503-CLASS20
CLASS 20. <PLOWED AGRICULTURE> 2MM PAN STATISTICS
04/30/73 10:38

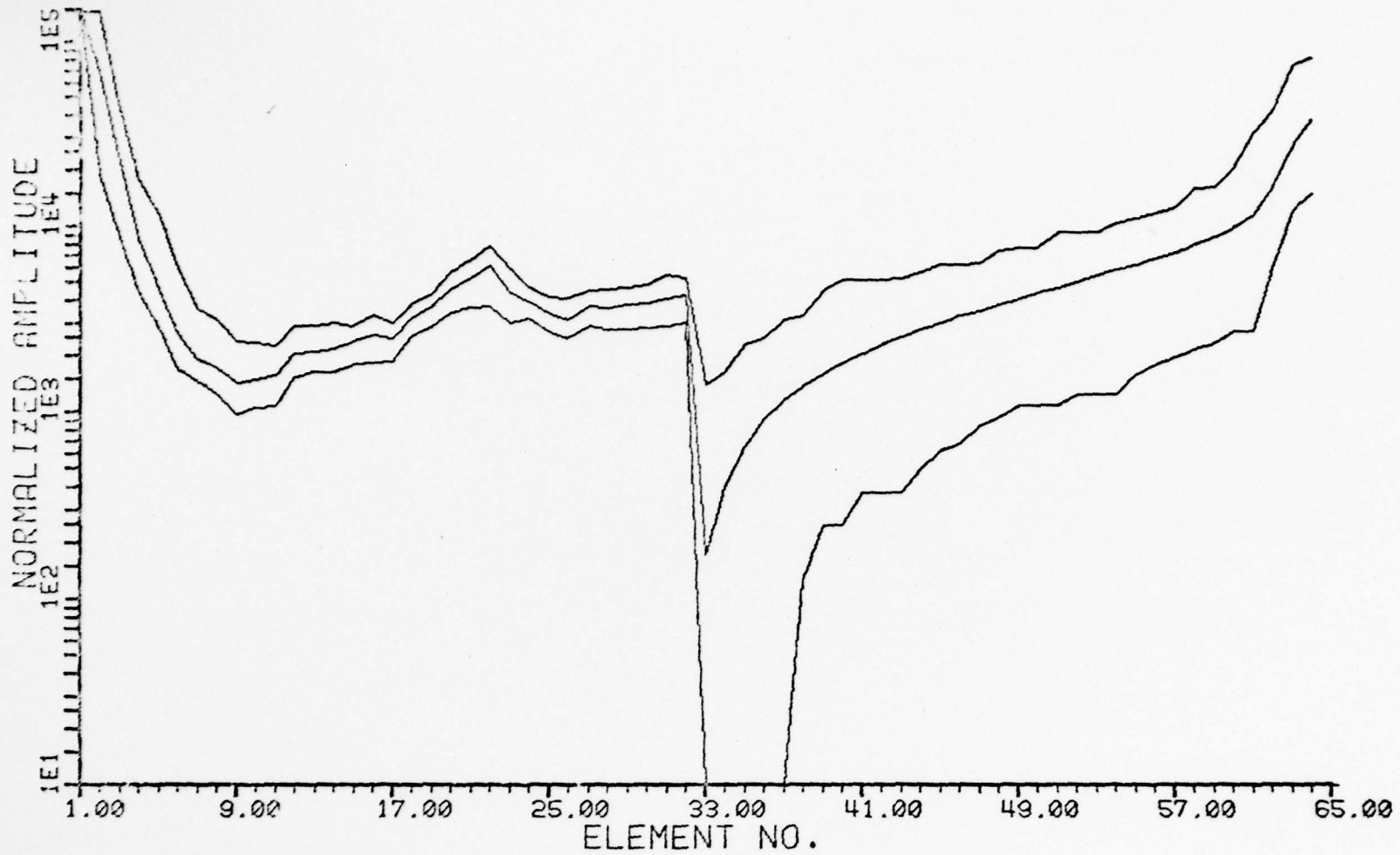

FILE D1.HLK5 .N34503- STATISTICS FROM NVN503-CLASS40
CLASS 40. <FOREST> 2MM PAN STATISYICS
04/30/79 10:40

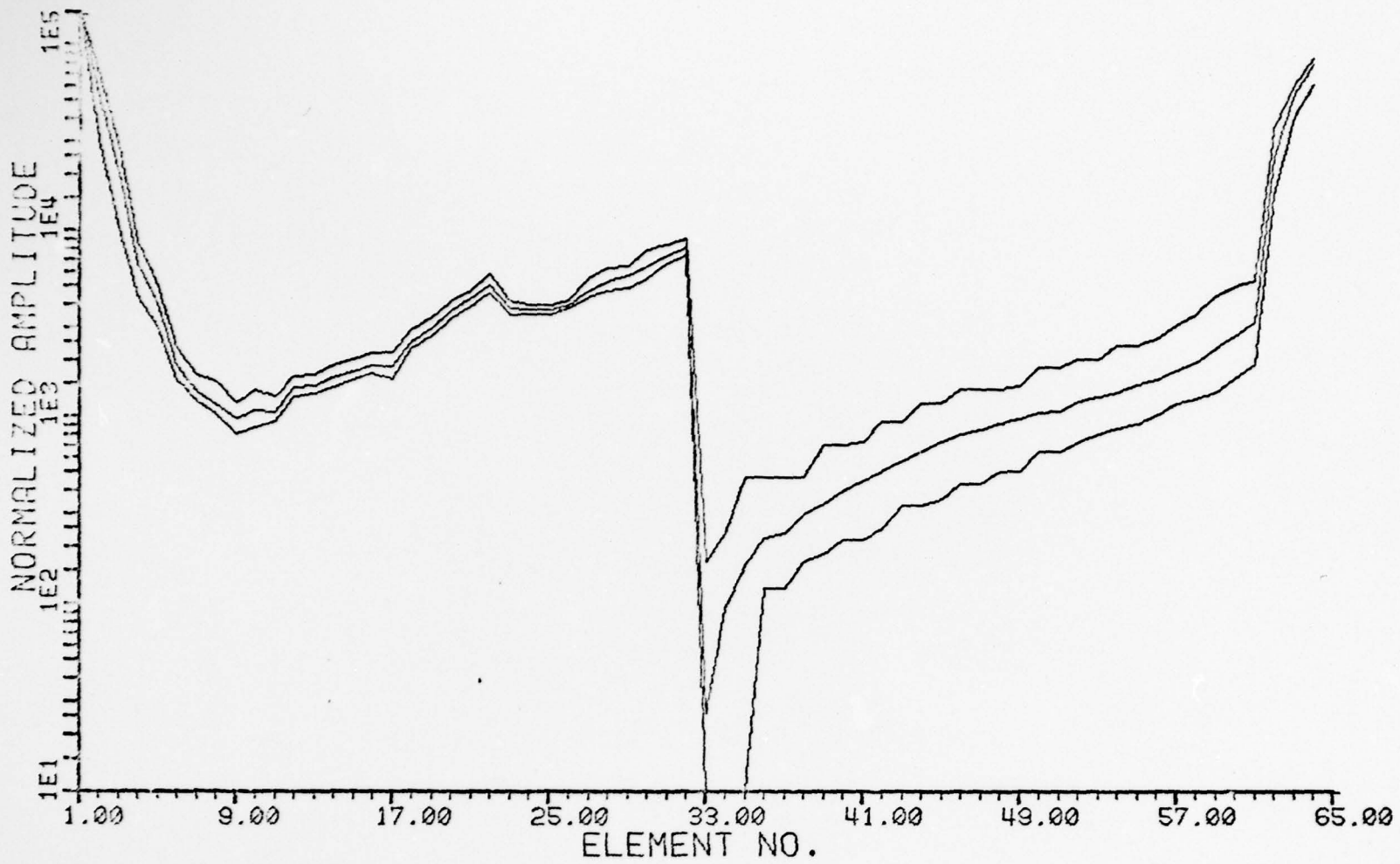

FILE D1.HLK5 .NS5503- STATISTICS FROM NVN503-CLASS50
CLASS 50. <WATER WITH 1XXXX DESIGNATORS> 2MM PAN STATISTICS
04/30/79 10:42

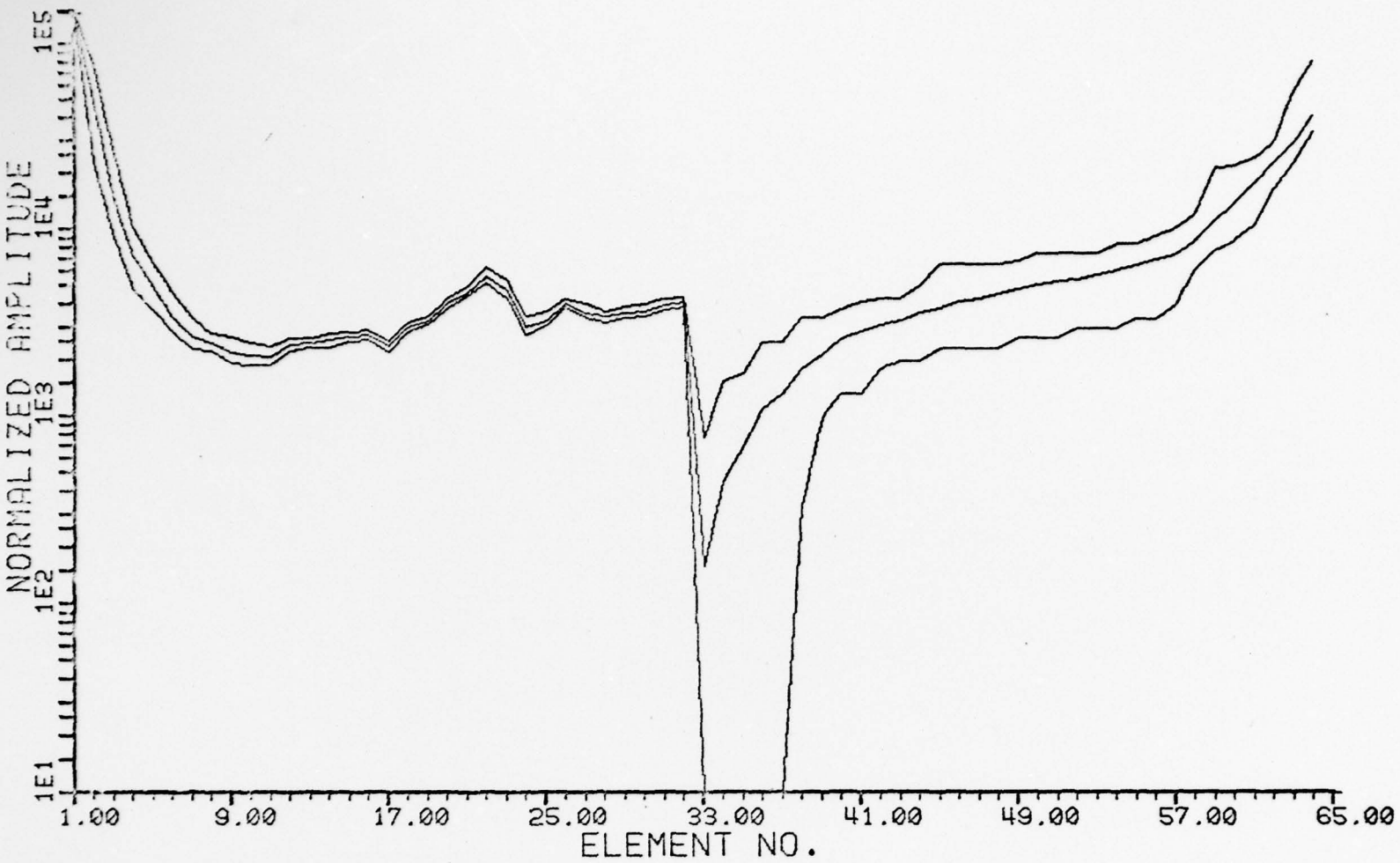

FILE D1.HLK5 .NS6503- STATISTICS FROM NVN503-CLASS60
CLASS 60. <WATER WITH DESIGNATORS 2XXXX> 2MM PAN STATISTICS
04/30/79 10:44

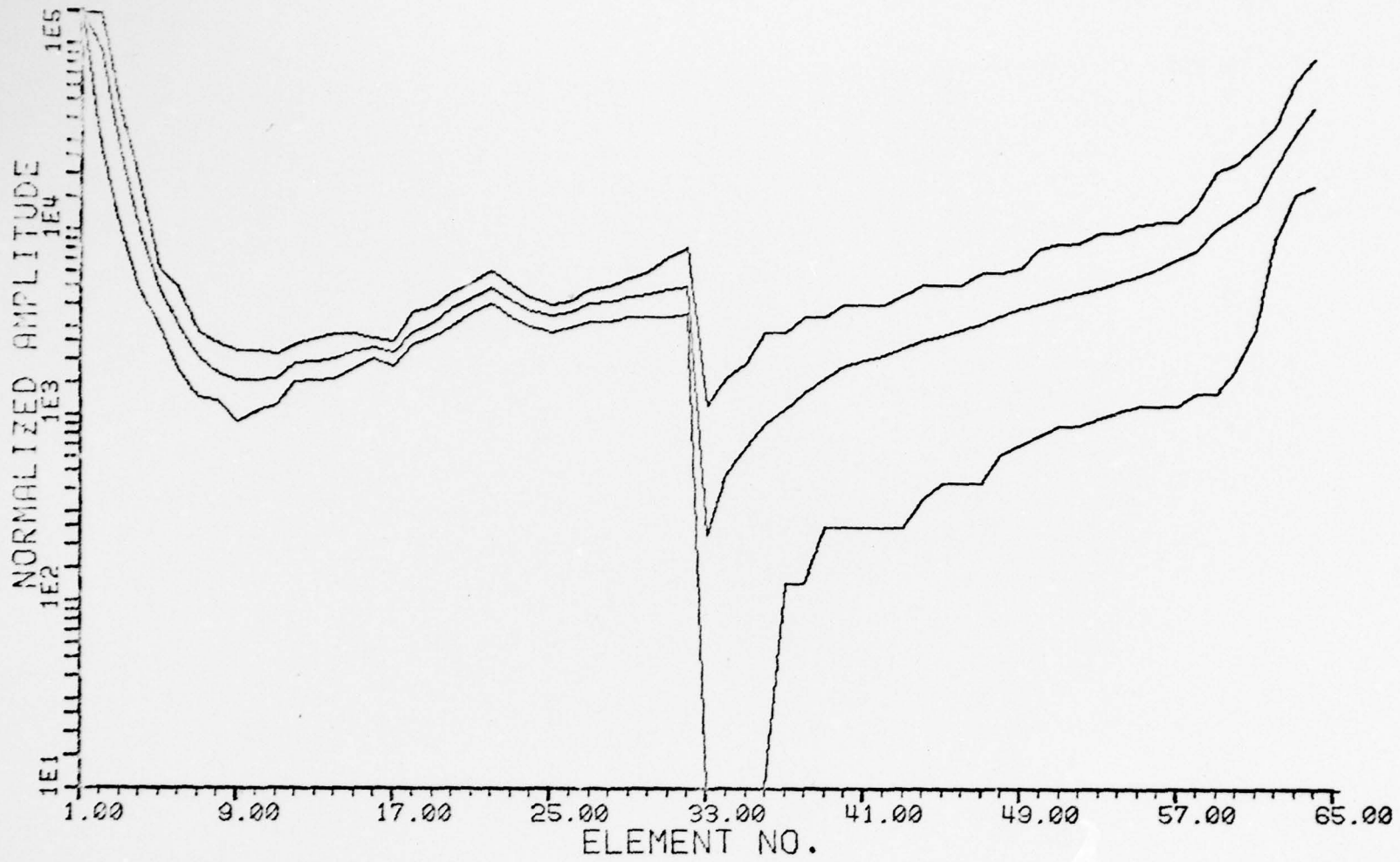

FILE D1.HLK5 .NS7503- STATISTICS FROM NVN503-CLASS10
CLASS 70. <NON PLOWED AGRICULTURE> 2MM PAN STATISTICS
04/30/79 10:46

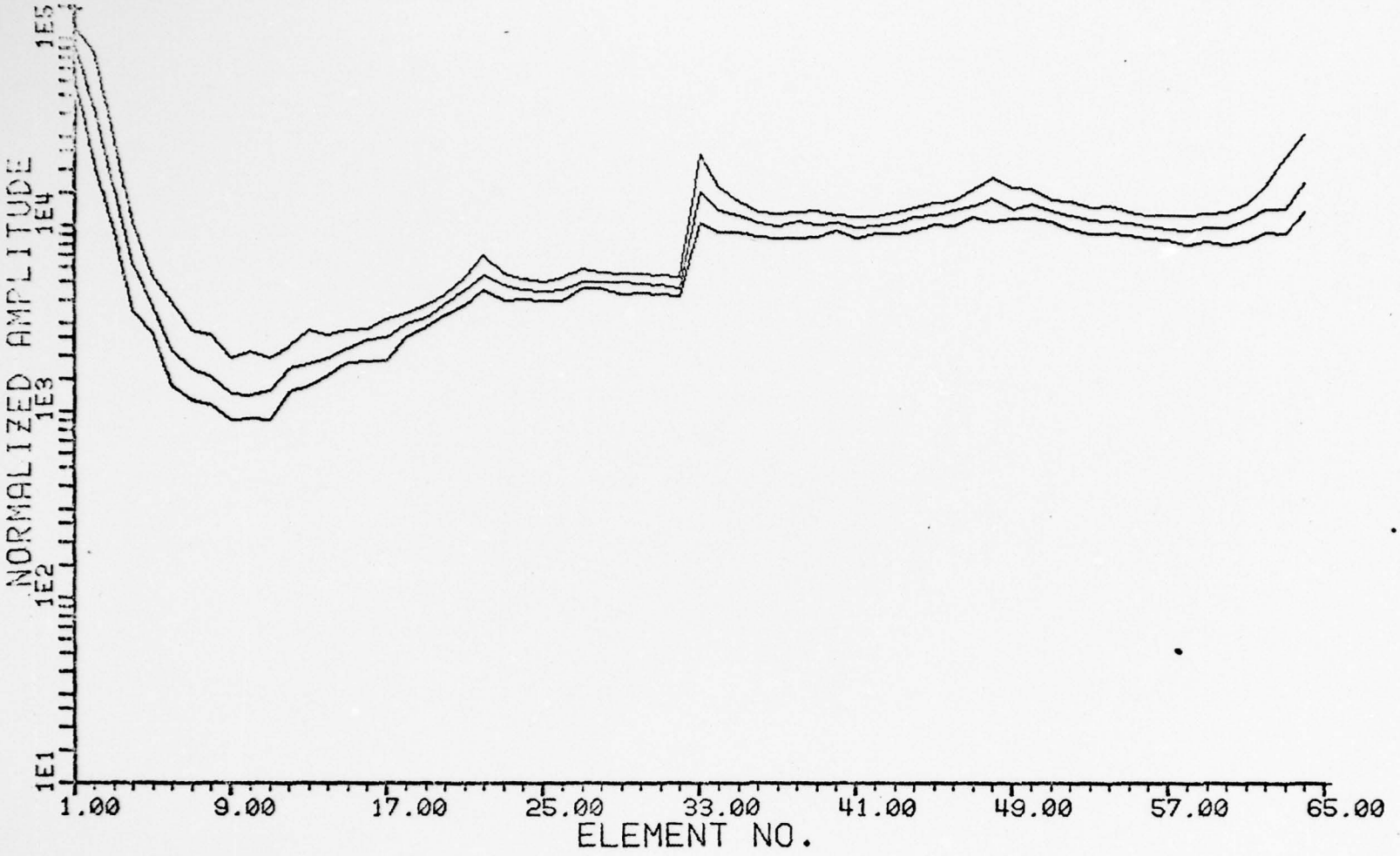

177

FILE D1.HLK5 .NS1008- STATISTICS FROM NVN008-CLASS10
CLASS 10. <URBAN> 2MM RADAR STATISTICS
04/30/79 10:49

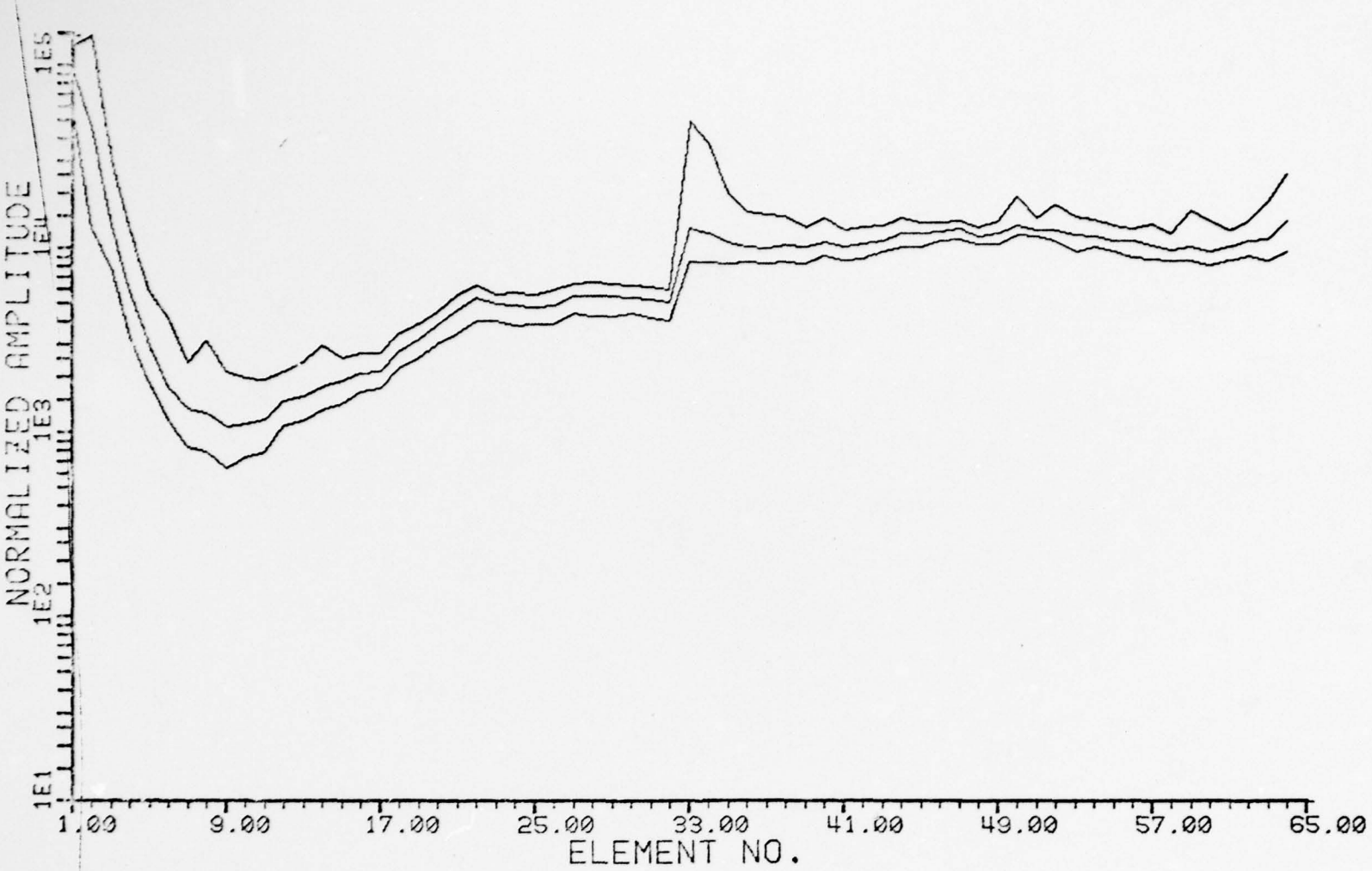

178

FILE D1.HLK5 .NS2000- STATISTICS FROM NVN008-CLASS20
CLASS 20. <PLOWED AGRICULTURE> 2MM RADAR STATISTICS
04/30/79 10:51

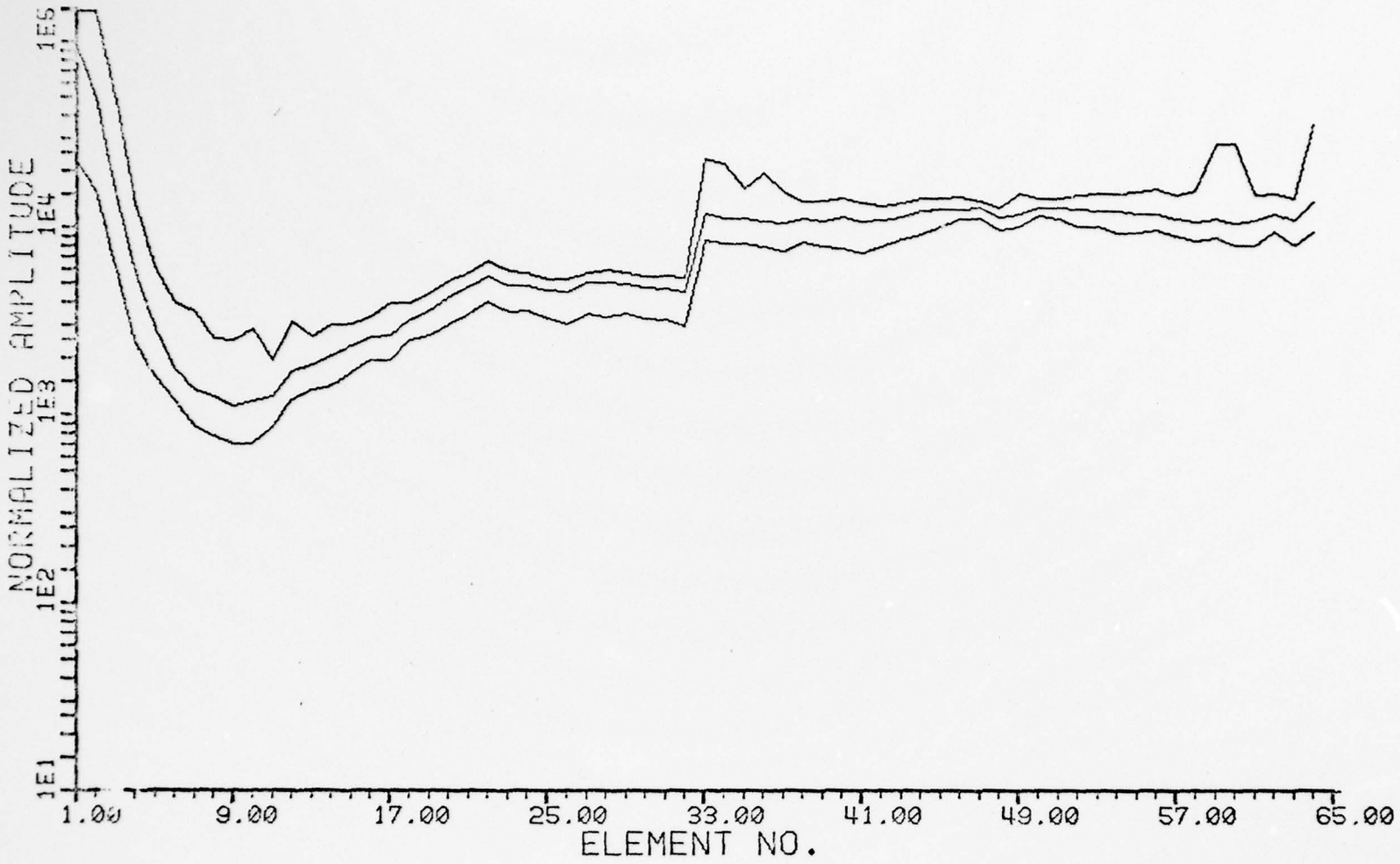

FILE D1.HLK5 .NS4008- STATISTICS FROM NVN008-CLASS40
CLASS 40. <FOREST> 2MM RADAR STATISTICS
04/30/79 10:59

AD-A076 566 RECOGNITION SYSTEMS INC VAN NUYS CALIF F/G 5/8
FEASIBILITY OF USING OPTICAL POWER SPECTRUM ANALYSIS TECHNIQUES--ETC(U)
JUN 79 H L KASDAN DAAK70-78-C-0019
UNCLASSIFIED KS-77-370 ETL-0186 NL

3 OF 3
AD
A076566

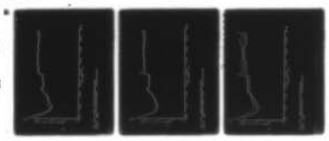

END
DATE
FILMED
12-79
DDC

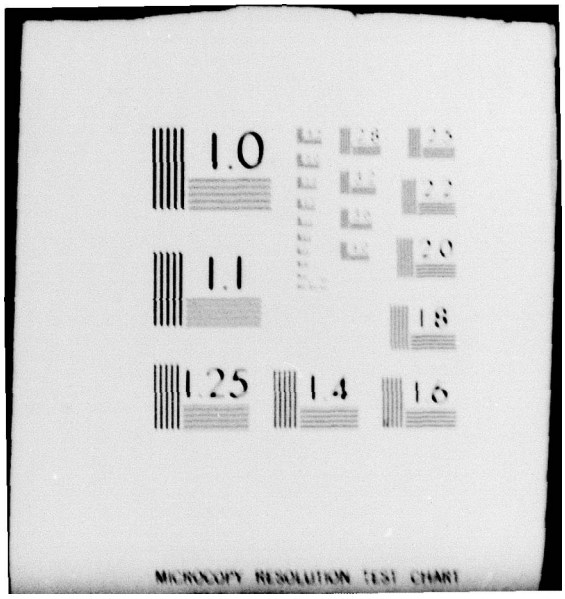
1.0
1.1
1.25
1.4
1.6
2.0
2.2
MICROCOPY RESOLUTION TEST CHART

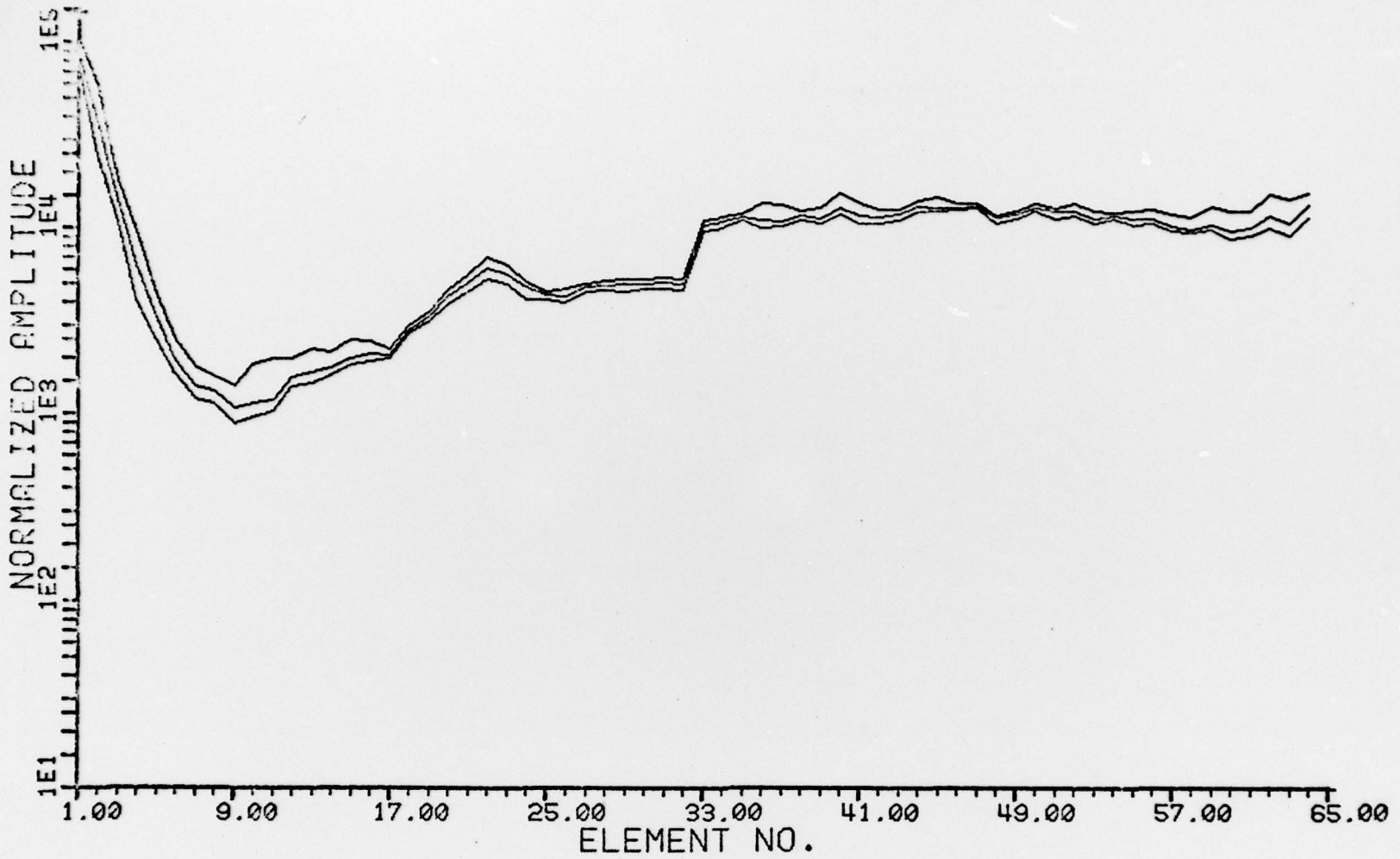

180

FILE D1.HLK5 .NS5008- STATISTICS FROM NVN008-CLASS50
CLASS 50. <WATER WITH 1XXXX DESIGNATORS> 2MM RADAR STATISTICS
04/30/79 10:55

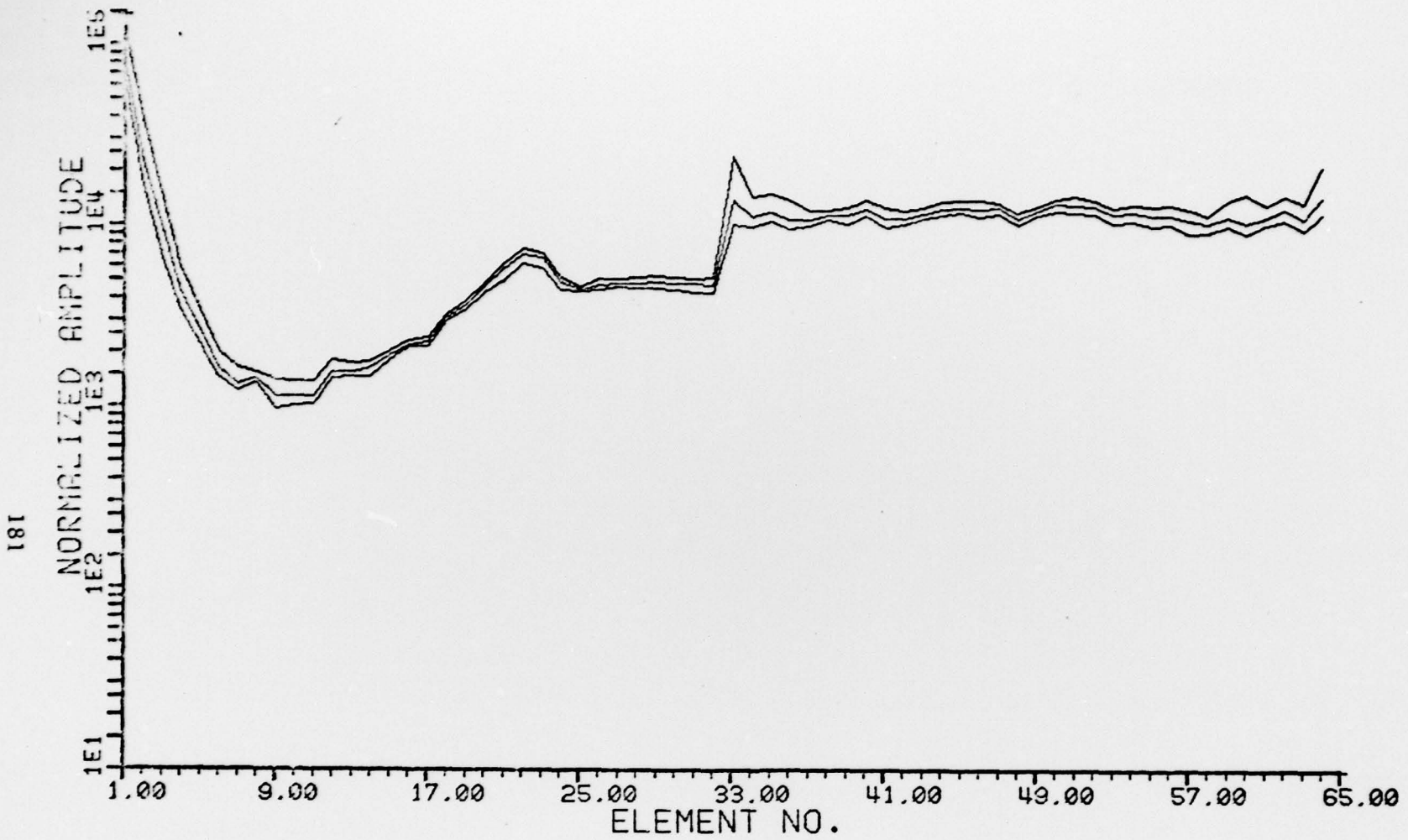

FILE D1.HLK5 .NS6008- STATISTICS FROM NVN008-CLASS60
CLASS 60. <WATER WITH DESIGNATORS 2XXXX> 2MM RADAR STATISTIC2
04/30/79 10:57

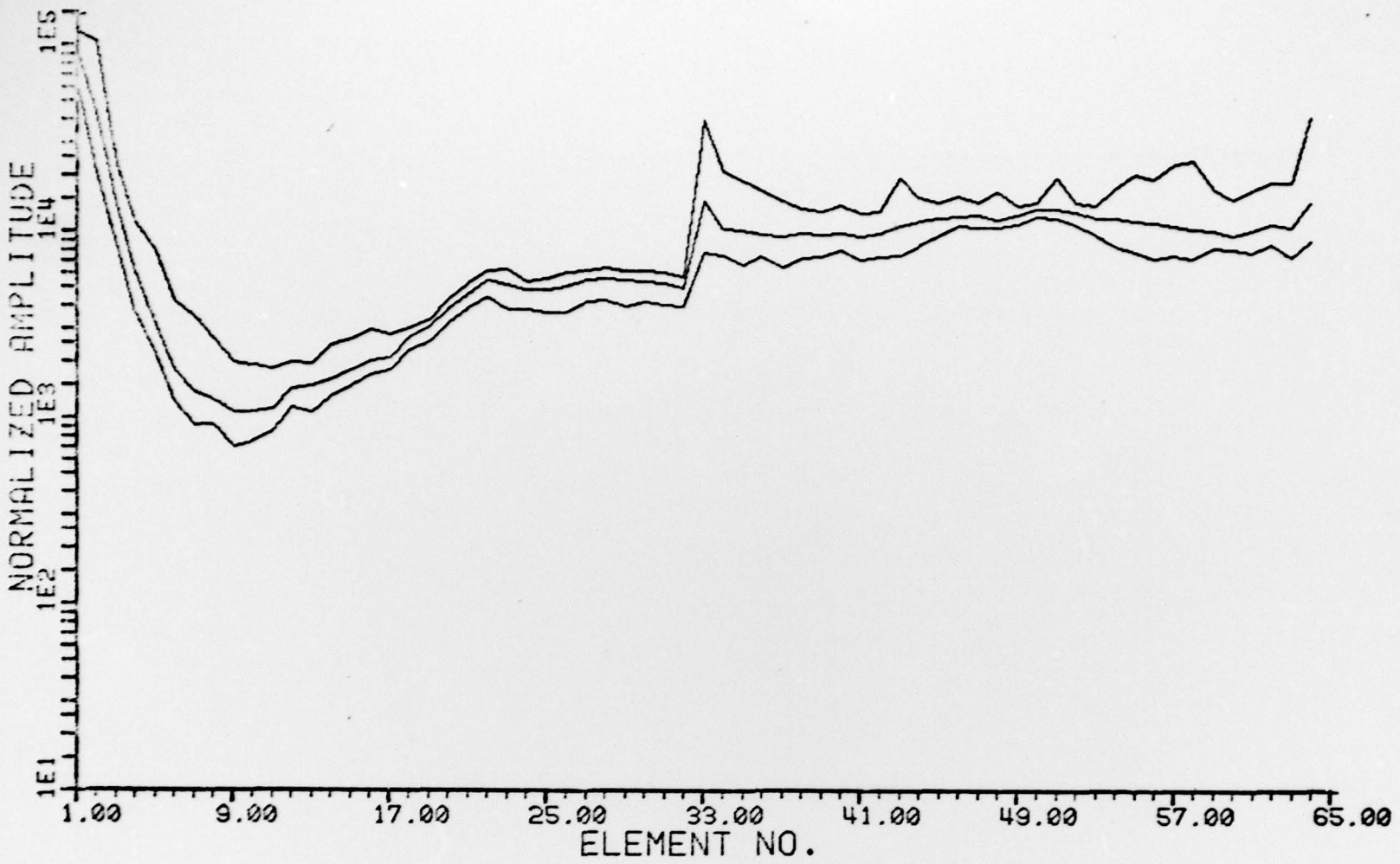

FILE D1.HLK5 .NS7008- STATISTICS FROM NVN008-CLASS70
CLASS 70. <NON PLOWED AGRICULTURE> 2MM RADAR STATISTICS
04/30/79 10:59